# DEFORMATION OF COMPACTS OF MAGNESIUM HYDROXIDE DURING DEHYDROXYLATION

PHILIP WILLIAM SUNDERLAND, P. ENG.
B. A. Sc., UNIVERSITY OF BRITISH COLUMBIA
1965

A THESIS SUBMITTED IN PARTIAL FULFILMENT OF THE REQUIREMENTS OF THE DEGREE OF MASTER OF APPLIED SCIENCE

in the Department

of

METALLURGY

We accept this thesis as conforming to the standard required from candidates for the degree of Master of Applied Science

Members of the Department of Metallurgy

THE UNIVERSITY OF BRITISH COLUMBIA

August, 1970

In presenting this thesis in partial fulfilment of the requirements for an advanced degree at the University of British Columbia, I agree that the Library shall make it freely available for reference and study. I further agree that permission for extensive copying of this thesis for scholarly purposes may be granted by the Head of my Department or by his representatives. It is understood that copying or publication of this thesis for financial gain shall not be allowed without my written permission.

Department of METALLURGY

The University of British Columbia
Vancouver 8, Canada

Date SEPT 21, 1970.

# ABSTRACT

The deformation behaviour of polycrystalline compacts of $Mg(OH)_2$ during dehydroxylation has been studied in an attempt to evaluate the nature of strain that can be introduced into the compact during the reaction. A study of neck-growth between tips of single crystals of $Ca(OH)_2$ and between two hemispherical tips of $Mg(OH)_2$ compacts showed both deformation and interaction at the contact point during the dehydroxylation reaction. Load-dependent deformation of the compacts gave a total strain proportional to the one-third power of the applied stress. The creep deformation of $Mg(OH)_2$ compacts during dehydroxylation was also studied under isothermal conditions. The overall creep behaviour can be divided into three stages. The initial stage is initiated by the dehydroxylation reaction. During the second or steady state creep stage the highest creep rate was obtained. The steady state creep rate was determined as a function of temperature, pressure, and relative density of the green compact. The results are represented by:

$$\dot{e} = \dot{e}_o + \frac{A\sigma}{\rho} \exp\left(\frac{-17500}{RT}\right) t^{-1}$$

Particle sliding was considered to be the most probable mechanism for creep during the second stage.

# ACKNOWLEDGEMENTS

The author wishes to acknowledge the assistance and encouragement generously given by Dr. A. C. D. Chaklader and others throughout this work. Thanks are also extended to the faculty and staff of the Department of Metallurgy for their advice. Financial assistance provided by Clayburn-Harbison Co. Ltd. in the form of a Fellowship is gratefully acknowledged.

# TABLE OF CONTENTS

Publications:


1) P. W. Sunderland and A. C. D. Chaklader, Mat. Res. Bull., 2, 1111-1118 (1967).

2) P. W. Sunderland and A. C. D. Chaklader, J. Am. Ceram. Soc., 52, 410-414 (1969).

# LIST OF FIGURES

LIST OF FIGURES - continued

LIST OF FIGURES - continued

# LIST OF TABLES

# CHAPTER I

## 1. Introduction

### 1.1 Reactive Hot Pressing

Several workers have recently [1-4] shown that the hot pressing of the decomposible compounds such as $Mg(OH)_2$, etc. during the decomposition reaction results in high density products. The process utilizes a transient "reactivity" resulting from either chemical decomposition [1-4] or a polymorphic phase transformation [5] to obtain dense, high strength ceramic bodies at comparatively low temperatures and pressures, usually below 1000°C and 10,000 psi. The process has all the advantages of conventional hot pressing: low porosity and hence high strength in the product, fine grain size since recrystallization and grain growth are minimized by the comparatively low temperatures, and accurate dimensions of the product, as well as requiring lower temperatures and holding times than the conventional hot pressing process.

The process has been applied to many ceramic systems. Chaklader and McKenzie [4] pressed several natural clays as well as synthetic hydroxides of aluminum and magnesium. Unstabilized zirconia was densified[5] by cycling it through the monoclinic $\underset{860^\circ C}{\overset{1100^\circ C}{\rightleftharpoons}}$ tetragonal phase transformation, and up to 99.8% of theoretical density was obtained. Another application[6] was to the production of cermets of alumina with iron, copper and chromium. The low temperature required for the decomposition of boehemite (600°C)

resulted in a minimal formation of interfacial phases which could reduce the strength of the product.

Morgan and Schaeffer [7] have reported work on the fabrication of magnesia by a process they call "pressure calcintering", which is essentially identical to reactive hot pressing; They conducted a series of investigation of the process, analysing such effects as the nature (chemical history) of the precursor and the effect of impurity content on densification.

Chaklader and Cook [8] have also studied the hot pressing characteristics of the $Mg(OH)_2 \longrightarrow MgO$ system, as well as boehmite and two clays.

1. 1. 1 Hypotheses for Reactive Hot Pressing

In the earlier papers they [8] suggested that the formation of strong, dense compacts by reactive hot pressing might be associated with an "enhanced reactivity" during or just after a phase change, which is known as the "Hedvall Effect". [9] The precise nature of this reactivity has not been established, although Chaklader has made the following statements regarding the mechanisms of reactive hot pressing:( 4 ).

"The idea of using the high reactivity of a solid during a decomposition reaction or a polymorphic phase change (the Hedvall Effect) for densification stems from the following hypotheses and observations:

(a) Broken bonds and unsatisfied valence links exist both on the surface and in the bulk of particles undergoing a decomposition reaction; these broken bonds and links may be available for interface reaction leading to interparticle bonding.

(b) Very transient instability of the atomic position during a reaction can produce a transient plastic state which may be utilized for densification".

The first proposition is easily accepted. It is well known that bonds of strength comparable to the bulk tensile strength of the material are formed by clean metal surfaces in frictional contact in high vacuum where surface contamination is prevented. Contact areas are obtained from electrical resistance measurements. While the nature of chemical bonding in ceramics is quite unlike the metallic bond, it is easy to understand the possibility of bond formation where clean oxide surfaces are brought together intimately on an atomic scale. It is the necessity of producing suitable contact that precludes the production of frictional bonding in ceramic systems. Plastic flow is required to bring finite areas into contact, and under low temperature conditions sufficient flow is not possible. Therefore it can be seen that the formation of interparticle bonds of finite strength depends upon some mass transfer mechanism, such as plastic flow or diffusion. It is to be expected that the large evolution of water vapour (or some other gas) would have a purging effect, reducing possible surface contaminants to such a low level that bonding can take place freely between contacting

asperities.

The second propostion, concerning a transient transformation plasticity*, is more important. To see exactly how plastic flow enters the densification process it is useful to consider the possible means of densification of a powder compact subjected to pressure at an elevated temperature (hot pressing).

1. 1. 2 Theories of Hot Pressing

The behaviour of a compact through a history of die filling in a gravitational field, vibratory compaction, applied pressure, densification up to the point of closed pore formation, and finally mechanisms of pore elimination can be followed. The factors which control the compaction of a powder to a dense body are manifold: particle size, particle size distribution, particle shape, the mechanical properties of the material - i. e. its susceptibility to fracture or flow, or its work hardening rate if plastic flow occurs, the anisotropy of mechanical properties, the melting point, surface energy and finally the rates of self diffusion and of grain growth. Some of these properties are obviously interrelated.

* Transformation plasticity is taken to denote an anomalous propensity for plastic flow, manifested by low flow stress and usually by large "ductility", accompanying a solid-solid phase transformation or decomposition reaction.

When a powder is placed in some container (say a die) the density obtained will be quite low since irregularly shaped particles may form bridges, or powder with a range of particle sizes may segregate, giving rise to less efficient packing than if the sizes were thoroughly mixed. (This segregation will not be altered by subsequent operations and therefore will not be considered further). If subjected to either vibration or pressure, particle rearrangement will occur, filling large voids. Vibration will quickly produce a packing density characteristic of the particle shape and size distribution. Application of pressure will cause densification by fracture and flow of the particles, depending on the strength and ductility of the particles. Only a very soft material can densify completely by the flow mechanism, and no useful ceramic material can by fabricated to high density by flow alone on a commercial basis. The constraint offered by surrounding particles probably prevents densification beyond the point at which a line contact between three or more particles is formed. From this point mass transport by bulk diffusion, surface (i.e. grain boundary) diffusion, or by evaporation - condensation is probably a more important factor than plastic behaviour, in most cases Nabarro-Herring (diffusional) creep may be operative, although this mechanism is not considered a likely one[10]. The elimination of trapped gas from pores may be a problem since the pressure will eventually counteract the available driving force (reduction of surface

energy plus applied pressure) unless the gas is soluble and therefore can diffuse through the structure. The densification of MgO by pressure calcintering of $Mg(OH)_2$ has been shown to occur in two stages. Approximately half the observed densification occurs simultaneously with the dehydroxylation of the brucite. The remainder of the densification takes place from about 550°C until the final density is reached, usually at about 850° to 900°C. Similar behaviour has been observed by Chaklader and Cook[8]. This is shown in Figure 1. Morgan and Schaeffer [7] have suggested that the first stage of densification is a result of a slip mechanism based on their observation of the formation of a (111) texture in magnesia resulting from the first stage. This departs from the theory earlier propounded by Morgan and Scala[2] who suggested that crumbling of the precursor brucite flakes into tiny periclase (MgO) cubelets was responsible for the initial densification.

The second stage is probably due to diffusional transport or grain growth processes. This is confirmed by the fact that no additional textural development has been observed during stage II. The previously determined properties of the experimental system are summarized in section 1.4.

## 1.2 Objectives of this Investigation

The purpose of this investigation is to study the flow characteristics of powder compacts of $Mg(OH)_2$ during the dehydroxylation reaction and thus to provide evidence of transformation

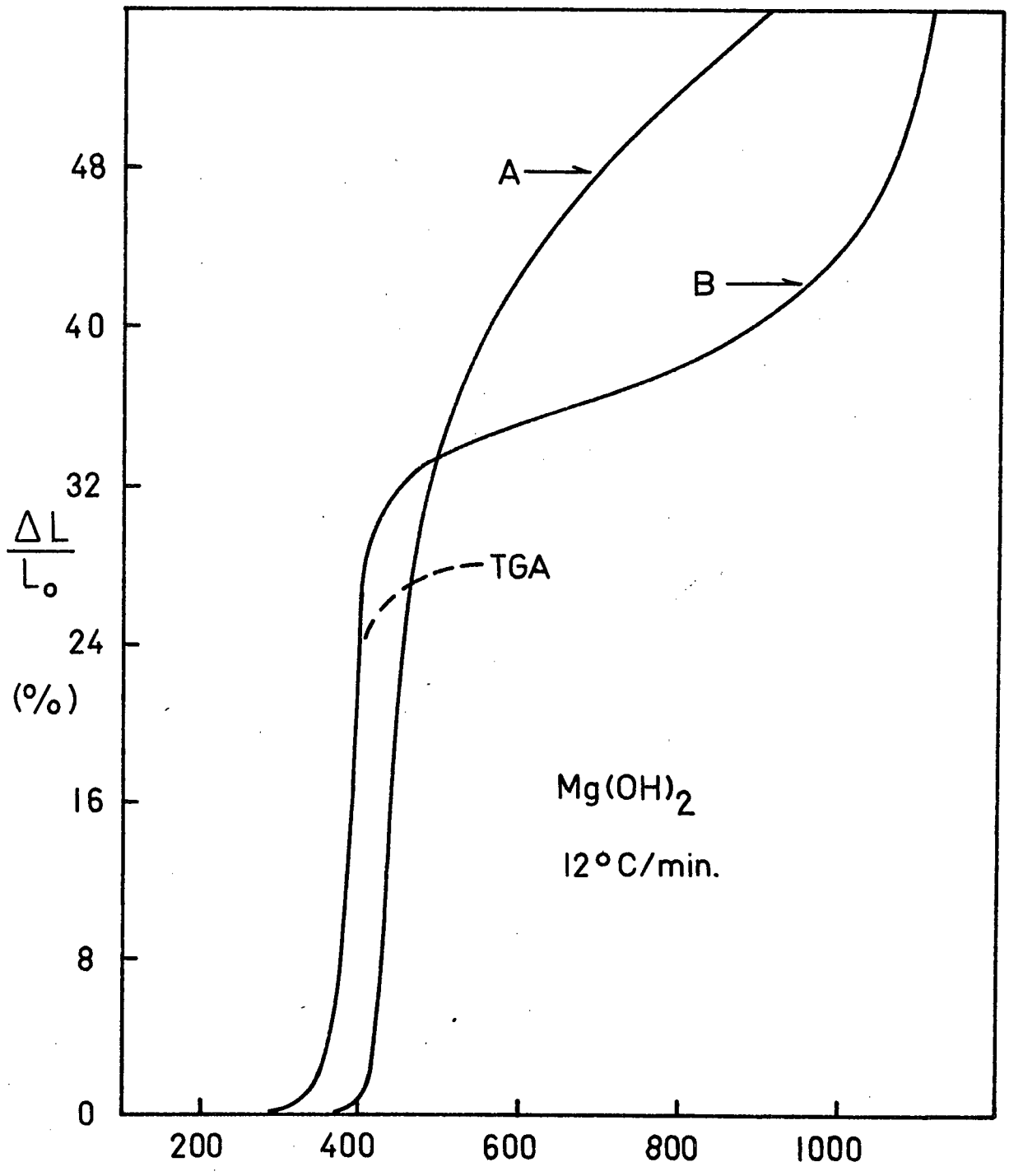


FIGURE 1 Compaction of $Mg(OH)_2$ as a function of temperature. (After Chaklader and Cook, B (8) and Morgan and Scala, A (2)).

plasticity. If a flow process is operating during the dehydroxylation, its presence should aid in understanding the enhanced densification observed during the reactive hot pressing of a decomposible compound.

An attempt has also been made to explore the possibility of bond formation across the interface between two single crystals while decomposing under load.

1.3 Choice of Experimental System

When this study was first being considered it was felt that some material available as natural or easily grown single crystals would make a suitable precursor. Calcite is an obvious choice, as very large and quite pure single crystals are commercially available. Unfortunately, however, the decomposition of calcite does not give a coherent CaO layer on the calcite surface, as has been demonstrated by several workers.[11] Thus, as expected, early experiments with this material were unsuccessful.

The second choice was the system $Ca(OH)_2$ (Portlandite) - CaO, as small crystals of $Ca(OH)_2$ are quite easily grown [12]. This system has the disadvantage that both the product and precursor transform readily to calcium carbonate upon exposure to moist air containing $CO_2$, i.e. the laboratory atmosphere, making handling difficult if contamination is to be avoided.

Therefore, in order to study quantitatively the nature of transformation plasticity cold compacts of synthetic magnesium

hydroxide powder were produced. These compacts were subjected to compressive creep deformation (at low stresses) during the dehydroxylation reaction, under varying conditions. Magnesium hydroxide was chosen for these experiments as it has several advantages over other possible choices: the structural relationship between precursor and product is simple, the crystal structures themselves are simple,and the reaction kinetics and morphology are quite well understood. The materials are also relatively easy to handle (although magnesia with high surface area rehydrates in moist air) and finally magnesia is a useful refractory. The relevant properties of this system are considered in the next section.

## 1.4 Properties of the Experimental System

The behaviour of the $Mg(OH)_2$ - MgO system has been the subject of considerable investigation, mainly because of the influence of the conditions of decomposition on the subsequent hot pressing or sintering behaviour of the product phase. "Active" MgO is produced by the calcination of $Mg(OH)_2$ at low temperatures, which produces high specific surface areas, as will be seen later.

### 1.4.1 Physical and Chemical Properties

Table I summarizes some important properties of the precursor-product pair. The decomposition $Mg(OH)_2 \longrightarrow MgO + H_2O$ occurs at temperatures in excess of 300°C, and is essentially complete (except for the removal of absorbed water) at about 400° C.

TABLE I

PROPERTIES of $Mg(OH)_2$ and MgO

| | Brucite $Mg(OH)_2$ | Periclase MgO |
|---|---|---|
| Formula Weight | 58.34 | 40.32 |
| Ratio | 1 : 0.691<br>1.449 : 1 | |
| Specific Gravity | 2.385 | 3.58 [20] |
| Structure | Hexagonal | Cubic |
| Type | $CdI_2$ | NaCl |
| Lattice Parameters | $a_o$ = 3.147Å<br>$c_o$ = 4.769Å | $a_o$ = 4.213Å [21] |
| Bond Lengths | O - O 3.13, 2.98Å<br>Mg - 6 O 2.16Å | O - O 2.98Å [22]<br>Mg - 6 O 2.10Å |

$\Delta H_R$ +19 Kcal/mol at 600° K

Decomposition of single crystals has shown [13-15] that a pseudomorphous product is obtained, with only a few percent shrinkage from the original dimensions. The product crystal is only 47 volume percent MgO, and is composed of an aggregate of very small (about 100 Å, [15]) crystallites having a definite crystallographic relationship to the brucite.

1.4.2 Structural Aspects of the Decomposition

Brucite ($Mg(OH)_2$) has a $CdI_2$ type structure, with the hydroxyl ions arranged in hexagonal (close packed layers) in hcp stacking sequence. The $Mg^{++}$ ions are in octahedral sites between every second pair of OH layers. The arrangement is shown schematically in Figure 2. This stacking of OH layers results in a pronounced basal cleavage and in the characteristic "platy" shape of the hydroxide (Figure 9 ).

Periclase (MgO) has a NaCl type (cubic) structure , (Figure 2), consisting of oxygen ions in close packed layers, forming the (111) planes, with Mg in all the octahedral sites.

A number of investigators [13-15] have considered the structural relationships involved in the dehydroxylation reaction. The most recent and authoritative work is that of Gordon and Kingery [15], which consists of electron and optical microscopy, and a kinetic study. The mechanisms proposed by various authors are summarized in Table II, which includes both morphological and kinetic aspects.

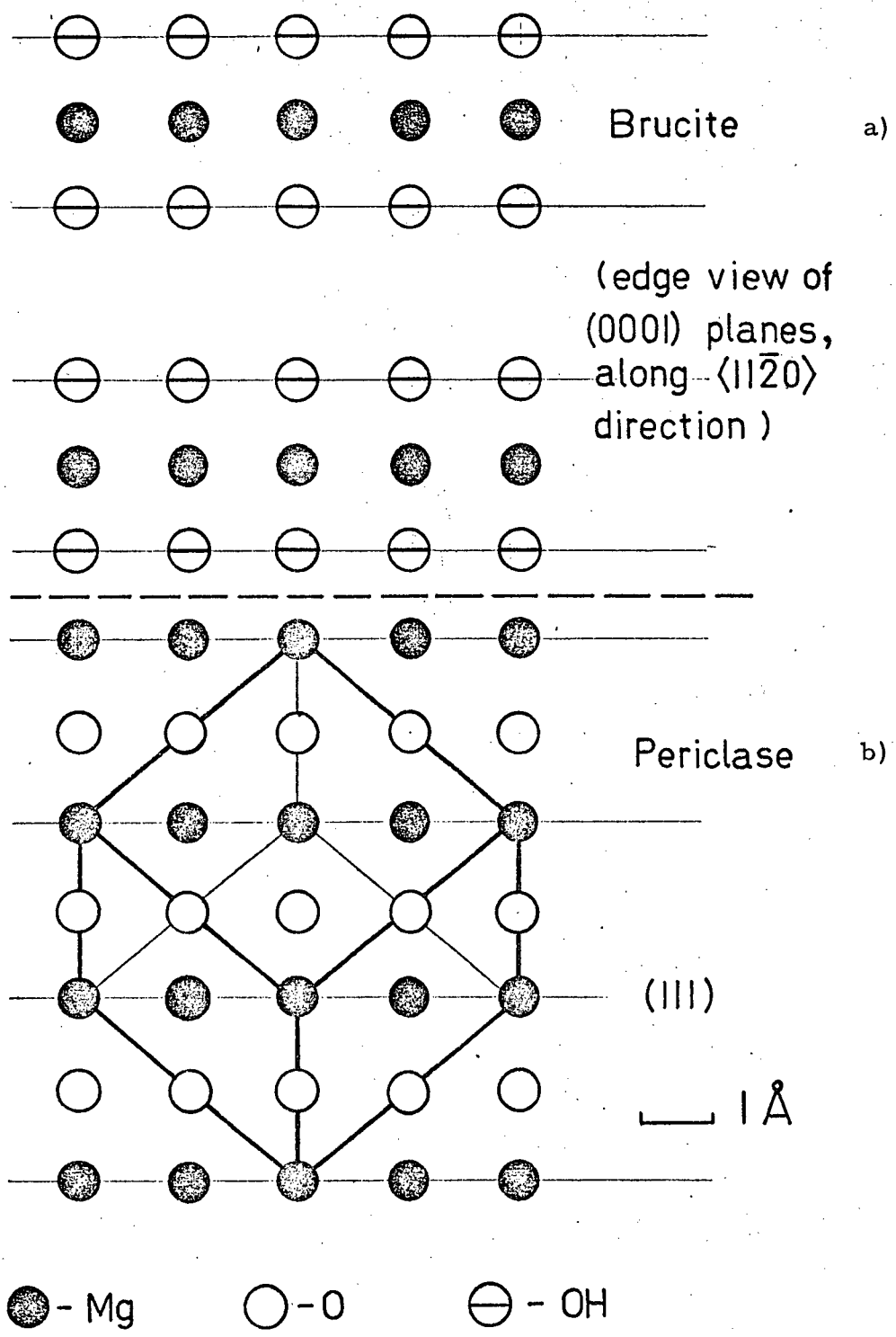


FIGURE 2 a) Structure of $Mg(OH)_2$ - Schematic representation
b) Structure of MgO - Schematic representation

TABLE II SUMMARY OF MECHANISMS AND KINETICS OF $Mg(OH)_2$ DEHYDROXYLATION

| Authors | Mechanism or Model | Type of Kinetics | Activation Energy, kcal/mol |
|---|---|---|---|
| Kingery and Gordon[15] | 1) Nucleation and growth process, with coherentnucleation, resultant large strains and fissuring. 2) A small amount of decomposition causes large changes in the physical state of the crystal, having a considerable effect on the subsequent process and product. The model explains: a) the structural relationship. b)the product crystallite size. c) the cracking process, and d) the d-spacing range. | First order for small particles, thick single crystals more complex. | 38 - 43 |
| Anderson and Horlock[14] | An interface reaction, described in terms of a contracting disc along the basal plane. | | 19 - 27 |
| Gregg and Razouk | Described weight loss data satisfactorily in terms of the contracting sphere model. | | 12 - 27 |
| Zhabrova and Gordeeva[18] | Showed that their data could be described equally well by the contracting sphere or unimolecular decay law. | | |

The list is not exhaustive, but includes the most recent and significant work in this field.

Various decomposition studies performed in the electron microscope have shown the crystallographic relationship developed between the periclase and the parent brucite [13-15]. One set of the (111) planes of the periclase are normal to the c-axis of the brucite. In addition, the ⟨110⟩ direction of the periclase is parallel to the ⟨110⟩ direction of the parent brucite.

Gordon and Kingery concluded that the decomposition of brucite is most likely a nucleation and growth process in which coherent nucleation of MgO results in large coherency strains and cracking, in the very early stages of weight loss as shown in Figure 3 . This cracking is a major change in the physical state of the crystal, and has a pronounced effect on the subsequent process and products. This model explains: a) the observed structural relationship, b) the small crystallite size of the product, c) the observed cracking process, and d) the observation of a range of d-spacings during the decomposition process.

Anderson and Horlock[4] found that the reaction proceeded from the edges of the brucite platelets (for large single crystals approximately 1 by 3 mm), producing a "polycrystallization" subsequently attributed to the coherency strain by Gordon and Kingery. The former authors found that the major part of the decomposition

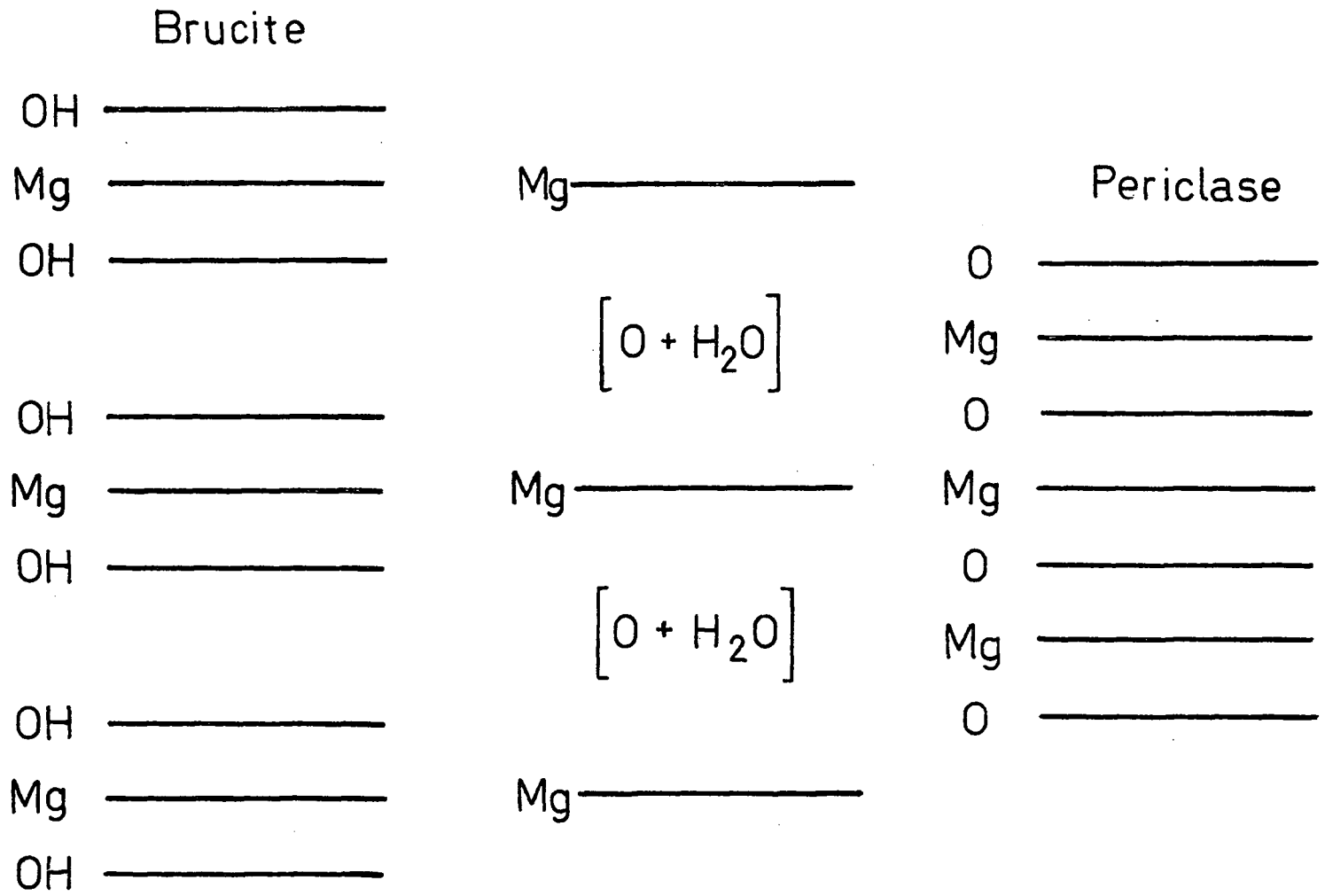


FIGURE 3 Goodman's [13] proposed mechanism for the dehydroxylation, showing collapse normal to the closed-packed oxygen planes in the formation of periclase.

originated at the "edge" of the platelets, an observation contradicted by Gordon and Kingery.

Goodman [13] was the first worker to use an electron microscope to study this decomposition, but he did not observe the initial cracking reported by the others. He was the first to recognize that the $O^{=}$ layers remained substantially undisturbed during the decomposition. This required diffusion of water (or its ionic components) between the $O^{=}$ layers, as schematically represented in Figure 3. Goodman proposed an atomistic mechanism that was essentially homogeneous. In this mechanism, he considered that $H_2O$ was uniformly removed from all parts of the decomposing crystal (though not necessarily at the same time) by a two stage process. Water would first be formed by reaction between hydroxyl ions, causing the first observed shift in lattice parameter, and then eventually escape between the oxygen layers of the partially decomposed crystal, as shown in the Figure.

Although Gordon and Kingery did not make specific comment on the mass transport necessary for decomposition, Ball and Taylor [16] point out that the movement of the product water would be extremely likely to cause disruption of the material. They felt that the observed behaviour was described better by the concept of an inhomogenous solid state reaction, operating as follows:

The decomposing crystal would develop donor and acceptor regions (Figure 4) between which diffusion of $Mg^{++}$ ( ionic

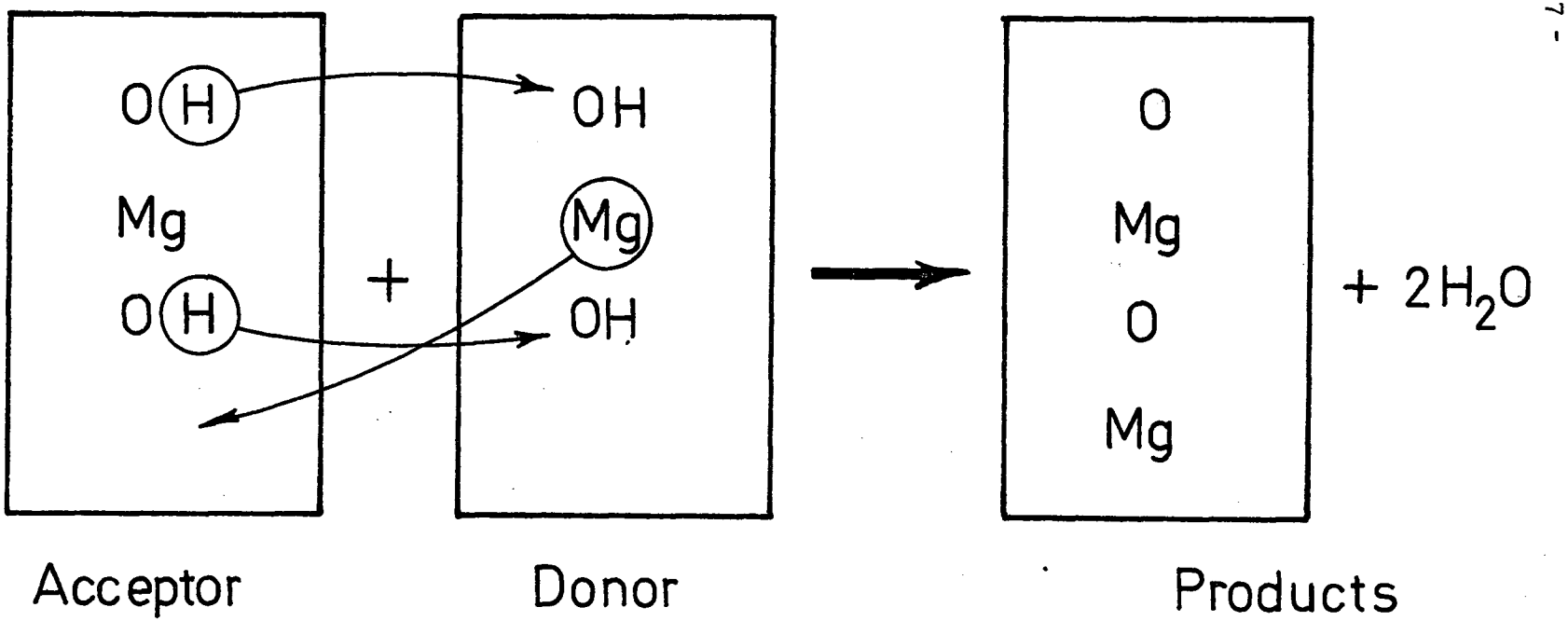


FIGURE 4 Ball and Taylor's proposed inhomogenous mechanism for the dehydroxylation, showing donor and acceptor regions, and the diffusion of Mg++ and H+.

radius = 0.78Å, compared to about 1.75 for water) and $H^+$ would occur as shown. The donor regions (probably adjacent to free surfaces or cracks) would eventually be completely destroyed. The close packed $OH^=$ layers of the acceptor regions would become close packed $O^=$ layers, with the addition of sufficient $Mg^{++}$ to form MgO.

1.4.3 Kinetics of Decomposition

The decomposition kinetics have been extensively investigated but no general agreement as to an exact mechanism has been made. Failure to obtain agreement has been attributed to variations in the material, experimental conditions, and in the size of the sample used (15).

Gregg and Razouk (17) interpreted their data by means of a contracting sphere model:

$$(1 - \alpha)^{1/3} = 1 - \frac{(k_2 t)}{R}$$

obtaining activation energies of 12 to 27 kcal/mole for $Mg(OH)_2$ powders, and 27.6 kcal/mole for brucite.

Anderson and Horlock (14) used a contracting disc model:

$$(1 - \alpha)^{1/2} = 1 - \frac{(k_2 t)}{R}$$

and obtained activation energies of 27.6 kcal/mole for powder, and 23.6 kcal/mole for two types of brucite.

Zhabrova and Gordeeva [18] had earlier shown that no single model could unequivocably be used: They fitted their data successfully to a contracting sphere relationship and to a unimolecular (first order) decay law of the form

$$\ln (1-\alpha) = k_1 t + \text{constant}$$

in which $k_1$ is a nucleation rate constant and $\alpha$ is the fractional weight loss.

Gordon and Kingery [15] concluded that their data could best be interpreted using the unimolecular model, because of the complete disruption of the starting material early in the decomposition. Large crystals probably show mixed control as the fragmentation may be incomplete, making both contracting disc and the first order mechanism operative. They also concluded that the effect of water vapour back pressure was considerable causing discernable variation of rate with sample size, and from worker to worker with various conditions. Horlock, Morgan and Anderson [19] studied the effect of water vapour on the decomposition, showing that the rate of weight loss is much higher in vacuum than in water vapour atmosphere.

# CHAPTER II

## 2. Experimental

### 2.1 Apparatus

The apparatus, shown in a schematic view in Figure 5, was constructed to permit the decomposition of various systems in a controlled atmosphere, since it was felt that gaseous atmospheres could produce considerable effects during and following decomposition. The design was intended to have fairly general applicability in the area of neck growth, sintering model studies, and for that reason incorporated some features not absolutely essential to the work forming the present study.

#### 2.1.1 Furnace and Load Frame

The specimens themselves were mounted in a loading frame (Figure 6) which was removeable from the furnace for specimen mounting. The load frame was fabricated from Inconel X-750. The pushrod slid in boron nitride bushings, gave fairly low values of coefficient of static friction (about 0.05 when clean), permitting the use of small loads for studies with single crystals. The various "grips" slid onto the pushrod and anvil, permitting ready change from one type of specimen to another.

When in position in the furnace the load frame was enclosed by a resistant element consisting of 10 turns of No. 6 A. W. G. Chromel wire, operating at 10 volts. The furnace had a power rating of one

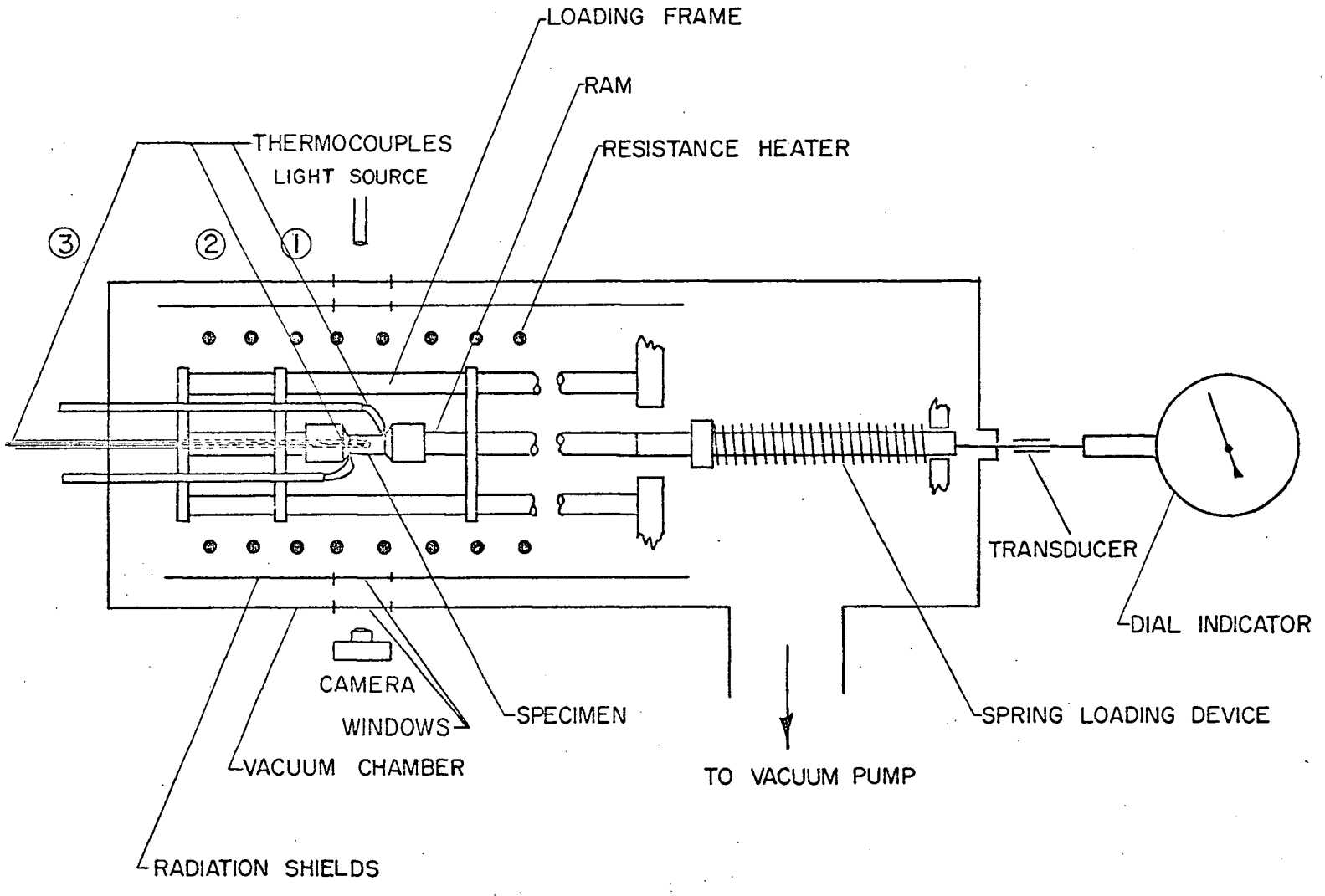


FIGURE 5 Schematic representation of the experimental apparatus.

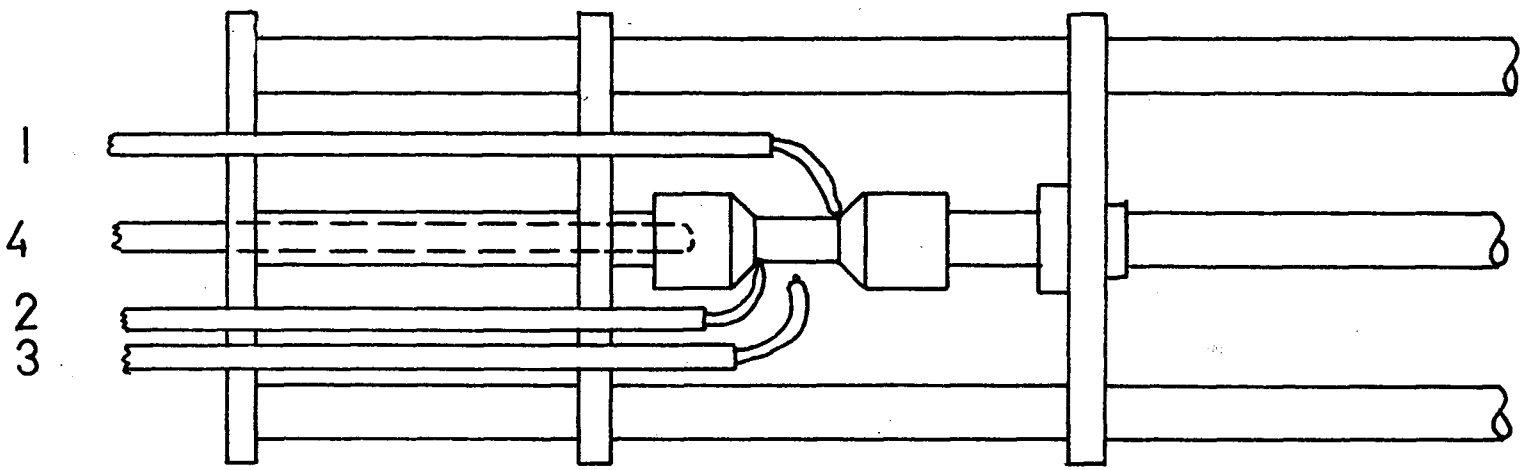


FIGURE 6 The loading frame, showing the thermocouples.

kilowatt with this winding. The heater was insulated from the water jacketted vacuum chamber by concentric silica tubes separated by corrugated stainless steel radiation shields, which provided reasonably efficient insulation with minimum surface area, permitting easy pump-down to high vacuums.

2. 1. 2 Vacuum System

The furnace chamber was fitted with two 2 inch diameter Pyrex windows, permitting viewing of the specimen when in position in the furnace. The sight path was through 3/4 inch holes in the furnace insulation and between turns of the heating coil.

The pumping system consisted of a 2 inch Edwards EO2 oil diffusion pump with liquid nitrogen trap and butterfly isolation valve, backed by a Balzers Duo 5 mechanical pump. Coarse and fine bleed valves permitted admission of any desired gas or vapour into the chamber, and by balancing bleed rate against pumping rate any desired pressure between 1 atmosphere and $1 \times 10^{-5}$ Torr could be obtained fairly easily.

Vacuum gauging was by means of an Edwards Piranni-Penning gauge unit.

2. 1. 3 Photography

Specimens in the furnace were photographed with one of two different lens systems, depending on the magnification required. A conventional 135 mm Telephoto lens with extension tubes permitted magnification slightly in excess of 1:1, and higher magnifications were provided by Leitz Optics, having a magnification of about 4 x . The

specimens were photographed in sihouette, being backlighted by a microscope illuminator. The camera was a 35 mm single lens reflex.

2.1.4 Loading and Displacement Measurement

The pushrod of the loading frame was contacted by a spring loading device. Substitution of different springs permitted loads from 10 grams to about 3 kilograms for the present experiments. This system had an inherent load variation with displacement but for the small displacements involved it was not felt that the variation would be significant. The springs were selected to minimize this effect. A piece of hardened 0.030 diameter drill rod passing through a slightly undersized hole in a piece of 1/8 inch thick neopren e rubber provided a means of transmitting the motion outside the vacuum system. The rod was smeared with vacuum grease and provided a very low friction force which was almost exactly balanced by the ram force of the dial indicator, about 20 grams, and was only used for loads in excess of 100 grams and so did not provide a large source of error in the load.

The displacement was measured in two ways; by an inductive displacement transducer connected to a Phillips strain gauge bridge and Heathkit strip chart recorder, or directly by a Starret dial indicator (0.0001 inch per division), connected in tandem with the transducer. Use of the transducer- recorder combination was terminated after experience showed that correction for the drift of the recorder involved more difficulty than manual recording of the dial indicator readings.

2. 1. 5 Furnace Temperature Control and Power Supply

Temperature measurement was by means of Chromel-Alumel thermocouples. These were either connected directly to a compensated potentiometer controller (Honeywell Servotronik or Versatronik) or connected to a Pye Potentiometer or Heathkit recorder with an icewater ($0^{o}C$) cold junction. Most of the experimental work with magnesium hydroxide was done using three thermocouples (Figure 6) of No. 32 A. W. G. wire. For the experiments two of the thermocouples were in contact with the specimen and grip (Nos. 1 & 2) while the third was free to measure radiant temperature within the furnace. Thermocouples 1 and 2 were generally in agreement within 5 degrees Centigrade, while the third was as much as 20 and 30 degrees different, depending on the particular thermal conditions.

For some of the early experiments temperature was measured by means of a 1/8 inch O. D. Inconel sheathed thermocouple, placed inside the fixed grip. This obviously was not representative of the specimen temperature except under isothermal (steady state) conditions, but it was used for temperature control during linearly increasing temperature runs.

The power to the furnace windings was supplied by 2 KVA Powerstat which was used in conjunction with the controllers to provide optimum control at a particular temperature setting.

## 2.2 Experimental Technique

### 2.2.1 Growth of $Ca(OH)_2$ (Portlandite) Single Crystals

The $Ca(OH)_2$ single crystals used were grown by the inter-diffusion of solutions of potassium hydroxide and calcium chloride by a technique due to Dave and Chopra [12], modified slightly as follows:

A 100 ml beaker was placed inside a 600 ml beaker, Figure 7, and the two were filled with $CO_2$ - free distilled water (prepared by bubbling nitrogen through distilled water) just above the top of the 100 ml beaker. In this work the solutions were introduced through two stopped funnels through fine glass tubing extensions rather than by pipette as suggested in the reference in order to prevent turbulence and premature mixing of the solutions.

When the distilled water had been added and the funnels filled with saturated solutions of KOH and $CaCl_2$ molten paraffin wax was poured onto the distilled water to a depth of about 1/4 inch to prevent contamination by atmospheric gases. 50 ml of the KOH solution and 40 ml of $CaCl_2$ was admitted to the beakers. In two or three days crystals started to appear on the outside of the small beaker and the inside of the larger one. In four days growth was essentially complete and the wax was lifted out and the crystals carefully removed from the walls of the beaker by scraping them off with a stirring rod equipped with a rubber scraper. The crystals were rinsed with distilled water and then stored in tightly capped jars. Each run produced about 500 small crystals. Only a small number of them were suitable for

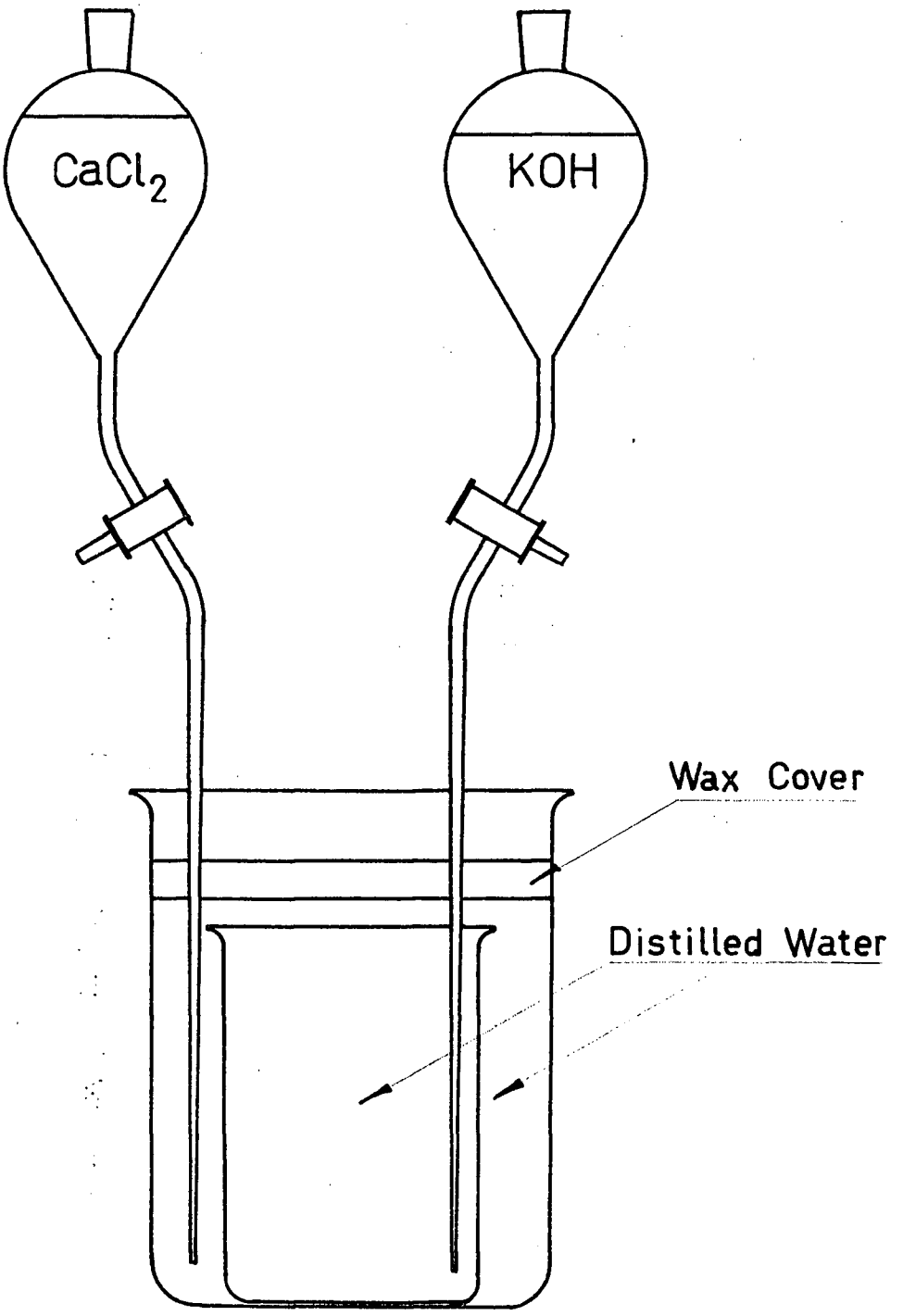


FIGURE 7 The apparatus used for growing $Ca(OH)_2$ crystals.

experiments as many were either very small, quite imperfect or broken fragments of larger crystals. The crystals had obvious hexagonal morphology and fractured very easily on the basal planes. Typical defects were pockets of trapped solution, or "pipe" extending some distance into the crystals from the root end.

The crystals were not analysed as purity was not felt to be of great importance at this stage of the investigation, but Dave and Chopra [12] quote 99.65% $Ca(OH)_2$ and 99.6% of the theoretical calcium in their crystals.

2.2.2 Experiments on Tip to Tip Contact

A. $Ca(OH)_2$ Crystals

For these experiments the camera set-up with 4 X magnification was used to view and record the behaviour of the crystals. During these early experiments the linear temperature programmer was not available so the heating rate was uncontrolled, giving a temperature - time profile similar to that shown in Figure 8.

The procedure of selection and mounting was tedious as the useful crystals were typically very small; less than 1 mm in diameter and 2 to 3 mm long. Crystals of good size and shape were selected from their storage jar, examined under a microscope (50X) to ensure suitable tip shape, then lightly etched in $10^{-4}$ N Hydrochloric acid solution; followed by rinsing in distilled water to give a fresh surface, then mounted, loaded and evacuated as quickly as possible to minimize surface transformation to $CaCO_3$.

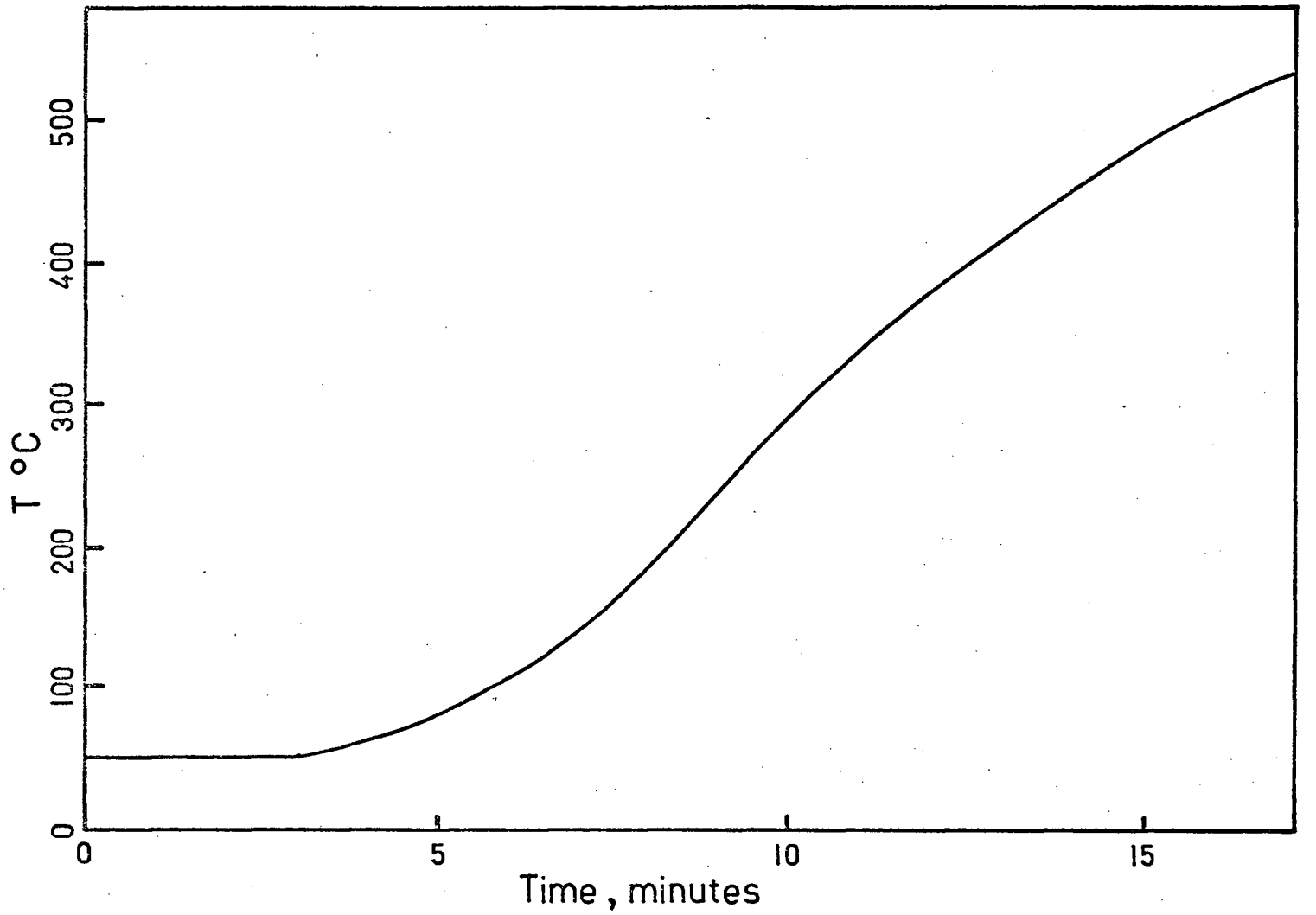


FIGURE 8 Time-temperature profile used for the decomposition of $Ca(OH)_2$ tips and for uniform heating rate experiments.

Mounting the crystals in the load frame was done with a commercial furnace cement "Sairset" as this provided a suitable mounting for the crystals inasmuch as it was quick setting, strong and yet easily removed from the grips after a run.

After the system had been evacuated to a vacuum of about 0.02 Torr, the furnace power was switched on and the run commenced. Photographs were taken before, during and after the decomposition, which could be followed easily, as the pressure in the furnace was to some extent proportioned to the decomposition rate.

2.2.3 Preparation of $Mg(OH)_2$ Compacts

B. $Mg(OH)_2$ Compacts

To study qualitatively both flow and bond formation, pairs of hemispherical tipped pellets were placed in the load frame and decomposed under various loads. Details of specimen preparation are given in the following section.

For deformation studies under compressive loading, $Mg(OH)_2$ compacts were prepared from Alcan magnesium hydroxide (Alcan Ltd., Montreal, Chemical Products Division). This material contained impurities as follows: MgO-96%-$Al_2O_3$+$Fe_2O_3$-1.5%, CaO+$SiO_2$-2.5%, (after ignition).

The particle size and shape was determined in an electron microscope by suspending a small amount of the powder in a dilute HCl solution, then placing a drop of this suspension on a grid with a carbon support film and allowing the water to evaporate. The powder is shown

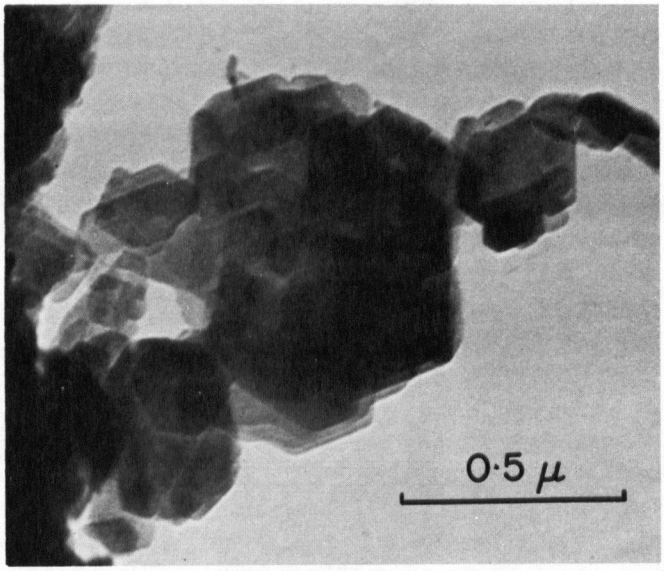


a) Before dehydroxylation

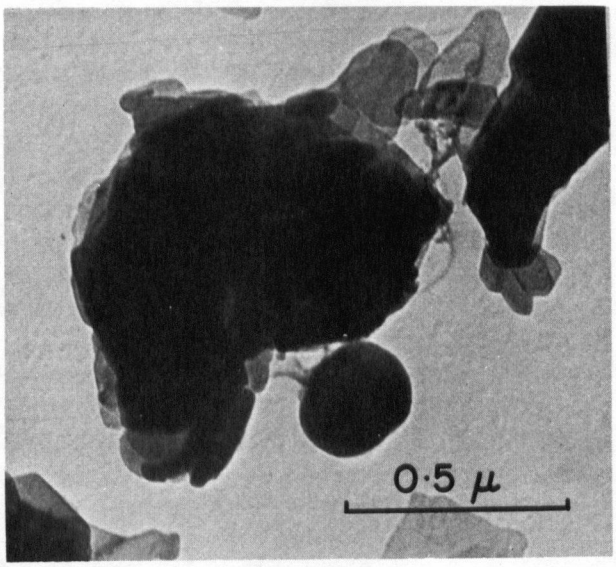


b) After dehydroxylation at 450°C

FIGURE 9 Electron micrographs of the $Mg(OH)_2$ powder.

in Figure 9. The mean particle dimension in the basal plane was estimated to be 1500 Å and the average thickness was about 250 Å. Surface area was approximately $15 m^2/gm$.

The powder was pressed into compacts in a 0.190 inch diameter die made from Atlas Keewatin steel, with plungers of drill rod. Both die and plungers were hardened and tempered, the die to $R_c 60$ and the plungers to $R_c 55$. The die was used successfully to 100,000 psi with $Mg(OH)_2$, although galling occured at much lower pressures with MgO in a similar die. The bore had a very slight taper (about 0.0005 inches/ inch), which facilitated removal of the compacts. It was felt that experiments with the tip to tip contact of decomposing bodies might demonstrate both flow and bond formation with this material and to this end a number of compacts were pressed from $Mg(OH)_2$ using a ram shaped to give a hemispherical end on the pellet, (shown later in Figure 13).

The compacts were produced using a floor model Instron Machine which was calibrated so that the chart read directly in pounds per square inch. By using the load cycle control it was possible to obtain very reproducible specimen density.

The pressing procedure was as follows:

1) The die was loaded (with pre-weighed charge).

2) The die was placed in the machine and preloaded to about 100 psi by means of the manual crosshead traverse.

3) The specimen was pressed under a constant crosshead speed of 0.05 inches/min.

4) The crosshead motion was stopped at a predetermined load.

5) The load was allowed to relax with constant crosshead position for 5 minutes.

6) The load was released at 0.05 inches/minute, and the specimen pressed out at 5 inches/minute.

The specimens were then weighed, measured for length and diameter and stored in stoppered vials until needed for experiments.

Practical considerations limited the densities available for study. It was found that below a relative density of 0.40 the specimens were too fragile to be handled easily, while above 0.70 they tended to develop circumferential cracks upon removal from the die.

The completed specimens were 0.1905 to 0.191 inches (4.839 to 4.851 mm) diameter, and approximately 0.32 inches (8.13 mm) long. Figure 10 shows the relationship between fractional density and the pressure used in compacting the specimens. The consistency of density was excellent; the range of densities observed was about $\pm$ 0.4% at 50% relative density.

2.2.4 Deformation of $Mg(OH)_2$ Cylindrical Compacts

Several different approaches were taken to the problem of characterizing the creep behaviour of the magnesium hydroxide compacts. In all cases the specimens were placed between the flat surfaces of the anvils or grips and the full load applied at room temperature.

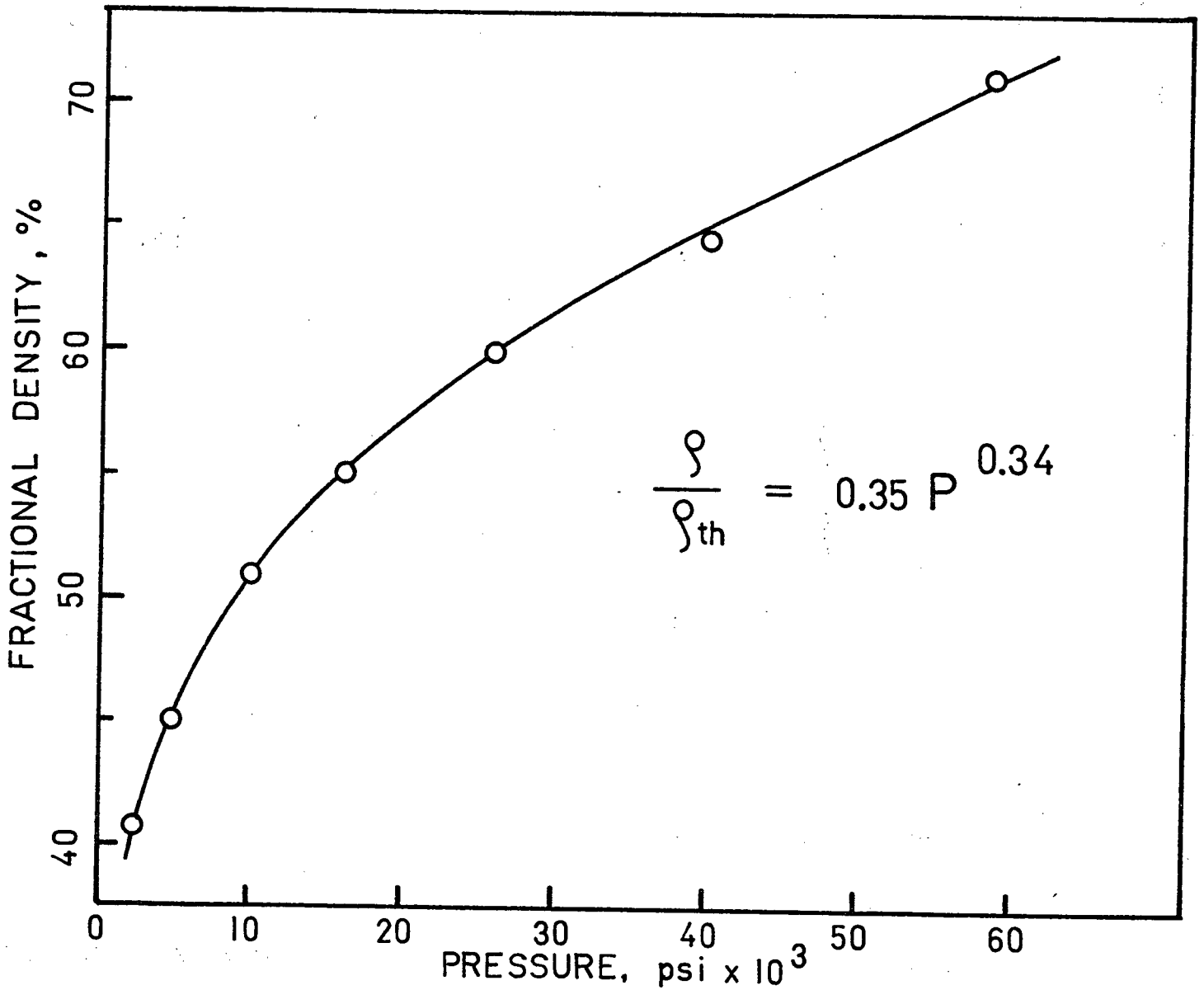


FIGURE 10 Relative density obtained in green compacts of $Mg(OH)_2$, versus pressure.

The types of experiments undertaken were as follows:

i) Quasi-uniform Heating Rate

The first series of runs were made to explore the reproducibility of the experiments, and to determine the effect of load on the creep behaviour under these conditions. The heating rate was obtained by using a fixed setting of the powerstat, giving the heating rate shown in Figure 8.

ii) "Isothermal" Runs

In order to facilitate the determination of an activation energy for the deformation, most of the experiments reported here were done under isothermal conditions. The maximum heating rate available was used to bring the specimen and load frame to the test temperature, and this was done within 10 to 12 minutes of the start of heating. The average heating rate was 40°C/minute, with an almost linear rate of 26°C/minute from 320°C to 405°C (the maximum temperature used in these experiments), as shown in a time-temperature profile, Figure 11. Temperature was recorded continuously during all experimental runs. Periodic checks of the recorder calibration was made during the runs.

Thermal expansion correction was necessitated by the rather rapid rise in temperature, which caused uneven thermal strains in the different parts of the loading frame. Two thermal expansion runs were performed for each run or pair of identical runs for given temperature and load conditions, using a dummy quartz specimen. The expansion

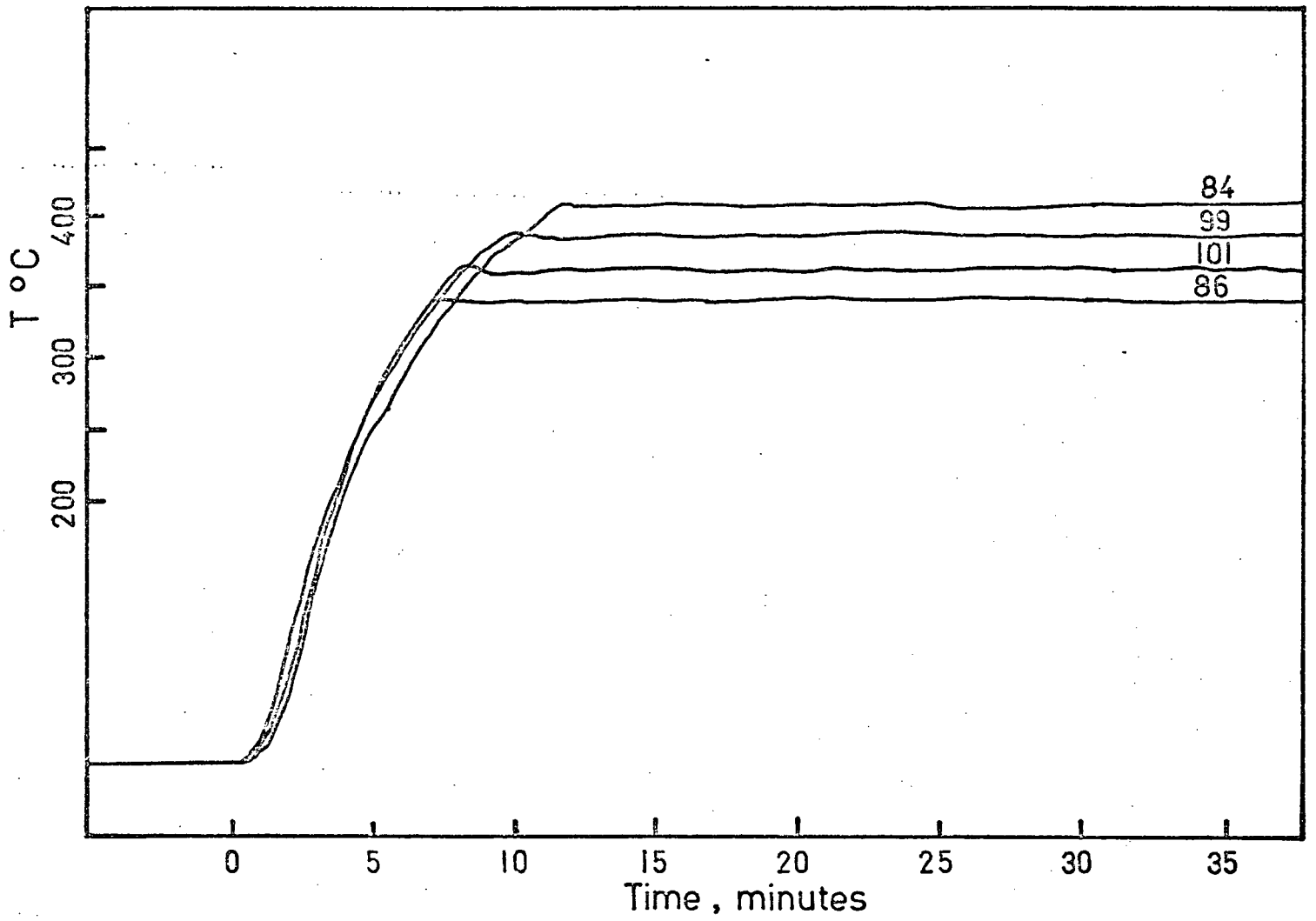


FIGURE 11 Specimen surface temperature as a function of time for the "isothermal" tests at four different temperatures.

data were subsequently used for correcting the deformation data. The thermal expansion correction was also verified using a travelling microscope (Appendix III).

The variables considered in this series of experiments were temperature, load (compressive stress) and specimen bulk density. Other factors which could conceivably be experimental variables, such as particle size, shape and chemical purity were held constant. The specimens were loaded into the load frame, then into the furnace, and the system way sealed and pumped down to about $10^{-2}$ Torr. The run was usually commenced as soon as pumpdown was complete, but extended holding periods at low pressures (as long as 46 hours) had no discernable effect on the creep curve.

Temperature measurements during this group of runs were made using the thermocouples described earlier, but several additional runs were made with a thermocouple inserted along the specimen axis to measure temperature at the centre of the specimen, as described in the following section.

2.2.5 Temperature Distribution in Specimens

The creep tests were performed "isothermally". However, since the specimen was taken to the temperature for creep study as fast as practically possible, there was a period at the beginning of each experiment during which large thermal gradients existed. There are two ways of determining the temperature distribution in the speciment

during the experiments: by theoretical consideration of thermal diffusivity, or by experimental determination of the temperature of the center and on the surface of the specimen.

A precise theoretical analysis was not possible because of the lack of data necessary for such calculations. However, a preliminary order of magnitude calculation was made using the method of Carslaw and Jaeger (22). This calculation, which indicates that an interior temperature of approximately 0.97 of the surface temperature will be reached in 8 to 10 minutes is presented in Appendix I.

The temperature distribution during the creep study was also determined experimentally. A thermocouple (No. 3) was inserted at the center of the specimen from one end, as shown by the dotted line in Figure 5. The temperature was measured continuously on the surface (using thermocouples 1 and 2) and at the centre. Experimentally determined temperature profiles for two surface temperatures, 345° and 408° C are shown in Figure 12. After a very large temperature gradient in the initial stages, a steady state, having a differential of from 10° to 12°C between the surface and the centre temperature was reached, within 10 to 12 minutes of the start of heating. Thus, for kinetic analysis, it was possible to assume the specimen to be at some "steady state" temperature characterised by the mean temperature.

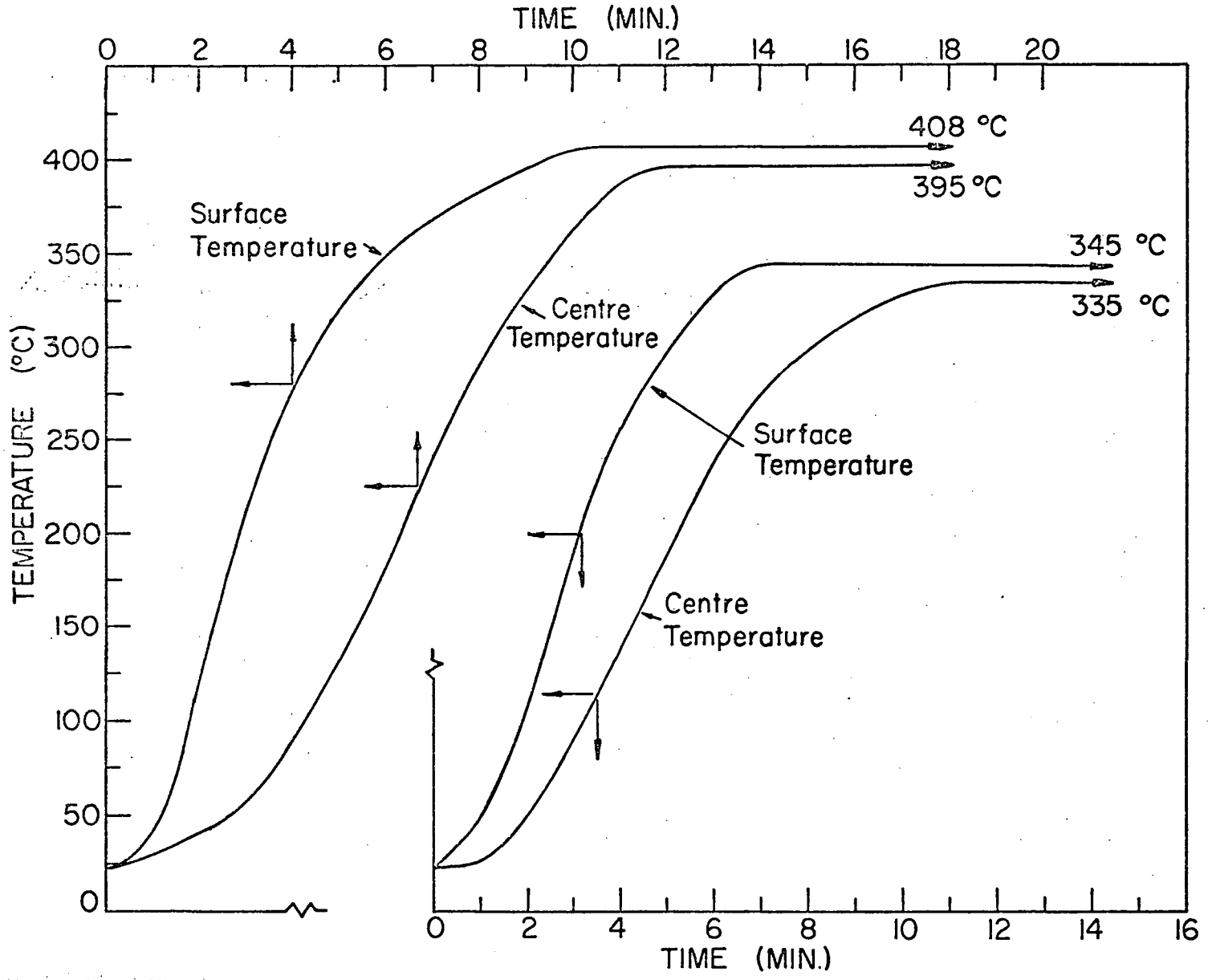


FIGURE 12 Specimen surface and centre temperatures for two different "isothermal" conditions.

# CHAPTER III

## 3 Results

### 3.1 Calcium Hydroxide Single Crystals

As discussed earlier only a very few specimens of single crystal calcium hydroxide were obtained with suitable properties for deformation study in tip to tip contact. Experiments were performed with single crystals 3 to 4 mm long, about 1 mm in diameter, and of hexagonal cross section. The specimen pair was placed under a load of 10 grams and decomposed. This load corresponds to a contact pressure of about 0.5 $kg/mm^2$, based on the final contact area.

Figure 13 shows a series of photographs of a particular pair of crystals before, during, and after decomposition. Due to the irregular geometry of the contact and the virtual impossibility of duplicating the curvature of the tips, no attempt was made to analyse the neck growth data quantitatively. However, the phenomenon of neck growth during decomposition is clearly demonstrated in this series of photographs. Microscopic examination of the contact faces of the crystals after the neck growth experiments indicated fusion had taken place. This was the first indication that deformation could take place in the presence of applied stress during the decomposition of hydroxide.

### 3.2 Tip to Tip Contact of Magnesium Hydroxide Compacts

Following a similar procedure, $Mg(OH)_2$ compacts with hemispherical tips were decomposed while loaded into contact (Figure 14). Deformation of the contact area resulted, as can be seen. Considerably

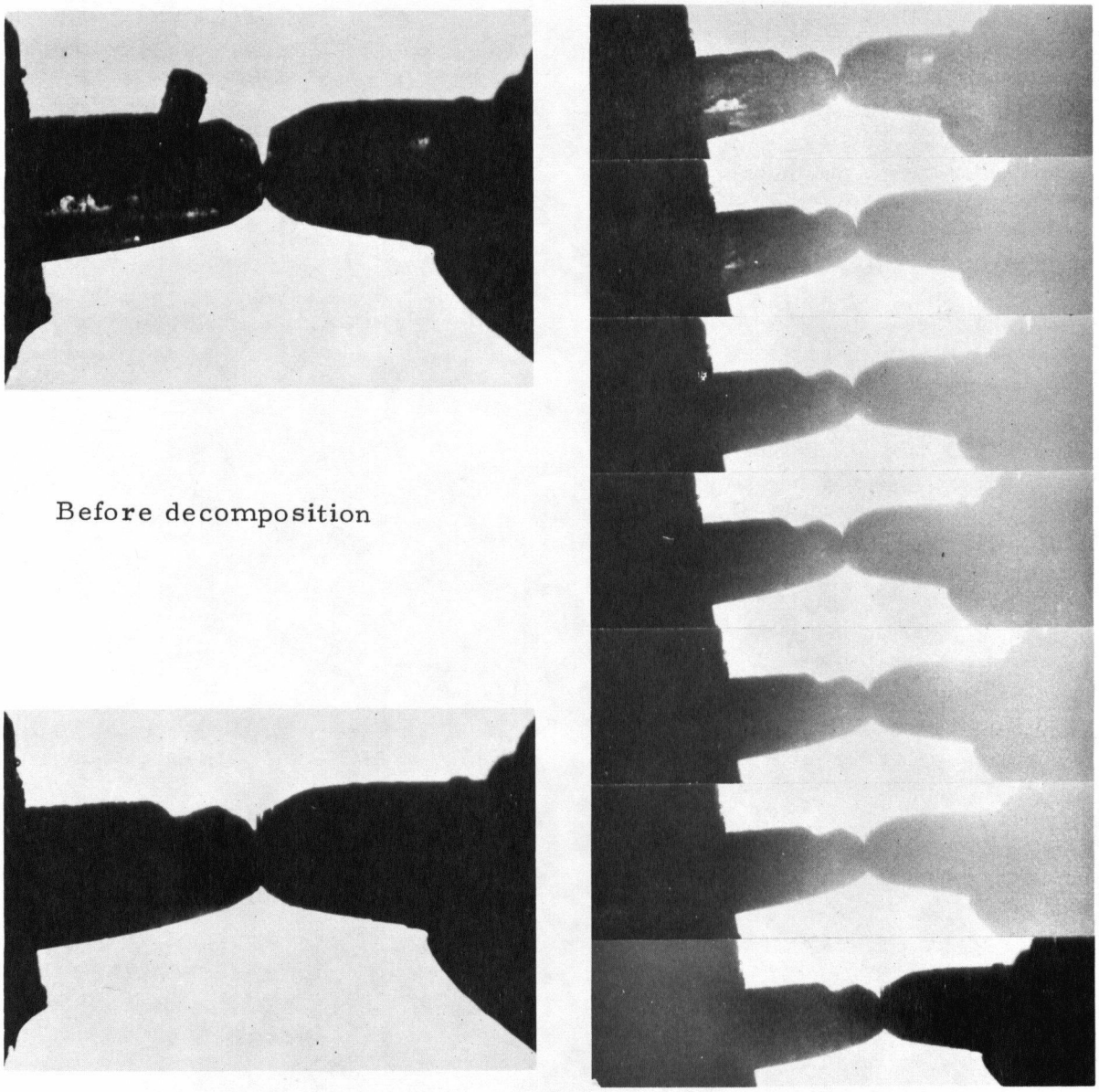

Before decomposition

After decomposition

FIGURE 13 Growth of contact area during the decomposition of $Ca(OH)_2$ tips under load.

more interesting was the explicit evidence of bond formation which is provided in the form of a small piece of one tip left on the other, when the tips were broken apart following the decomposition (Figure 15). This showed that the adhesion between the two tips was at least as great as the cohesion within them.

### 3.3 Deformation of Magnesium Hydroxide Compacts

After the initial experiment just described, attempts were made to study quantitatively the deformation behaviour of magnesium hydroxide compacts during dehydroxylation, both at a uniform heating rate and under isothermal conditions. The experiments at uniform heating rate under different loads were carried out to determine the extent of deformation obtained, and to establish limit on loads, temperature, and density which could be used in subsequent studies. These experiments also showed the relative amount of shrinkage and load-dependent deformation which were produced under these conditions.

#### 3.3.1 Uniform Heating Rate

The specimens used in this series of tests all had a nominal relative bulk density of 0.50 (Table III). A set of temperature-deformation curves for this series of runs is shown in Figure 16. The curves show a tendency to increasing maximum slope and increasing total deformation with increasing load.

The total deformation obtained during decomposition was measured from the initial and final length at the end of the decomposition,

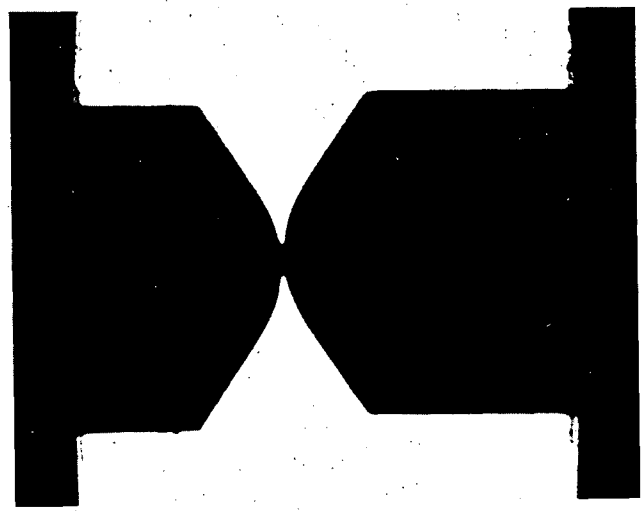

a) Before decomposition

b) After decomposition

FIGURE 14 Growth of contact area during decomposition of $Mg(OH)_2$ Compact tips under load.

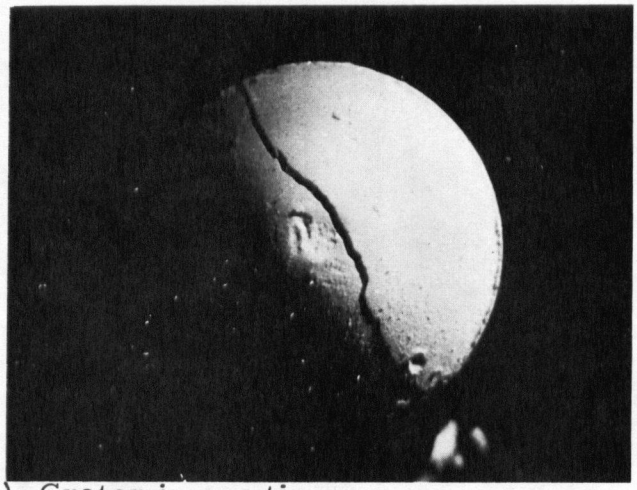

a) Crater in one tip

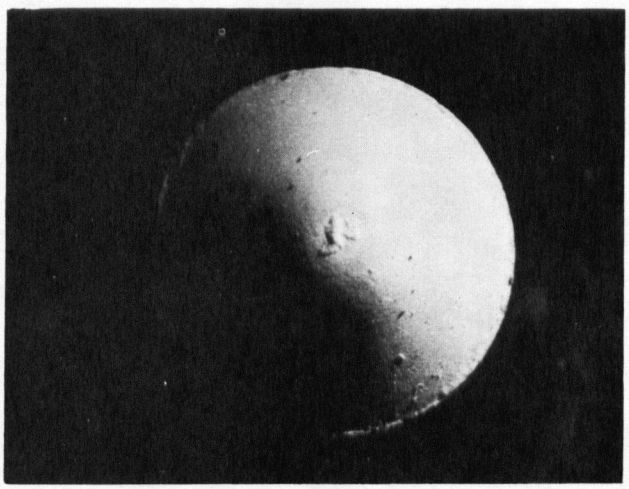

b) Material removed from the crater adhering to the other tip.

FIGURE 15 Evidence of bond formation during the decomposition of $Mg(OH)_2$ compact tips under load.

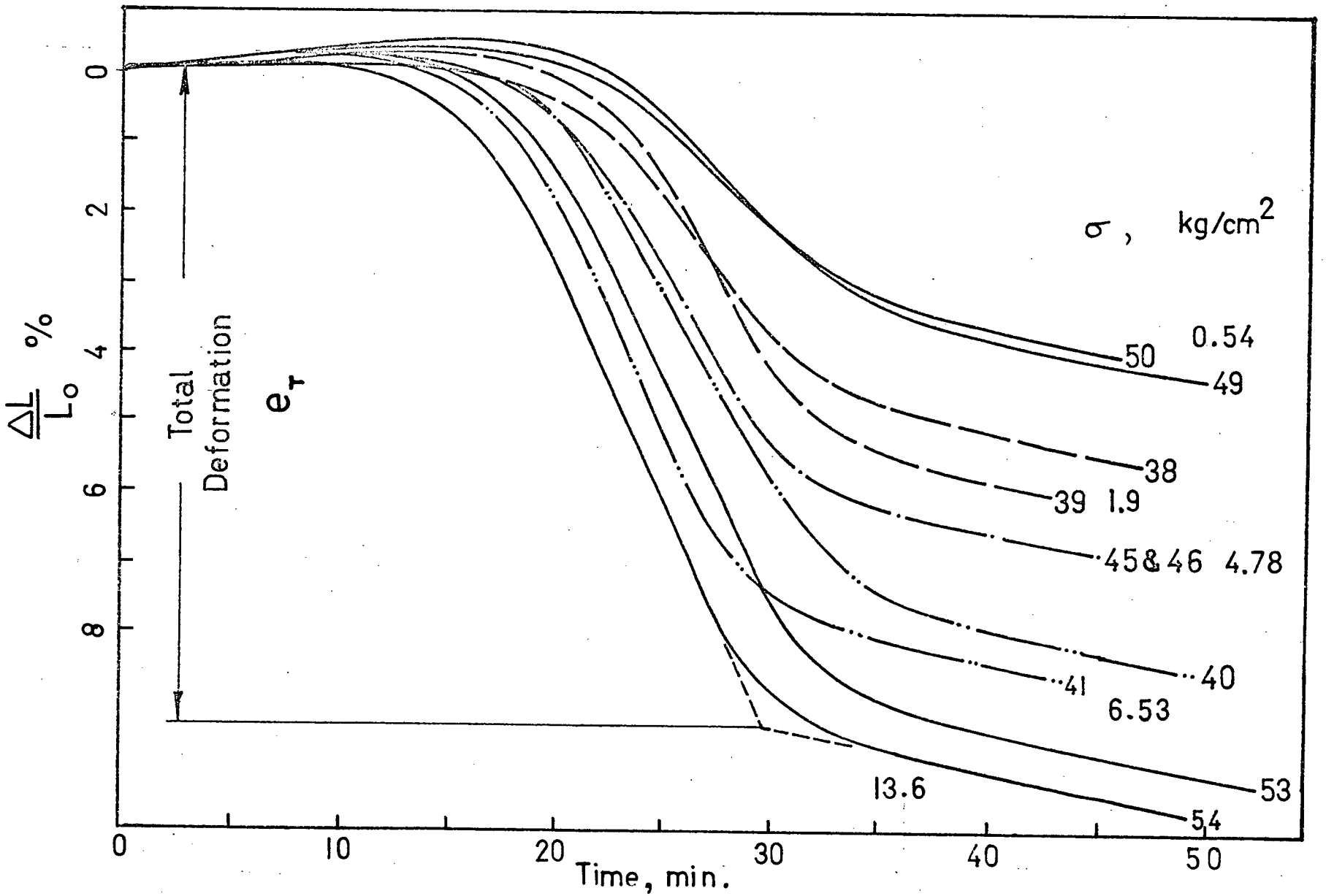


FIGURE 16 Family of Deformation - time curves for experiments under various loads at a uniform heating rate, showing the method of measuring the total deformation ($e_T$).

TABLE III

DEFORMATION DATA FOR UNIFORM HEATING RATE

| SPECIMEN | LOAD, kg | $kg/cm^2$ | $\frac{\Delta L}{L_o}$ (%) | $\rho_o$, $\frac{gm}{cm^3}$ |
|---|---|---|---|---|
| 49 | 0.10 | 0.54 | 2.62 | 1.19 |
| 50 | 0.10 | 0.54 | 2.69 | 1.20 |
| 38 | 0.35 | 1.9 | 3.56 | 1.19 |
| 39 | 0.35 | 1.9 | 4.08 | 1.19 |
| 45 | 0.66 | 3.58 | 4.78 | 1.19 |
| 46 | 0.66 | 3.56 | 4.69 | 1.20 |
| 42 | 0.88 | 4.78 | 5.15 | 1.18 |
| 43 | 0.88 | 4.78 | 5.20 | 1.19 |
| 40 | 1.2 | 6.53 | 5.65 | 1.19 |
| 41 | 1.2 | 6.53 | 5.96 | 1.18 |
| 47 | 1.63 | 8.76 | 6.22 | 1.19 |
| 48 | 1.63 | 8.76 | 6.47 | 1.19 |
| 33 | 2.06 | 11.2 | 6.72 | 1.20 |
| 34 | 2.06 | 11.2 | 6.90 | 1.20 |
| 52 | 2.5 | 13.6 | 7.26 | 1.21 |
| 53 | 2.5 | 13.6 | 6.85 | 1.20 |
| 54 | 2.5 | 13.6 | 7.10 | 1.20 |

as shown in Figure 16. This total deformation was then converted to percent total strain and is plotted against load in Figure 17. A log-log plot of this data (Figure 18) suggests a relationship of the form

$$e_T = e_{o_T} + K\sigma^n$$

where n is approximately 1/3, and the extrapolated change of length under zero load was calculated to be 0.3%.

3.3.2 "Isothermal" Deformation (Creep)

As previously discussed, the optimum relative density that could be easily achieved by cold pressing was 0.50 of the density of magnesium hydroxide. For this reason most of the experiments under isothermal conditions were carried out using compacts of 0.50 relative density. All creep curves presented have been corrected for thermal expansion of the loading frame as outlined in Section 2.2.4, (ii). The compressive load was applied to the cold specimen, and maintained throughout the test. A typical time deformation curve is shown in Figure 19, along with the specimen surface temperature and pressure in the vacuum chamber. The apparent relationship between the pressure of the water vapour produced by the decomposition (as noted from the vacuum gauge on the system) and the deformation is notable; the peak of the pressure curve coincides in time with the region of maximum slope (maximum creep rate) of the deformation curve. The significance of this result will be discussed in more detail later.

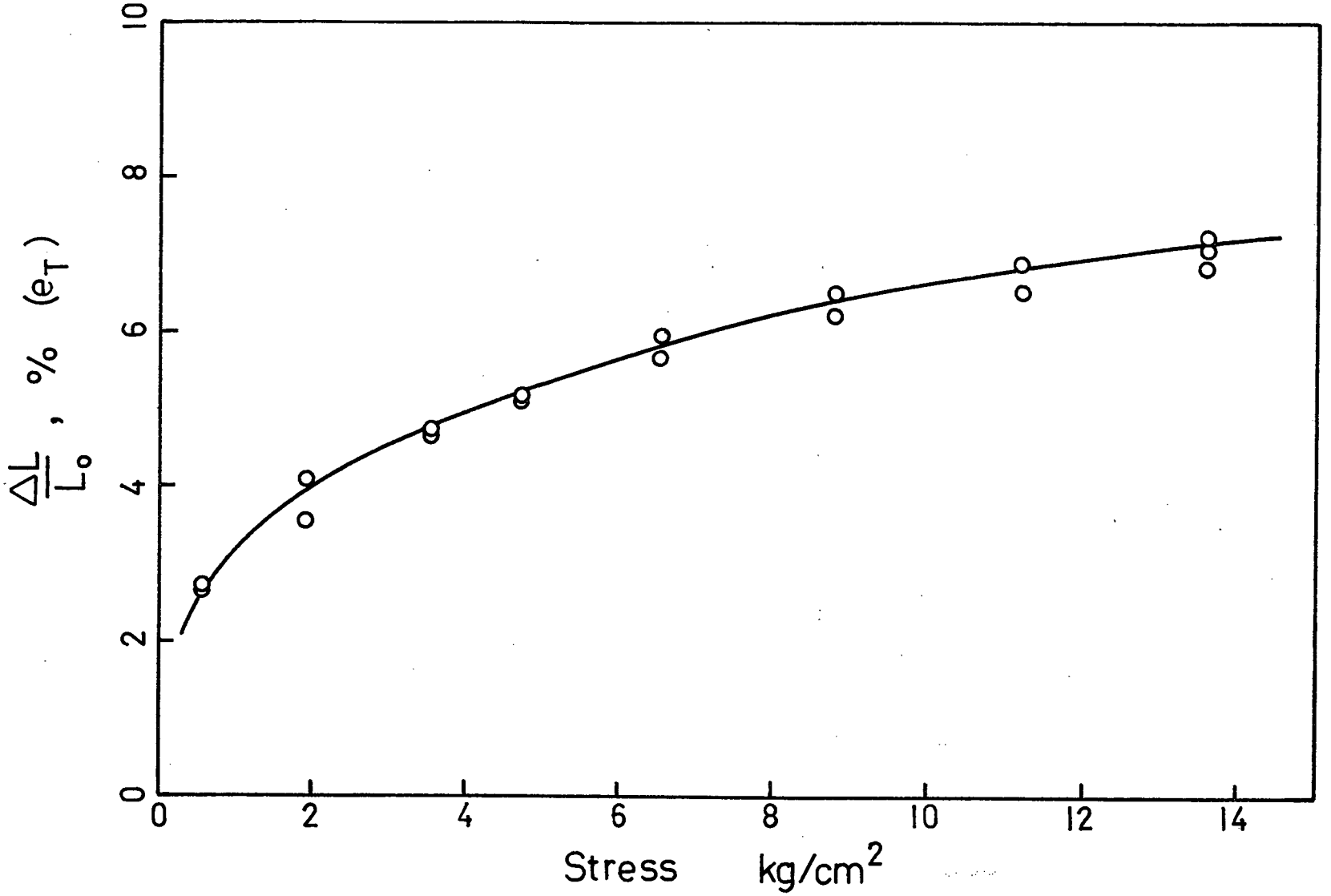


FIGURE 17 Total deformation as a function of load (uniform heating rate).

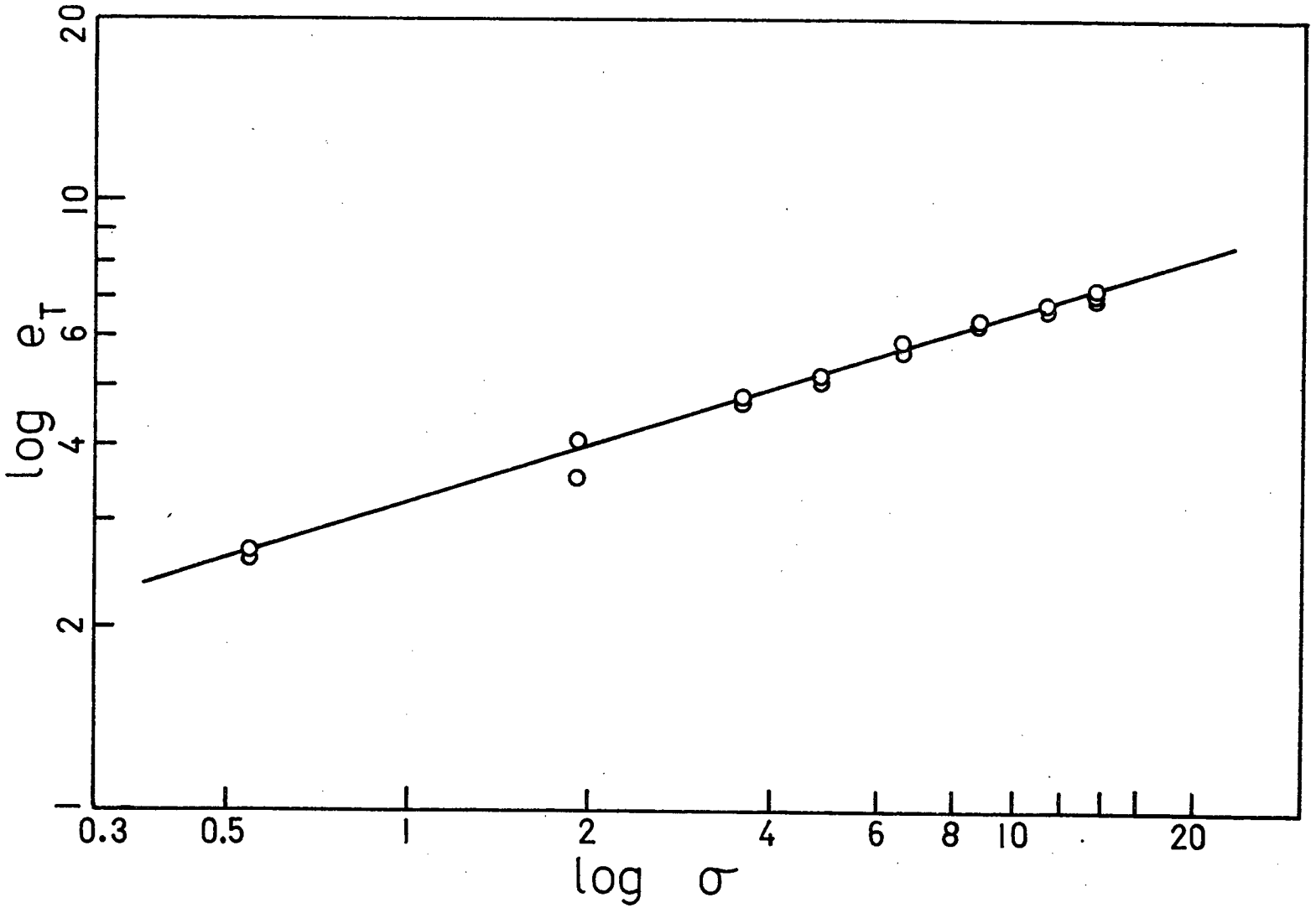


FIGURE 18 Log-Log plot of total deformation as a function of load (uniform heating rate).

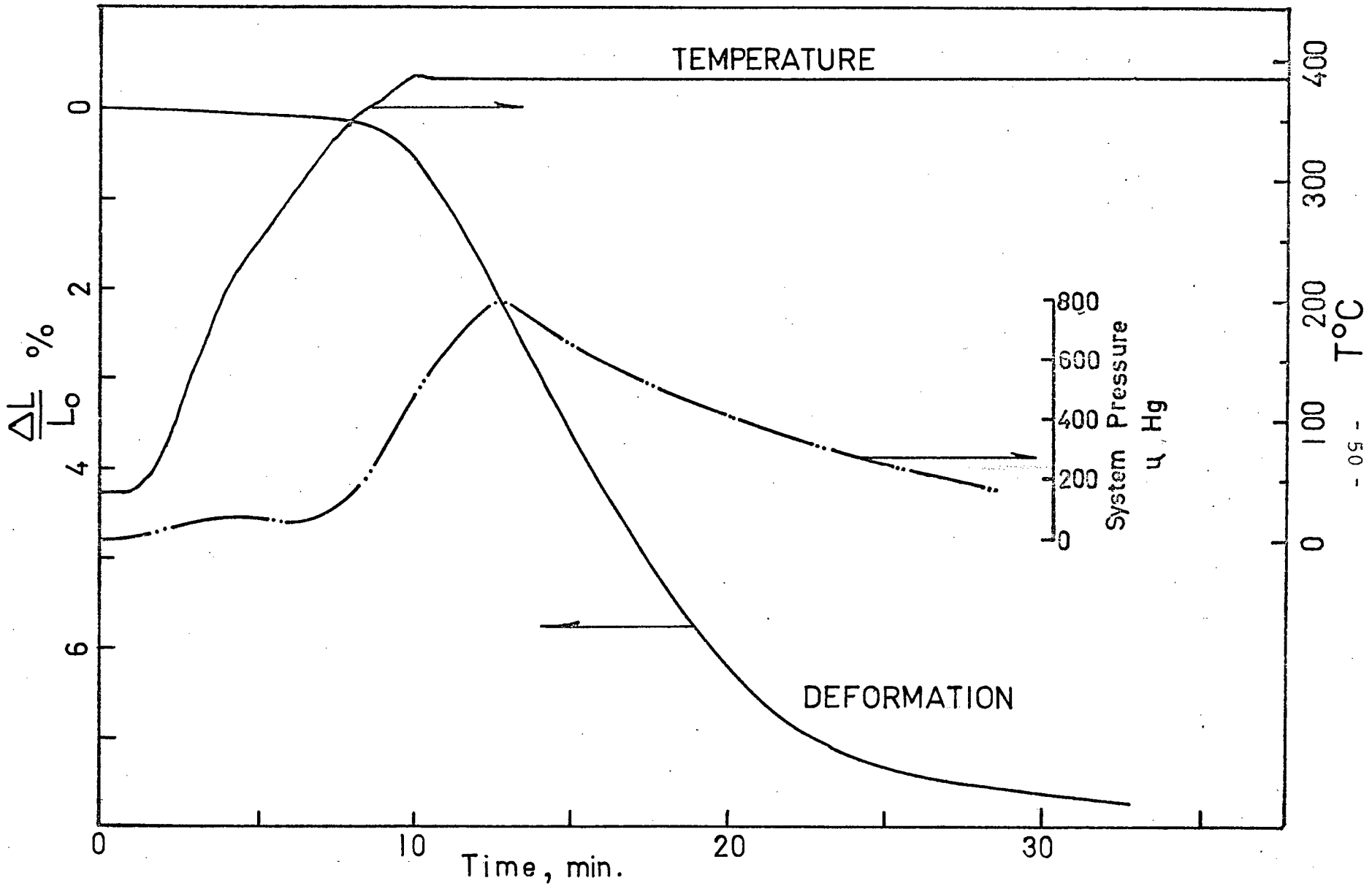


FIGURE 19 Temperature, deformation, and system pressure versus time for a typical "isothermal" run.

(a) Effects of Temperature on Deformation

The first series of runs were performed using a load 2.50 kg (13.6 kg/cm$^2$) at different temperatures in the range of 340° to 405° C. At least two runs were made for a given set of experimental conditions, to test reproducibility. Four pairs of representative time-deformation curves are shown in Figure 20, and time-temperature deformation data are tabulated in Appendix II (a).

The second series of runs were performed with a load of 1.1 kg, (6.0 kg/cm$^2$), and the same temperature was used in the previous series. Four pairs of curves for this series are shown in Figure 21, and data are presented in Appendix II (b).

(b) Effect of Stress at Constant Temperature

Following the same procedure outlined above, isothermal creep tests were performed to determine the effect of load on deformation, using specimens of 0.50 relative density. A temperature of 360°C was chosen for this study as it allowed a maximum range of loads to be used without fracture of the compact. Five stresses between 0.55 and 13.6 kg/cm$^2$ were used for these experiments. The results are plotted in Figure 22 and recorded in tabular form in Appendix II (c).

(c) Effect of Green Density

Previous creep studies of porous ceramic bodies have shown that the creep rate varies with the relative density of the compact[24]. In order to determine the effect of the green density of

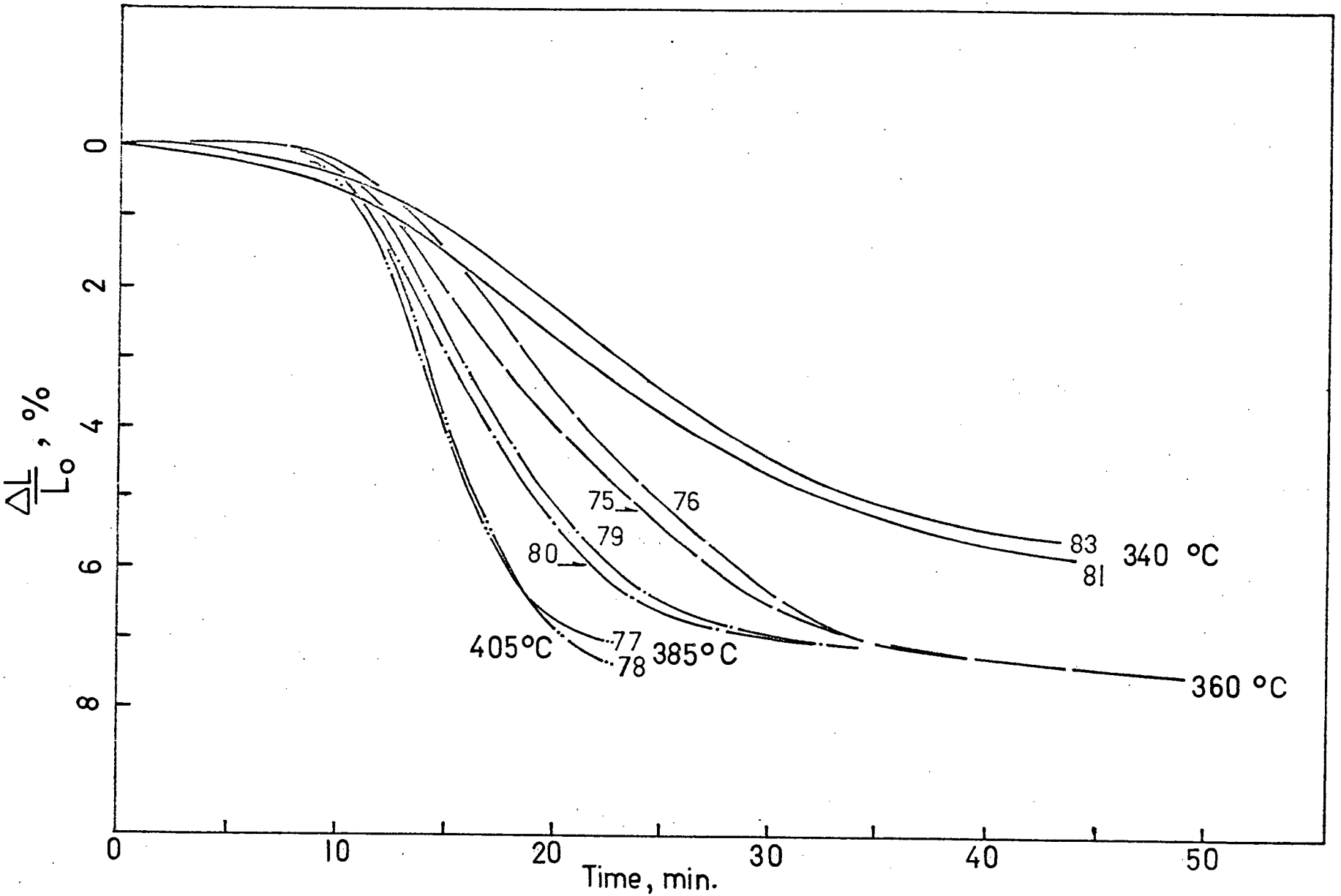


FIGURE 20 Deformation versus time for specimens of 0.50 relative density, at "isothermal" temperatures as shown. Stress 6.0 kg/cm$^2$.

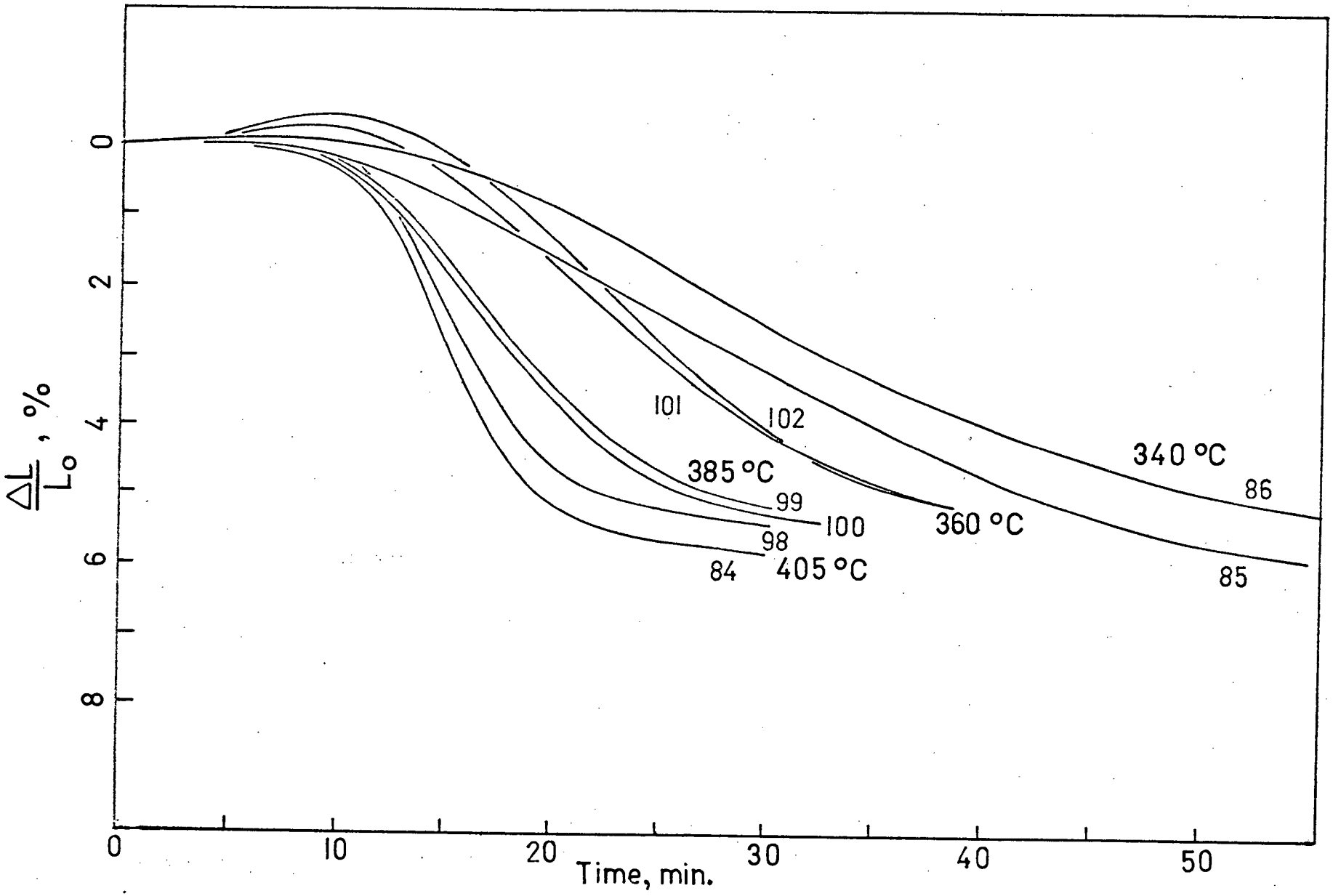


FIGURE 21 Deformation versus time for specimens of 0.50 relative density, at "isothermal" temperatures as shown. Stress 6.0 kg/cm$^2$.

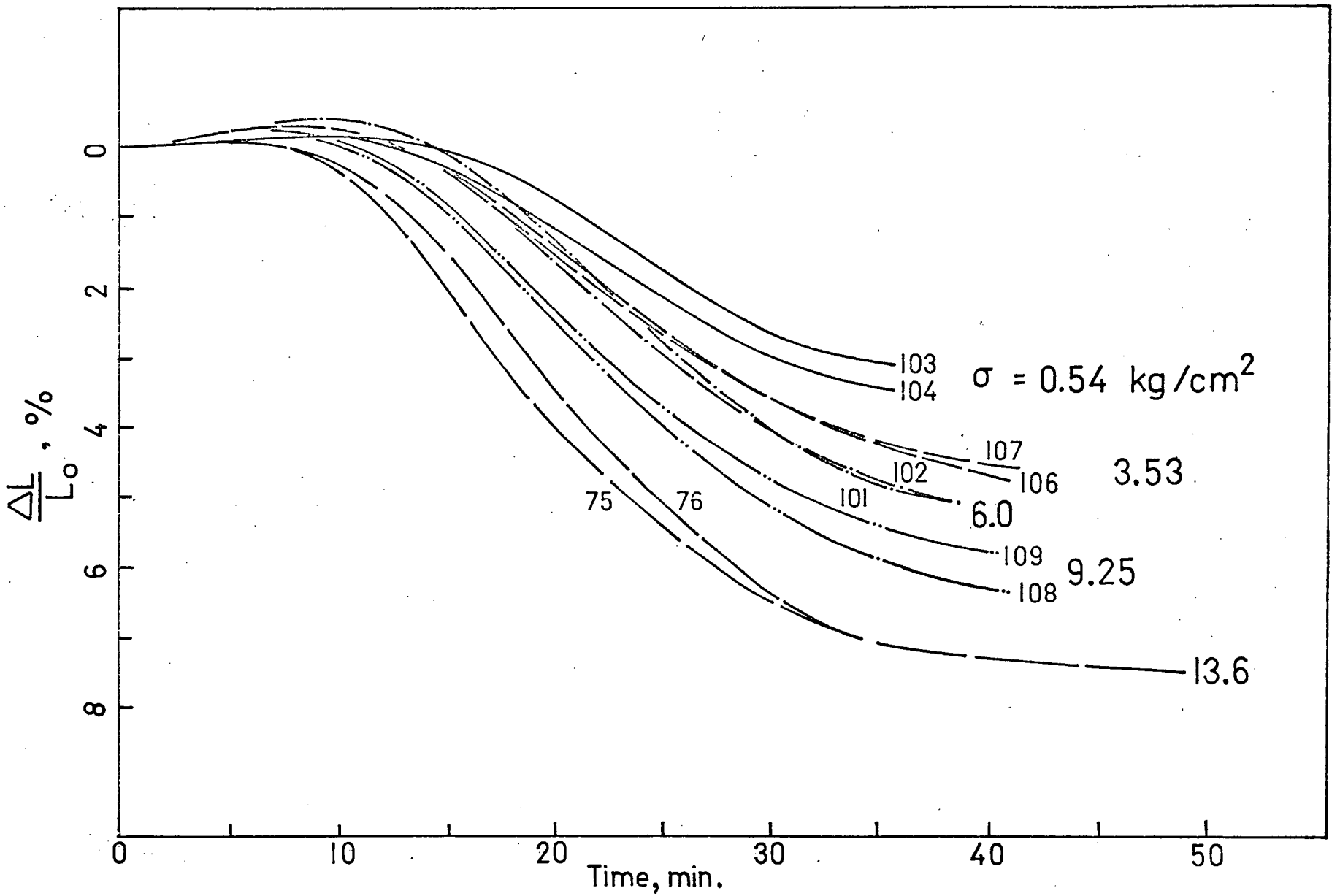


FIGURE 22 Deformation versus time for specimens of 0.50 relative density, at 360°C, for stresses as shown.

the compact on the deformation behaviour, a series of experiments were carried out under isothermal conditions. For this series a temperature of 360°C and a load of 9.25kg/cm$^2$ was used. As the specimens could be produced with relative densities in the range 0.4 to 0.7, compacts having densities in this range were used. As expected, the variation in green density signifigantly affected the creep behaviour as can be seen in Figure 23. The creep data are also presented in tabular form in Appendix II (d).

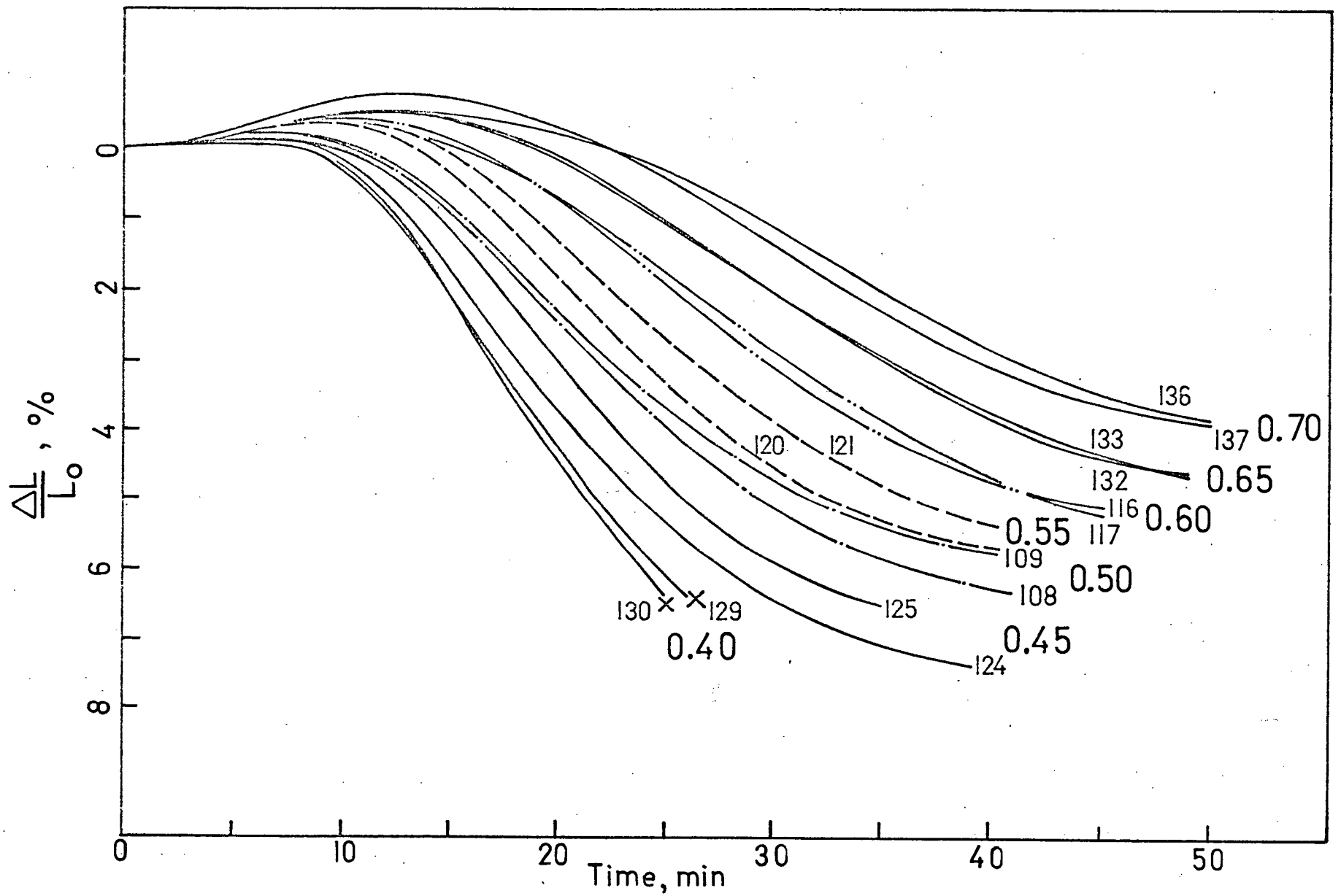


FIGURE 23 Deformation versus time for specimens of various relative densities as shown, at 9.25 kg/cm$^2$.

# CHAPTER IV

## 4 Discussion

### 4.1 Shrinkage Versus Creep

The first consideration requiring clarification is that of the nature of the deformation observed. It must first be established that the deformation produced during the decomposition of magnesium hydroxide compacts under load, either with a uniform heating rate or under isothermal conditions, is not due simply to mass loss associated with the decomposition. The reaction involved in decomposition is -

$$Mg(OH)_2 \longrightarrow MgO + H_2O$$

and this results in a theoretical weight loss of 30.9% of the initial specimen. It can easily be shown that a fully dense specimen of brucite would if fully transformed to periclase occupy only 47% of its original volume. Thus, there is a net volume reduction of 53% associated with this decomposition. However, it is well established [15] that the decomposition of brucite produces pseudomorphous relics with only slight dimensional change.

It was therefore necessary to experimentally determine the extent of shrinkage directly associated with mass loss so that this could be differentiated from the creep deformation resulting from the externally applied stress (during dehydroxylation). However, with the apparatus used, a finite load on the specimen was required to ensure

the function of the measuring system, so direct measurement of shrinkage without load in the experimental setup was not possible. Therefore, several specimens were decomposed under the same conditions of temperature and vacuum in the furnace of the creep apparatus. The cylindrical specimens were set vertically on a foil pan to ensure that unrestricted shrinkage could occur during decomposition. The dimensional changes of the specimens, heated at temperatures in the range of 300° to 500° C, were determined with a conventional micrometer (sensitivity 0.0001 in.). As the specimens were quite fragile after decomposition, precise shrinkage measurement was difficult. However, the results indicated that the shrinkage was less then 0.4%.

The results presented in Section 3.3.1, for the deformation of magnesium hydroxide compacts subjected to varying loads and decomposed under a uniform heating rate also support this estimate of the shrinkage. The extrapolated value of total strain at zero load was calculated to be 0.3% on the basis of the experimental data. This value compares favourably with that obtained by direct shrinkage measurements.

Thus this shrinkage, due to the mass loss only, can be considered insignificant in comparison with the 6 to 8% linear dimensional change observed during the creep study. No attempt has been made to correct the creep curves for the shrinkage, which is smaller than other potential experimental sources of error. This observation firmly establishes for the first time that the material can be deformed plastically during a decomposition reaction.

4.2 Weight Loss Versus Creep

The shape of the creep curve (as opposed to the shrinkage curve) is similar to that of the weight loss curve determined thermogravimetrically. This is shown clearly in Figure 24, where a creep curve and a weight loss curve prepared under identical heating conditions are compared. A load of 6.0kg/cm$^2$ and a linear heating rate of 25°C/min were used, on compacts having the same relative density (0.50). A shrinkage curve is also included for comparison with the observed deformation. The conditions of decomposition differed slightly in that the thermogravimetric analysis was carried out in a nitrogen atmosphere. This may explain the non-coincidence of the creep and weight loss curves in Figure 24.

4.3 Stages of Creep

The creep curve is of sigmoidal form (Figure 25 and Figures 20 - 23), with three apparent stages. These can be termed:

Stage I

The initiation period, where a rapid increase of creep rate occurs.

Stage II

A period of rapid creep, which in several cases appears to approach linearity.

Stage III

A decay region, during which the rate decreases rapidly and appears to approach zero asymptotically.

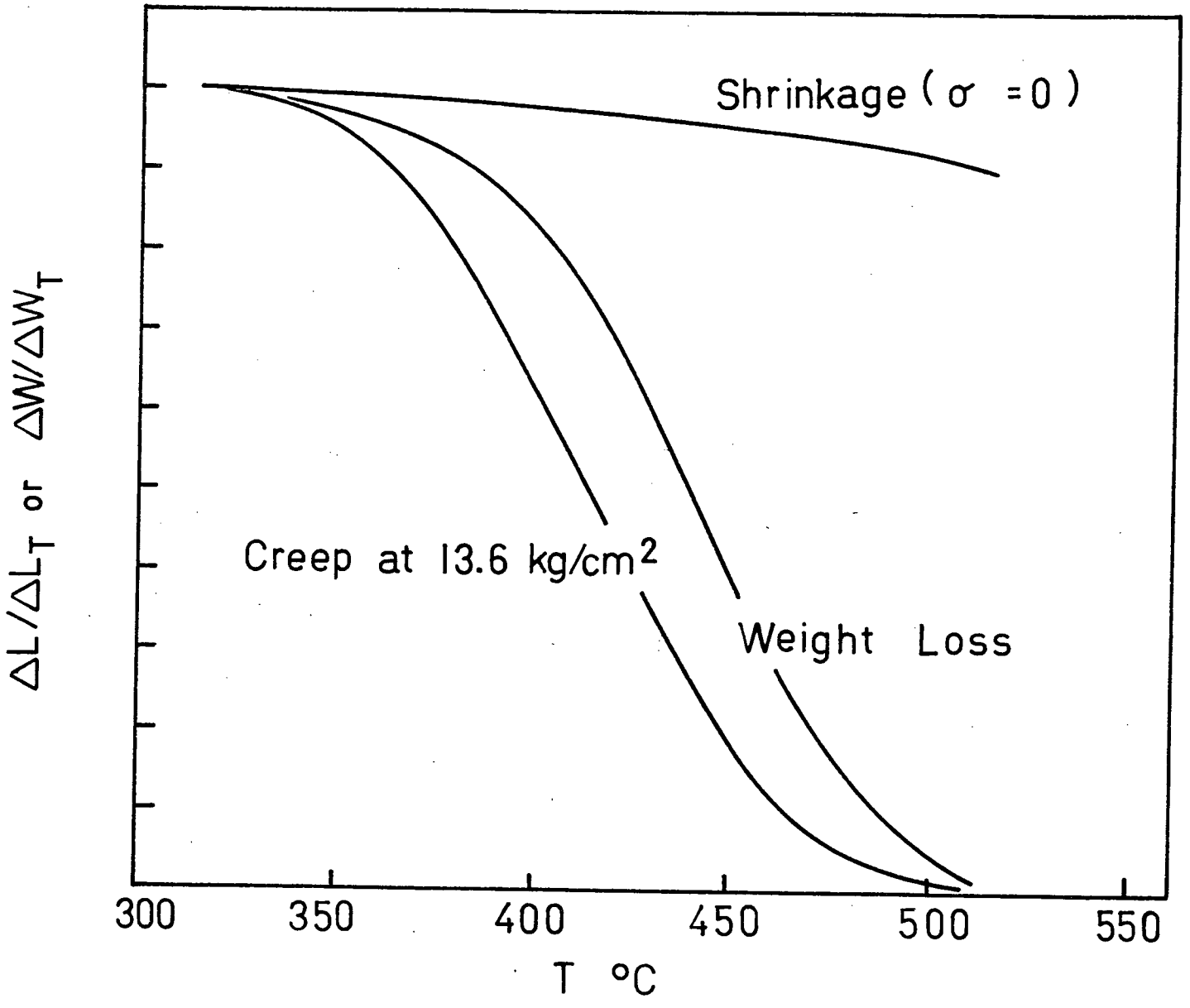


FIGURE 24 Creep, weight loss and shrinkage versus time.

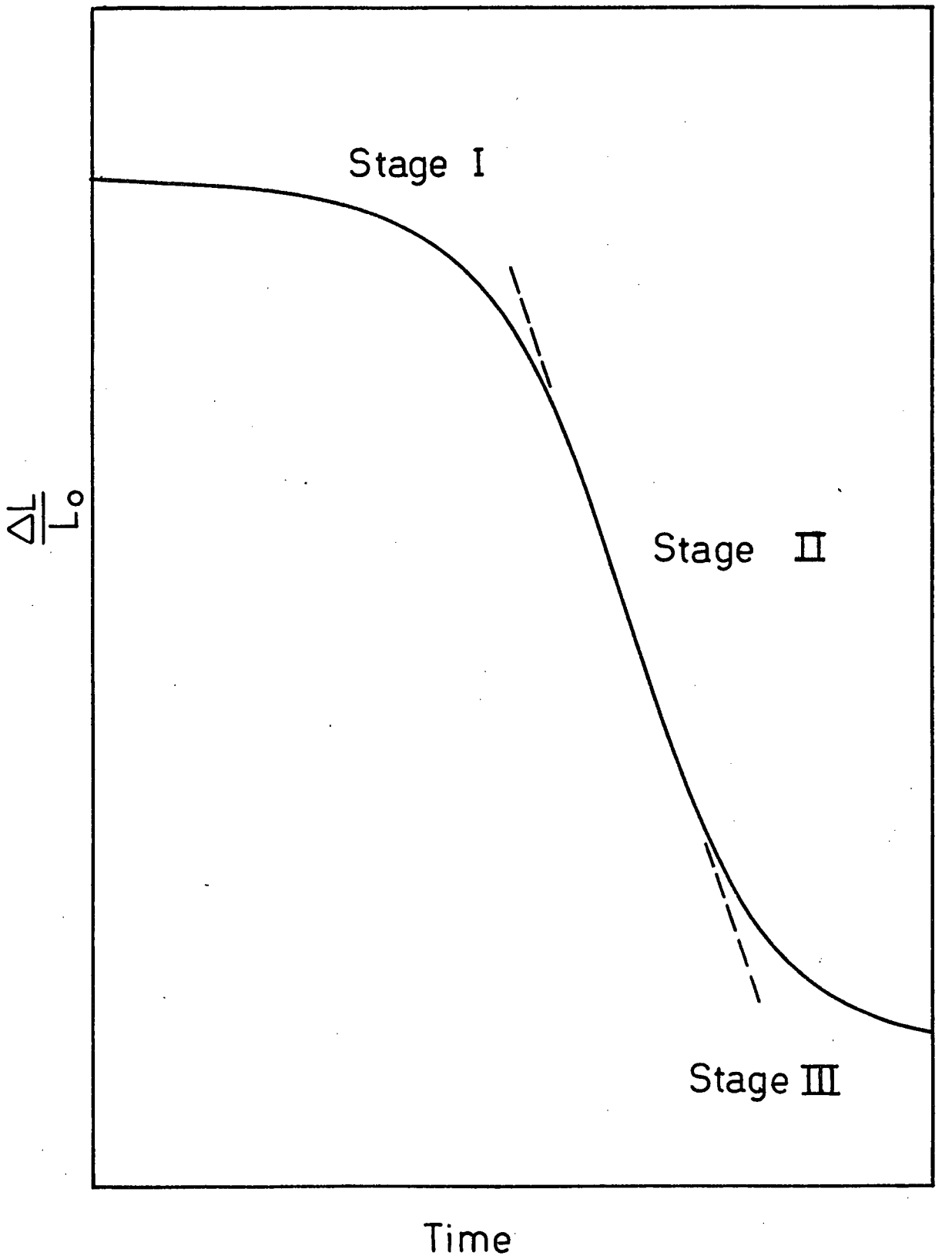


FIGURE 25 Stages of Creep

The first stage appears to be initiated by the dehydroxylation reaction. This is shown in Figure 19, where the beginning of Stage I coincides with the rise of pressure in the vacuum system. This stage appears to last for the first 10 to 20% of the total creep. In the second stage, the creep rate is highest. During this stage the temperature of the surface and the inside of the specimen reached a steady state thermal condition, with a differential of 10° to 12°C throughout the decomposition, as discussed in Section 2. 2. 5, and shown in Figure 12. This stage of the deformation coincides with the most rapid evolution of water vapour from the specimen, and hence the highest system pressures. The tendency of the system pressure to form a sharp peak, as shown in Figure 19, depends upon the temperature of the run, (specimen surface temperature). At 385° and 405°C the peak is quite pronounced; temperatures of 340° and 360° produced a broader and flatter pressure curve, as is expected, if the creep is directly related to the decomposition. Several more time-deformation-pressure relationships are shown in Figures 26 and 27 . These demonstrate clearly the relationship between the system pressure and deformation.

The relationship between the system pressure and the rate of mass loss accompanying dehydroxylation is in principle a simple one. The pumping rate is probably a function of the absolute system pressure, and if the exact pumping rate is known it should be possible to determine reasonably accurately the rate of mass loss during

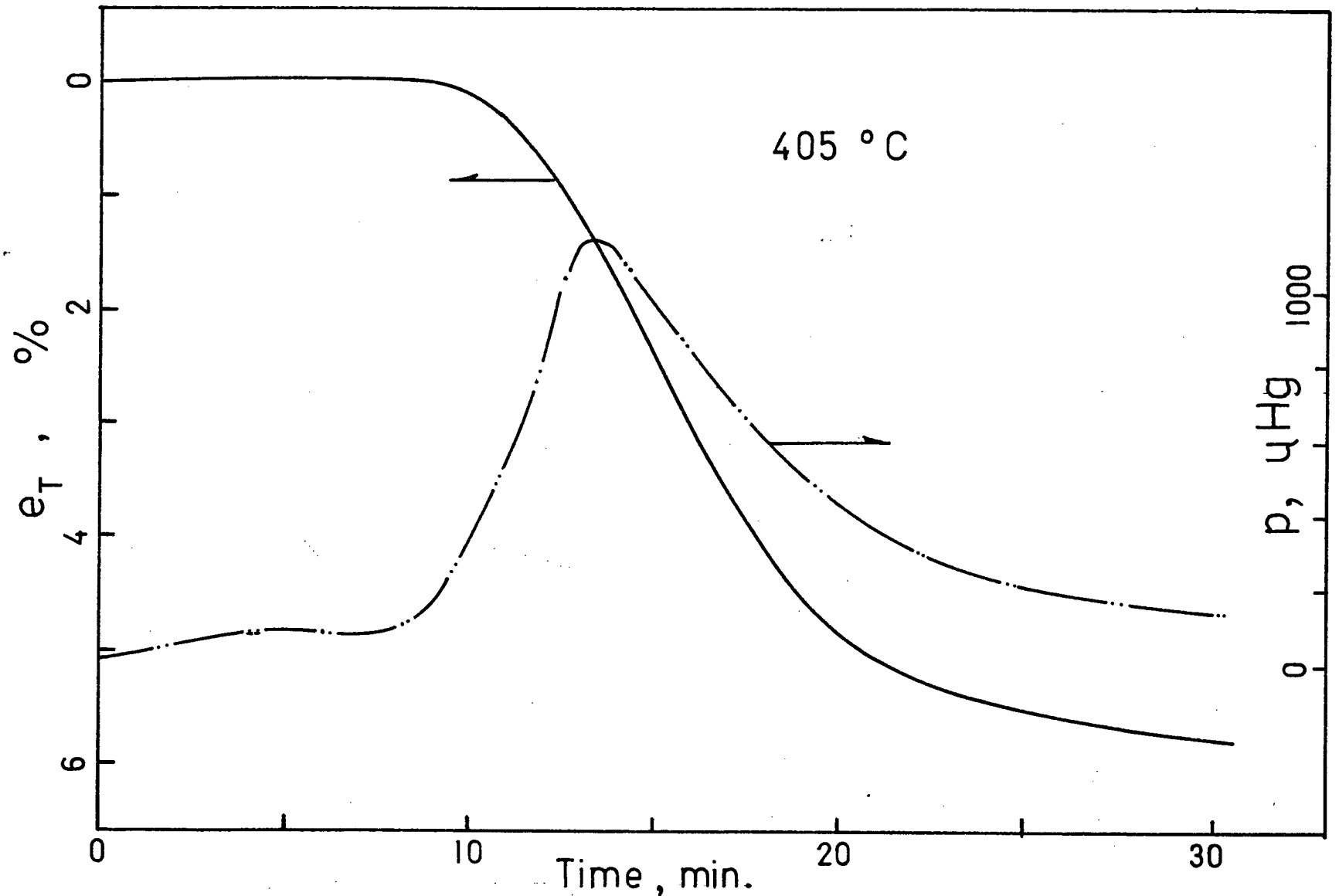


FIGURE 26 Deformation and system pressure versus time.

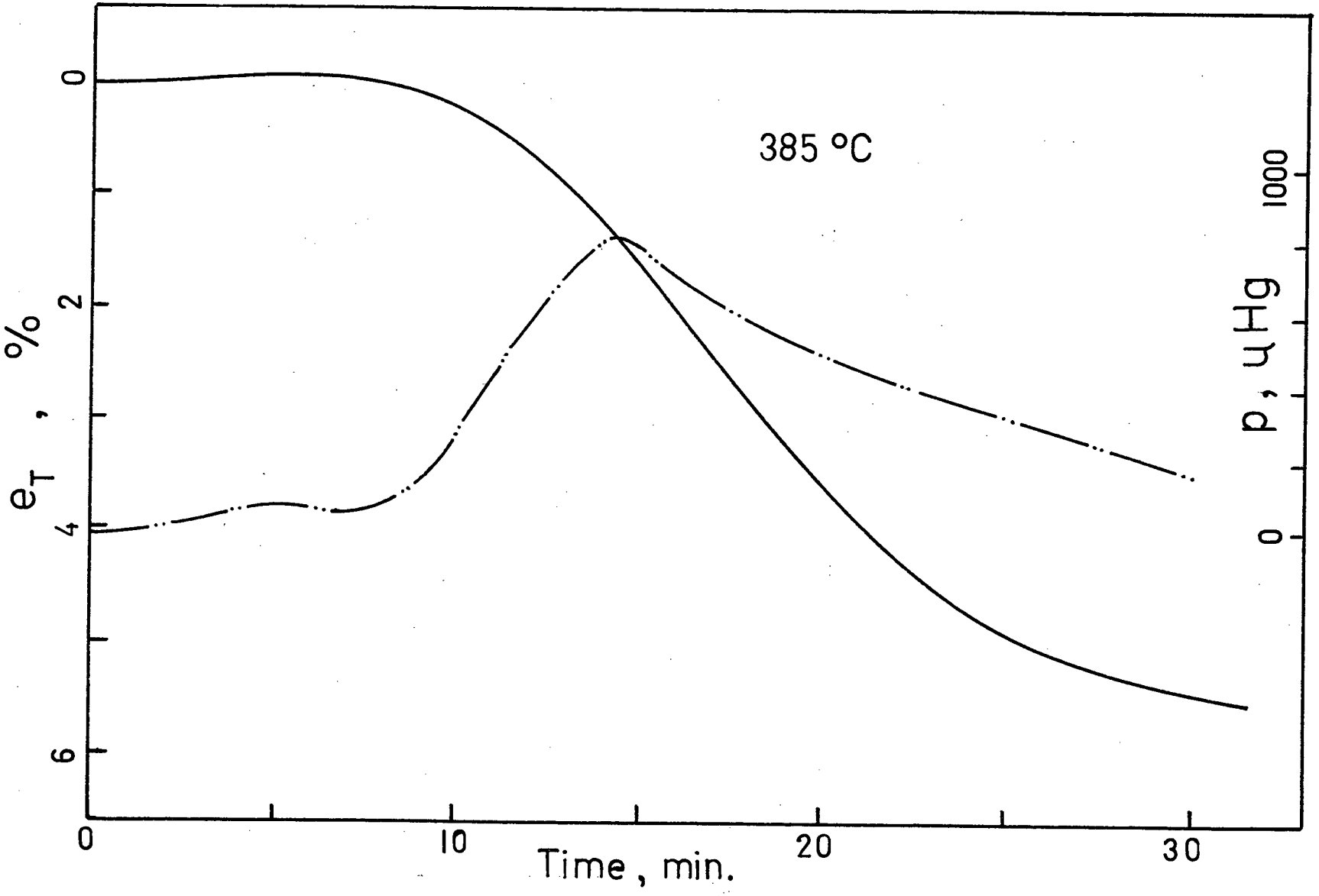


FIGURE 27 Deformation and system pressure versus time

the dehydroxylation. From this, the mass loss versus time curve could be obtained by integration.

This approach is complicated, unfortunately, by the variation of such parameters as the pumping rate, which depends to some extent on the mechanical condition of the backing pump , the type of gas previously pumped, the system temperature, and other factors. These factors are probably controllable, however, and the measurement of system pressure represents a potentially useful technique for correlating mass loss with mechanical deformation during dehydroxylation in this type of experiment.

In order to characterize the observed creep quantitatively, different aspects of the time-deformation curve should be considered. The beginning of Stage I seems to be related directly to the onset of dehydroxylation, and the extent of this stage varies with the temperature, load and density of the specimen as can be seen in Figures 20 - 23. Lower temperatures, and consequently lower rates of dehydroxylation produce a more prolonged initiation period.

The duration of Stage II varies with the temperature and applied load. At higher temperatures and loads, and lower densities, a longer and nearly linear Stage II is observed. At lower temperatures, higher densities and lower stresses, the Stage III decay region seems to form a larger portion of the curve. In all cases, however, the slope of the curve (maximum creep rate) is strongly influenced by variations

in stress, density and temperature .

The parameters selected to characterize the creep phenomenon are, therefore, the total creep strain developed under isothermal conditions and the maximum rate of creep. The total deformation was measured following the procedure shown in Figure 16, and the maximum creep rate was determined from the slope of a line drawn tangent to the steepest part of the creep curve. The creep rate is expressed as inches/inch/minute (or minute$^{-1}$).

These two parameters are somewhat arbitrarily defined. but as is shown in the following sections, they provide a basis for analyzing quantitatively the creep behaviour.

In the following sections, the effects of temperature, stress and relative density on the maximum creep rate and the total observed strain are considered.

## 4. 4 Creep Rate

### 4.4.1 Effect of Temperature

To determine the activation energy for the creep process, the maximum creep rates have been plotted against reciprocal absolute temperature in Figure 28. The Arrhenius plot of both sets of creep rates, determined using specimens of relative bulk density 0. 50 and stresses of 6. 0 and 13. 6 kg/cm$^2$ produced an activation energy of 17. 5 kcal/mol. The specimen properties, temperatures, stresses and creep rate are summarized in Table IV.

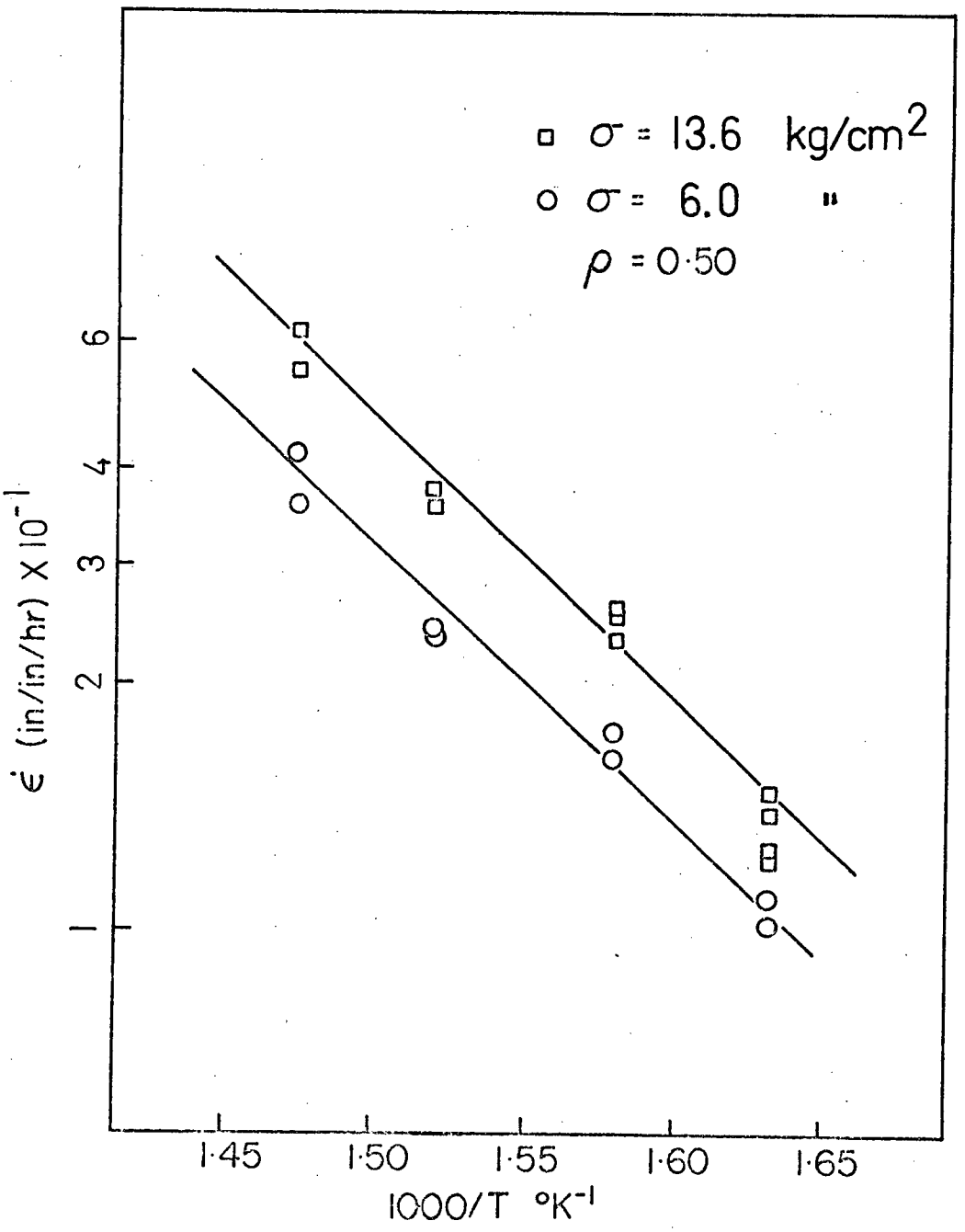


FIGURE 28 Arrhenius - type plot of creep rate versus temperature.

TABLE IV

TEMPERATURE DEPENDENCE OF ISOTHERMAL CREEP

Nominal Relative Bulk Density = 0.50 $\sigma$ = 13.6 kg/cm$^2$

| SPECIMEN | T°C | $\dot{e}$ min$^{-1}$X10$^4$ | $e_T$ % | $\rho_o$ |
|---|---|---|---|---|
| 81 | 340 | 24.6 | 7.55 | 1.206 |
| 83 | 340 | 22.9 | 7.48 | 1.206 |
| 76 | 360 | 43 4 | 7.25 | 1.208 |
| 75 | 360 | 42.9 | 7.25 | 1.203 |
| 82 | 360 | 39.0 | 6.86 | 1.196 |
| 79 | 385 | 66.6 | 6.95 | 1.202 |
| 80 | 385 | 70.6 | 6.94 | 1.206 |
| 77 | 405 | 90.3 | 7.26 | 1 204 |
| 78 | 405 | 100.8 | 7.52 | 1.199 |
| | | | $\sigma$ = 6.0 kg/cm$^2$ | |
| 85 | 340 | 16 35 | 5.97 | 1.204 |
| 86 | 340 | 17.9 | 5.40 | 1.203 |
| 96 | 340 | 20.8 | 5.43 | 1.217 |
| 97 | 340 | 20.0 | 5.08 | 1.216 |
| 101 | 360 | 27.6 | 5.39 | 1.208 |
| 102 | 360 | 30.0 | 5.38 | 1.214 |
| 99 | 385 | 41.3 | 5.40 | 1.217 |
| 100 | 385 | 40 2 | 5.36 | 1.209 |
| 84 | 405 | 70.0 | 5.68 | 1.210 |
| 98 | 405 | 60.2 | 5.42 | 1.219 |

4.4.2 Stress Dependence

The observed maximum creep rate is plotted as a function of stress in Figure 29. The stress dependence is essentially linear, showing pseudo-Newtonian behaviour, with an apparent intercept on the rate axis, i.e. finite rate at zero stress. A direct proportionality between creep rate and stress is generally attributed to viscous flow, grain boundary sliding or Nabarro-Herring creep. Details of possible mechanisms of creep during dehydroxylation will be discussed later. The data is summarized in Table V.

4.4.3 Density Dependence

The maximum creep rate varied strongly with the green density of the specimen. A similar density dependence was also observed by Coble[24] for the creep of alumina at elevated temperatures.

To explain the density dependence of creep rate, the effective stress acting within the specimen must be considered. In a particulate compact, the effective stress acting on contact area A, (on a cross section of the compact), and the stress are related by -

$$\sigma_{eff} = \sigma \frac{applied}{A}$$

Any increase in the relative density increases the contact area (assuming constant packing geometry) and thus reduces the effective stress. The contact area in a powder compact of spheres after deformation and the relative density of the compact are related by [25]

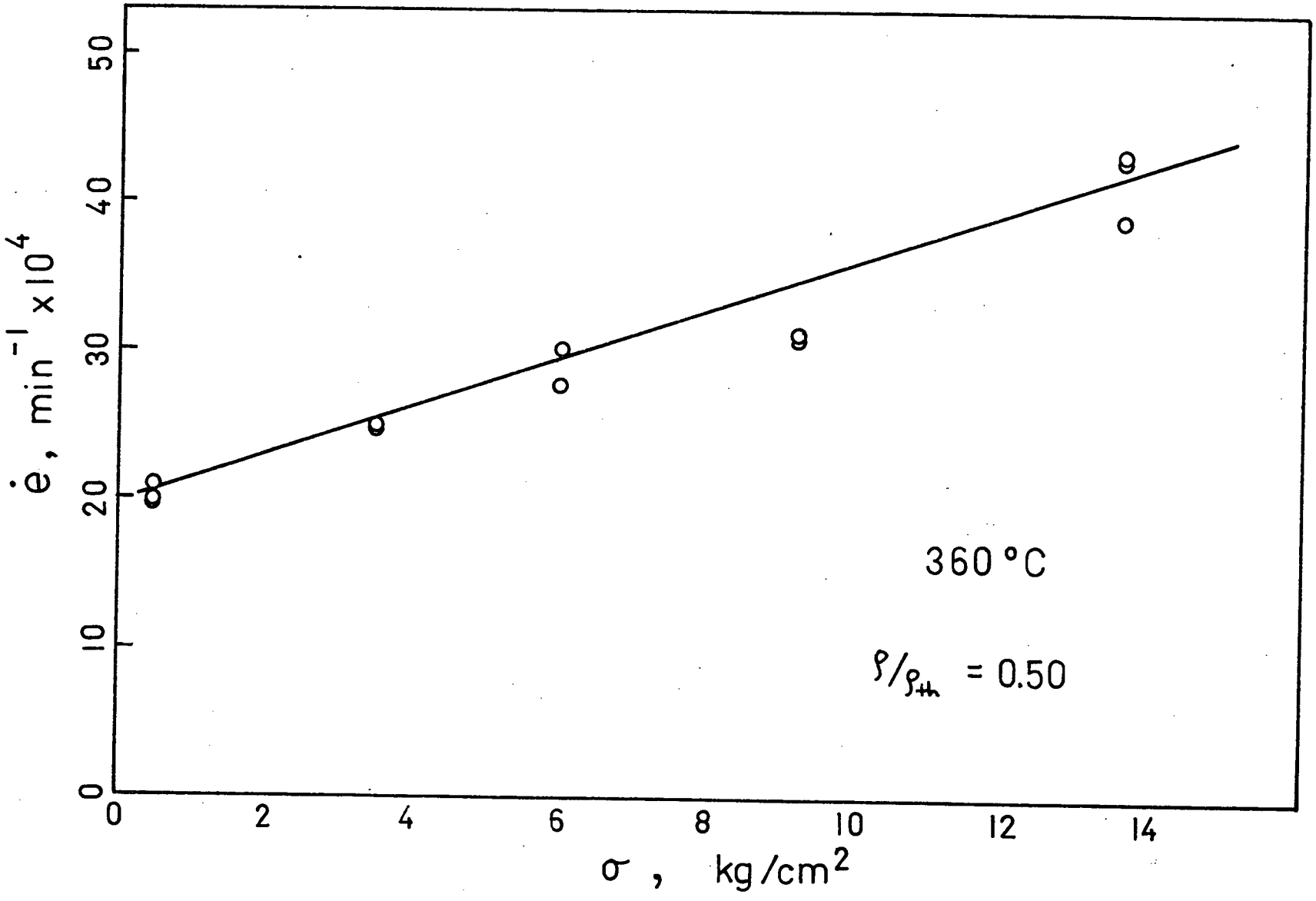


FIGURE 29 Stress dependence of maximum creep rate

TABLE V

STRESS DEPENDENCE OF ISOTHERMAL CREEP

Isothermal Creep — Stress Dependence

$T = 360^{\circ}C$ — Nominal relative bulk density = 0.50

| SPECIMEN | STRESS $kg/cm^2$ | $\dot{e}$ $min^{-1} X10^4$ | $e_T$ % | $\rho_o$ |
|---|---|---|---|---|
| 103 | 0.54 | 20.9 | 3.16 | 1.214 |
| 104 | 0.54 | 19.9 | 3.48 | 1.214 |
| 105 | 0.54 | 17.7 | 2.53 | 1.212 |
| 101 | 6.0 | 27.6 | 5.39 | 1.208 |
| 102 | 6.0 | 30.0 | 5.38 | 1.214 |
| 108 | 9.25 | 30.6 | 6.58 | 1.212 |
| 109 | 9.25 | 31.2 | 6.27 | 1.220 |
| 106 | 3.53 | 24.9 | 5.02 | 1.205 |
| 107 | 3.53 | 24.7 | 4.70 | 1 212 |
| 75 | 13.6 | 42.9 | 7.25 | 1.203 |
| 76 | 13.6 | 43.4 | 7.25 | 1.208 |
| 82 | 13.6 | 39.0 | 6.86 | 1 196 |

$$\rho = \rho_0 + \frac{3\rho_0}{2}\left(\frac{a}{R}\right)^2$$

where $\rho$ and $\rho_0$ are the relative densities at any face of radius a and a =0, respectively, and R is the radius of the deformed sphere. This means that $\rho \propto a^2$ or contact area, for a constant initial packing density. Hence,

$$\sigma_{eff} \propto \frac{1}{\rho}$$

This relation may also be obtained by considering the solid area fraction in a plane cut through the specimen, the stress effective on this area, and the relative density of the specimen. A similar conclusion was also drawn by Fryer [26]. Finally, since the strain rate is proportional to the stress,

$$\dot{e} \propto 1/\rho$$

The experimental validity of the relation is shown in Figure 30, where the creep rate is plotted as a function of $1/\rho$. The data of Coble and Kingery [24] for the creep behaviour of $Al_2O_3$ of varying relative densities are also plotted. It can be seen that this relation satisfies both sets of data. This result implies that the density dependence of the creep rate arises from the stress concentration on the grain boundaries or the contact area between the particles because of the porosity in the specimen.

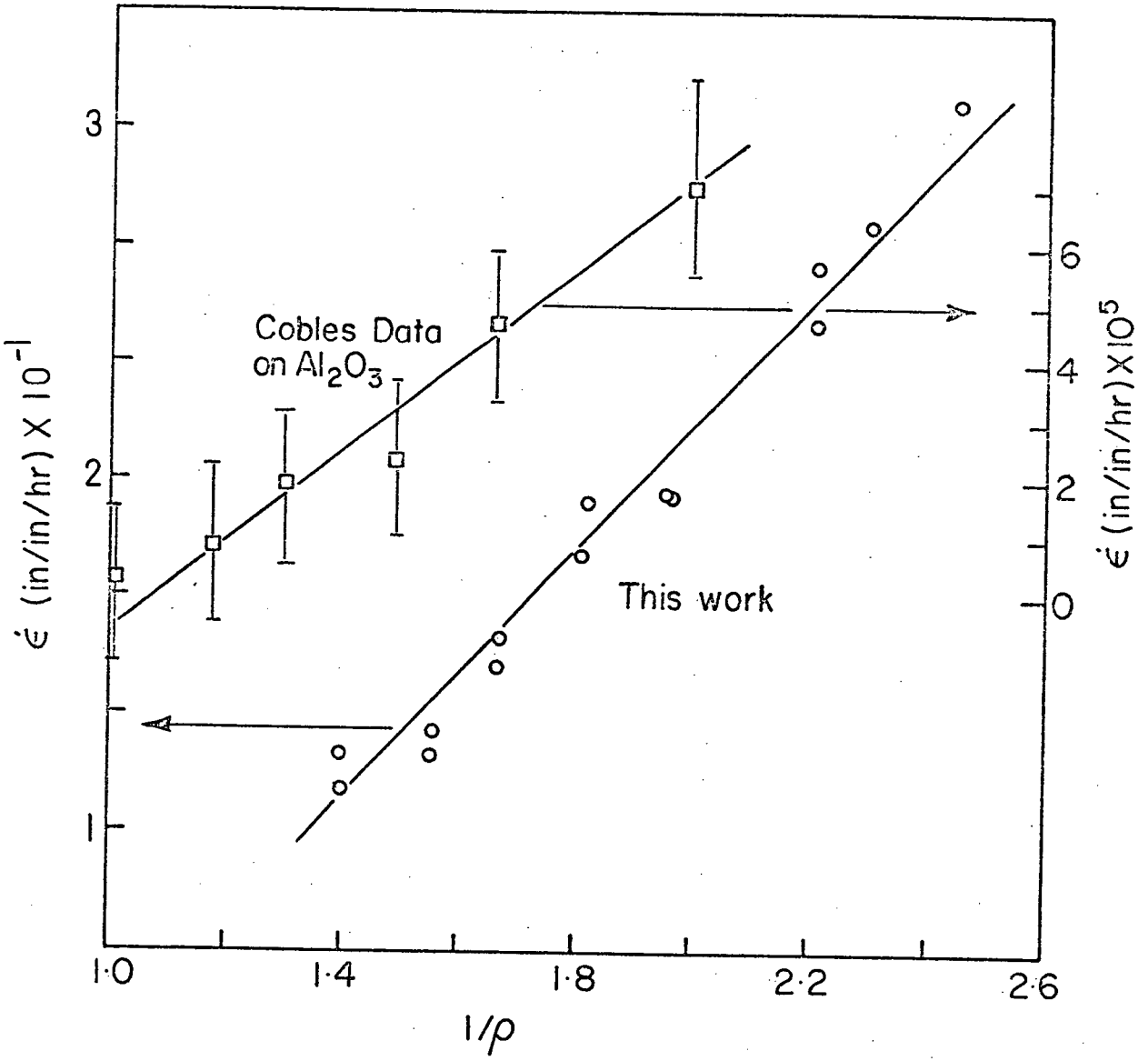


FIGURE 30 Density dependence of maximum creep rate.

TABLE VI

DENSITY DEPENDENCE OF ISOTHERMAL CREEP

Stress 9.25 $kg/cm^2$

Temperature 360°C.

| SPECIMEN | $\rho_o$ | NOMINAL RELATIVE DENSITY | $\dot{e}$ $min^{-1} X10^4$ | $e_T$ % |
|---|---|---|---|---|
| 129 | 0.963 | 0.40 | 44.9 | collapsed |
| 130 | 0.972 | 0.40 | 51.3 | collapsed |
| 124 | 1.072 | 0.45 | 41.2 | 7.62 |
| 125 | 1.073 | 0.45 | 40.7 | 7.05 |
| 108 | 1.212 | 0.50 | 30.6 | 6.58 |
| 109 | 1.220 | 0.50 | 31.2 | 6.27 |
| 120 | 1.313 | 0.55 | 31.4 | 5.96 |
| 121 | 1.317 | 0.55 | 29.2 | 6.04 |
| 116 | 1.425 | 0.60 | 25.5 | 5.42 |
| 117 | 1.430 | 0.60 | 24.3 | 5.59 |
| 132 | 1.537 | 0.65 | 21.3 | 5.02 |
| 133 | 1.535 | 0.65 | 20.2 | 4.87 |
| 136 | 1.702 | 0.70 | 19.1 | 4.28 |
| 137 | 1.700 | 0.70 | 20.1 | 4.21 |

It should be pointed out that the actual density of the compact at the instant of maximum creep rate is not the same as the green density, since a certain amount of decomposition (and hence mass loss) has taken place at the time the maximum creep rate is measured. The fact that the density dependence may be described by as simple a relationship as $\dot{e} \propto \frac{1}{\rho}$ shows that: 1) $\dot{e}$ is independent of weight loss during Stage II, or 2) the maximum rate occurs at a certain fraction of the total weight loss in all cases.

The creep rate during Stage II appears to be relatively constant, even though the system pressure variation shows that the reaction reaches maximum rate and diminishes very rapidly, indicating that the dehydroxylation rate has the same behaviour. This suggests strongly that the creep rate may be independent of the extent of dehydroxylation as long as the reaction is actually in progress.

4. 5 Total Creep Strain

The total percent strain is summarized for a particular set of conditions in each of the tables mentioned in the preceding section. (Tables IV - VI). The effects of temperature, stress and green density upon the total strain will now be considered.

4. 5. 1 Effect of Temperature

The total strain in plotted in Figure 31, for two different stresses (6. 0 and 13. 6 kg/cm$^2$) and a range of temperatures. A least squares fit performed on the data gave lines through both sets of points having a zero slope. That is, the total strain developed is independent

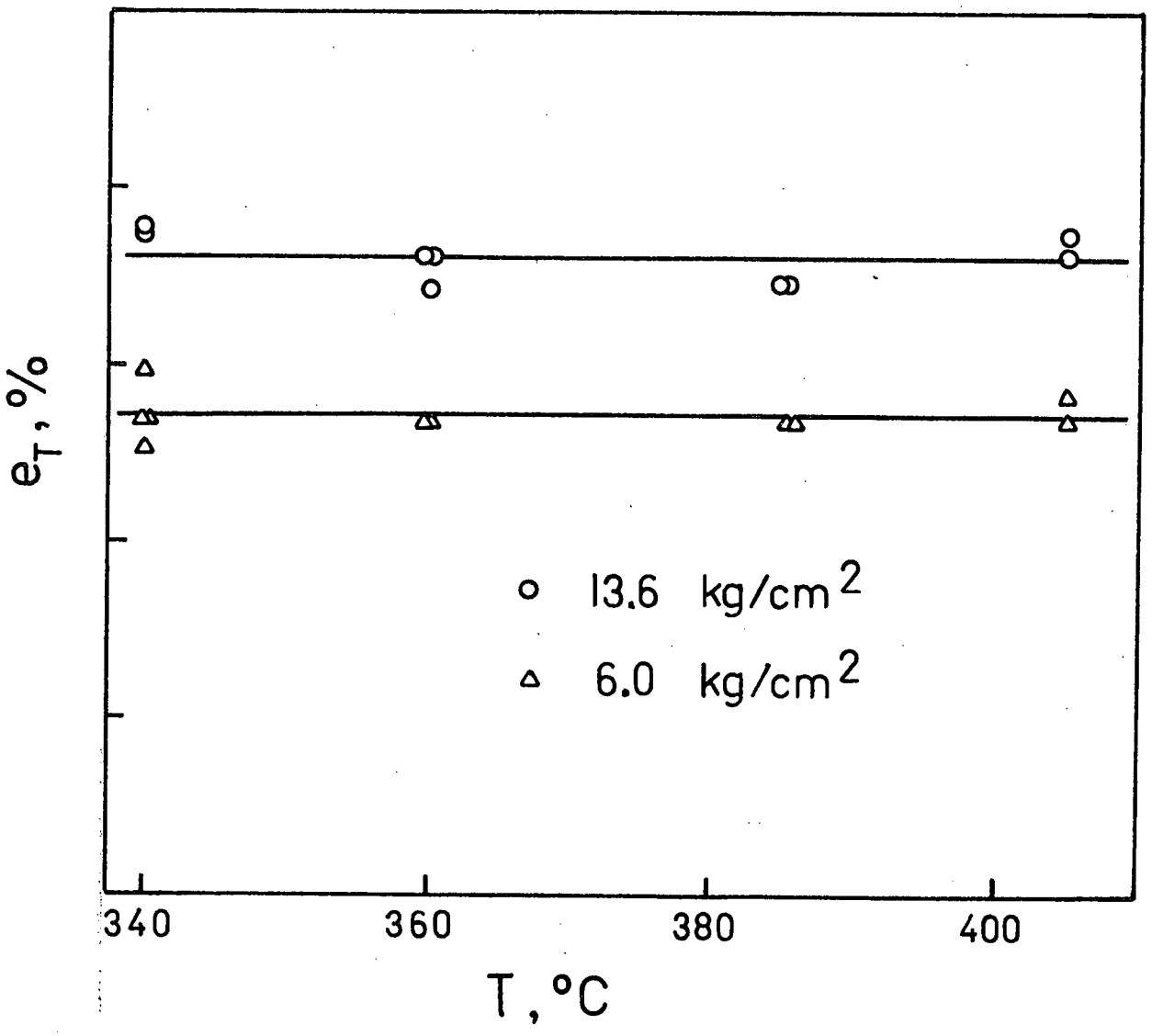


FIGURE 31 Total Strain Versus Temperature

of temperature.

4.5.2 Effect of Stress

The total percentage strain under isothermal conditions is also plotted as a function of stress in Figure 32. In order to find the stress dependence of the total strain, a log-log plot of the data is made (Figure 33). The equation which adequately represents the data is found to be $e_T = e_{oT} + k\sigma^n$, where the value of the power n is approximately one third. $e_{oT}$ is very small, and so can not be determined from this plot. This behaviour is strikingly similar to that observed earlier (Section 3.3.1) for total strain at a uniform heating rate.

4.5.3 Effect of Density

The values of total strain observed following isothermal creep at 360°C, for a constant stress of 9.2 kg/cm$^2$, are plotted against density in Figure 34. The data have also been tested on a log-log plot, on which a line drawn through the point gives a slope of approximately -1, suggesting a reciprocal relationship. The data are therefore plotted against $1/\rho$, as shown in Figure 35. The experimental scatter in these data makes it impossible to determine with certainty the form of the relationship.

However, as the strain rate was shown to be inversely proportional to the density, it is likely that the density dependence of the total strain under isothermal conditions also arises from the effective stress acting on the compact, making the reciprocal relationship more probable.

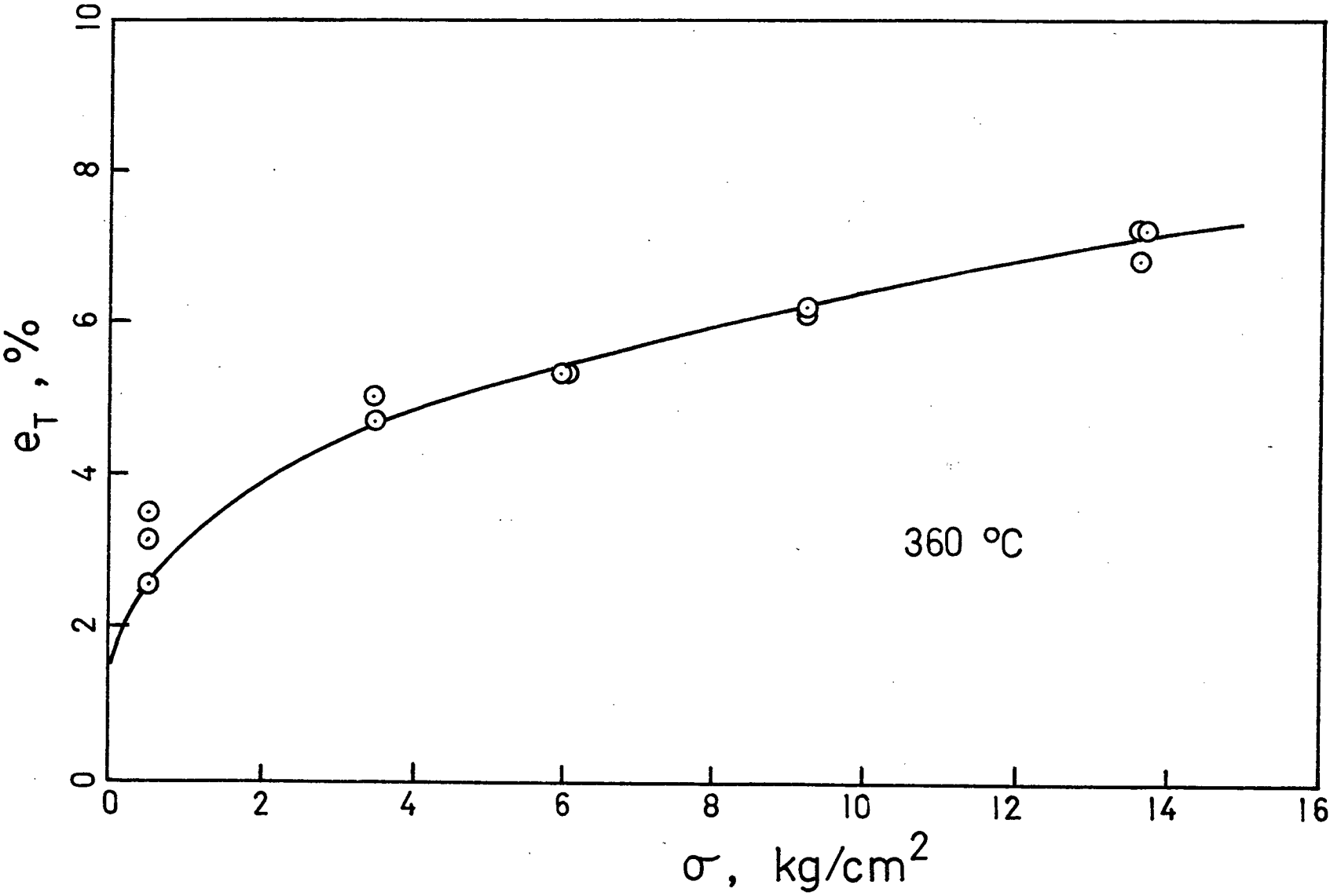


FIGURE 32 Total strain versus stress

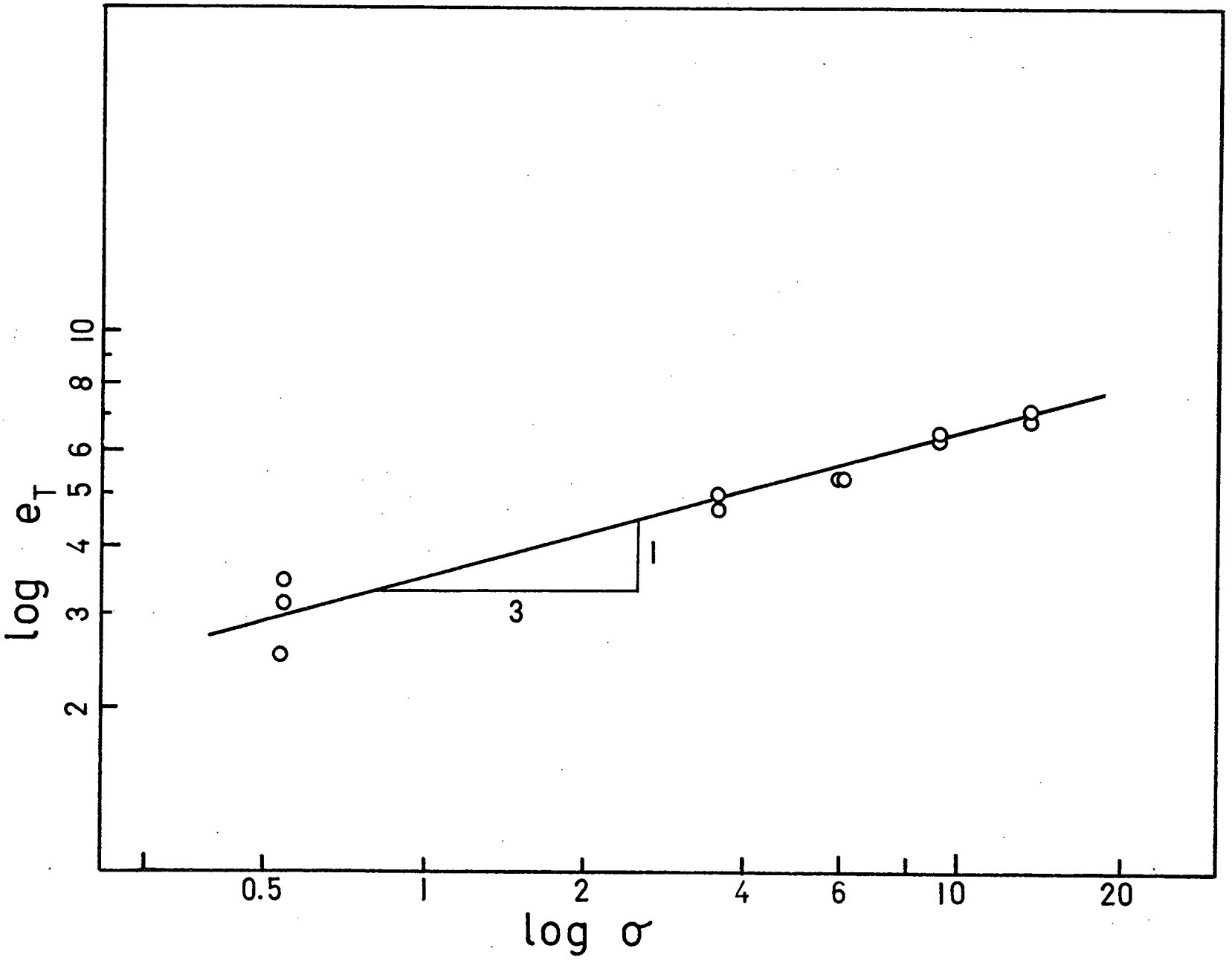


FIGURE 33 Log-Log Plot of Total Strain Versus Stress

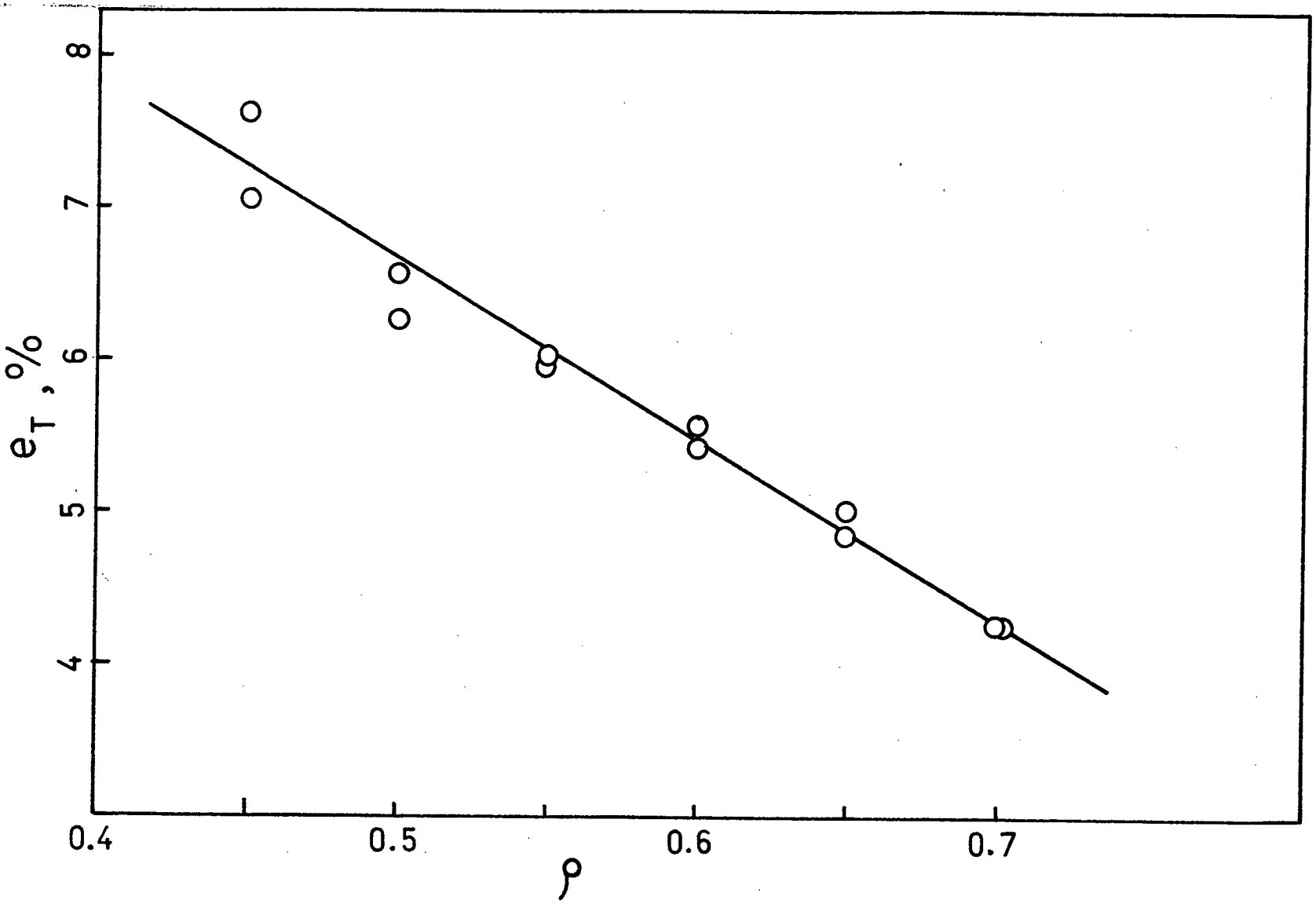


FIGURE 34 Total Strain Versus Density

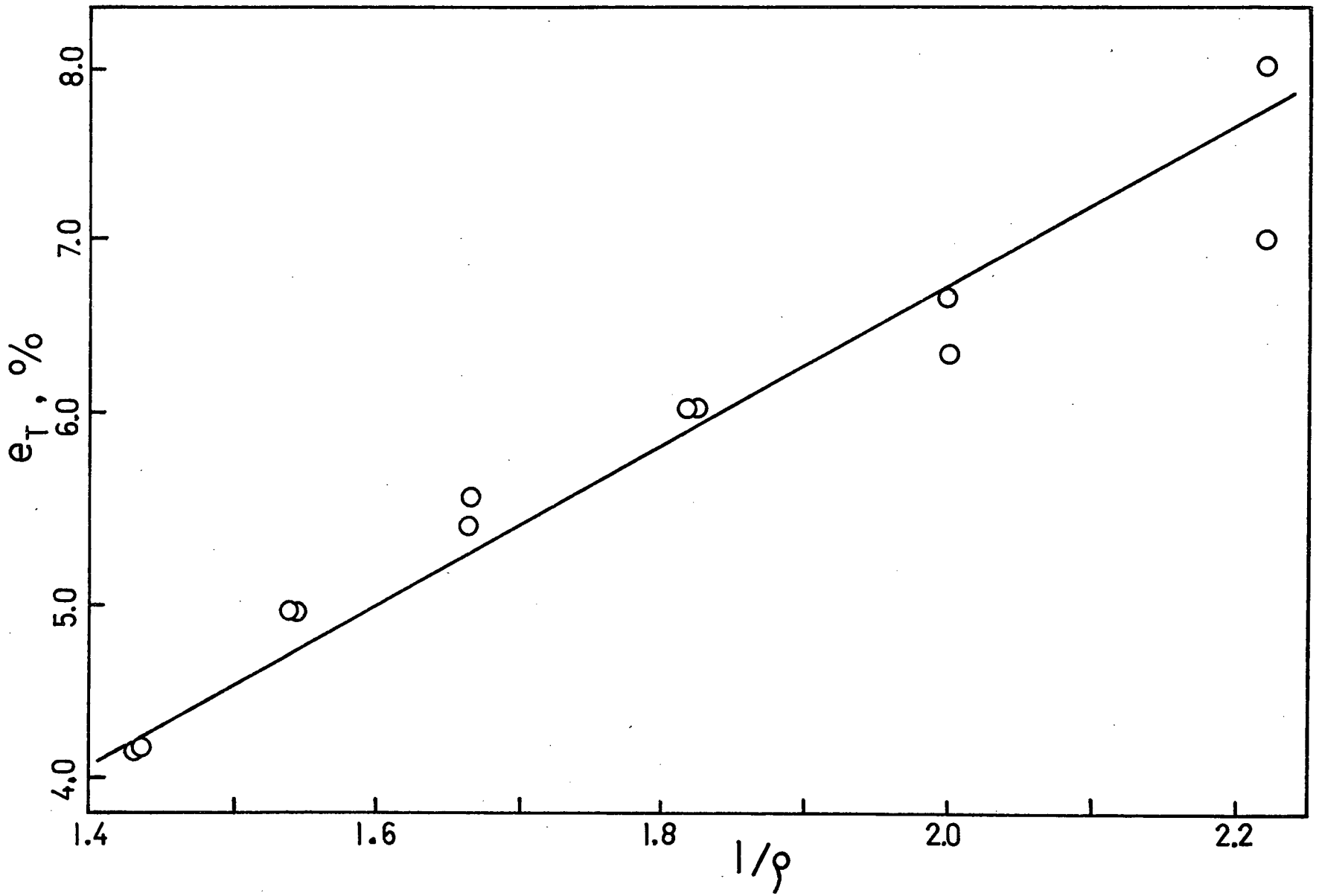


FIGURE 35 Total Strain Versus $1/\rho$

4.5.4 Phenomenological Behaviour

The relationship observed between total strain and stress, i.e.

$$e_T \propto \sigma^n \quad , \text{ where } n \approx 1/3$$

is similar to the dependence of the cold compacted density of the material, which gave

$$\rho = \rho_0 P^n \quad , \text{ with } n \text{ also } \approx 1/3$$

The similarity of the stress dependence suggests some possible mechanistic relationship, perhaps particle sliding, but no theoretical argument can be advanced for this power law. A similar power law dependence of density on stress has also been reported by Smith [30], also on the basis of experimental data.

## 4.6 Postulated Mechanisms of Creep

### 4.6.1 Physical Changes Accompanying Dehydroxylation

In order to postulate a mechanism for the observed creep it is necessary to consider the changes which accompany the decomposition. As discussed in the Introduction, the dehydroxylation of $Mg(OH)_2$ forms particles of MgO, approximately 100 Å diameter. Calcination of the $Mg(OH)_2$ used for this study (specific surface area $15 m^2/gm$) in the temperature range $350^\circ$ to $400^\circ C$ has produced surface areas of up to $250 m^2/gm$ on the product MgO. This corresponds to free cubes of average 66 Å to a side. This calculated size is in good agreement with X-ray line broadening experiments on the same material, calcined between $400^\circ$ and $500^\circ C$, which produced a particle size range of 60 to 75 Å[27].

Samples of the $Mg(OH)_2$ have been examined before and after dehydroxylation in the electron microscope. The magnesium hydroxide powder was placed on carbon support films on copper grids, then calcined in a vacuum furnace ($10^{-5}$ Torr) at temperatures from $350^\circ$ to $500^\circ C$. The samples were then examined to determine the extent of visible change at various temperatures. At the temperatures used for this study (below $450^\circ C$) the hexagonal brucite platelets retained their characteristic shape, although completely transformed to MgO.

These experiments served to confirm that the behaviour of this material was qualitatively similar to that observed by others (Section 1.4) on materials from different sources.

4.6.2 Activation Energies of Concurrent Processes

It is interesting to compare the activation energy obtained here for the creep process with the activation energies of other processes which may occur concurrently during dehydroxylation. Although this approach may not reveal the exact mechanisms involved in the deformation process, it is a basis for comparing quite different phenomena. Such comparison may lead to a hypothetical mechanism for the deformation observed in this investigation.

The dehydroxylation itself is the most important process associated with the creep, as the creep process observed is activated by the decomposition reaction. The most authoritative work on the dehydroxylation kinetics is that of Gordon and Kingery [15], who have shown that the activation energy of the process varies with the specimen geometry, primarily due to the back pressure of the water vapor created by the dehydroxylation. The activation energy for the dehydroxylation, when corrected for the specimen geometry appears to be in the range of 38 to 40 kcal/mol. This activation energy is more than double that determined for the creep process, which indicates that although the decomposition reaction initiates the deformation, the rate controlling mechanism for the creep is probably different from that of the dehydroxylation. The observation that the creep rate during the second stage is independent of the rate of dehydroxylation lends support to this argument. (Section 4.4.3).

Studies of the rehydration of MgO prepared by the calcination of $MgCO_3$ at 1000°C were carried out by Layden and Brindley[28]. These studies indicated that the temperature dependence of the reaction rate constant may be described by an Arrhenius - type relationship with an activation energy of about 16 kcal/mol. The exact mechanism was not determined, but it was felt most likely that the overall rate was governed by the rate of an interfacial reaction. This could presumably itself be diffusion controlled.

A grain growth study of MgO prepared by the calcination of $Mg(OH)_2$ has been performed by Kotera, Saito and Terada[29]. Working in air in the temperature range 500° to 900° C they found an activation energy of 17 kcal/mol for the grain growth, using material prepared from precipitated $Mg(OH)_2$. On the basis of the low activation energy of the process and the time exponent of grain growth ( $t^n$ , n = 1/6), Kotera et al suggested that the rate may be controlled by surface diffusion.

The good agreement between the activation energy of the grain growth process as determined by Kotera et al, and that of the creep process investigated here suggests that the rate controlling mechanisms for these two processes may be the same.

4. 6. 3 Viscous Flow and Grain Boundary Sliding

The stress dependence of the maximum creep rate is linear, suggesting that the mechanism of the deformation may be either viscous flow or grain boundary sliding (interparticle sliding).

Grain boundaries in the proper sense do not exist in a particulate compact of the type used, so particle (equivalent to grains) sliding is considered to be synonymous here. Grain boundary creep is generally important only at temperatures above 0.5 $T_m$. This suggests that some form of increased atomic mobility must be present for this mechanism to be operable at the temperatures used in this study.

4.6.4 Possible Mechanisms of Deformation

From the foregoing it appears that the creep deformation observed during the decomposition of $Mg(OH)_2$ may be diffusion controlled, as the activation energy of the creep process is similar to those of grain growth and rehydration. On the other hand, it is possible that the deformation occurs by some other means. For example, it has been demonstrated recently[33] that a loose particulate compact of a mixture of tungsten and oxalic acid can be densified during the decomposition of the oxalic acid, apparently without any chemical reaction between the two materials. In this case the enhanced densification of the tungsten powder was attributed to the effect of gas phase lubrication.

At present it is difficult to choose between these two mechanisms:

a) Deformation controlled by diffusion, and

b) Deformation controlled by gas phase lubrication.

This system is further complicated by the fact that the

$Mg(OH)_2$ disintegrates into very fine crystallites of MgO ( about 70 Å ), thus creating a large number of new interparticle contact areas for sliding. In addition, the possible contribution of slip to the observed deformation must be considered.

4.6.4.1 Slip Mechanisms

As near theoretically dense bodies have been produced just above the decomposition temperature, the deformation of individual crystallites must occur during the hot pressing process at higher stresses, indicating that the freshly formed MgO is plastic.

This plasticity may be manifested even at low stresses, giving rise to some or all of the creep deformation observed in this study. Hulse, Copley and Pask[31] showed that fully dense polycrystalline MgO ( of a certain and grain size ) can yield plastically at as low as 400°C. (at 35,000 psi ). They also showed that the yield stress on the $\{100\}\langle 110\rangle$ slip system of single crystal MgO is approximately 10,000 psi at 400°C. In the present investigation the particles are not constrained in the same manner as grains in a solid body, and the individual contact areas may be very small, giving rise to very high stress concentrations. Also, the freshly formed MgO particles may be highly defective as a result of the type of structural rearrangement involved in the decomposition. A combination of all these effects may contribute to the creep deformation observed.

4.6.4.2 Stacking Rearrangement

Another possible stress dependent mechanism of deformation of the particles may stem from the effect of stress on the rearrangement of the stacking sequence necessary for the transformation from the hexagonal to the cubic lattice configuration. In considering the transformation of $Mg(OH)_2$ to MgO, none of the previous investigators have studied in detail the required change of stacking sequence. Two basic models have, however, been proposed for the removal of water vapor from the material during the reaction.

The model suggested by Goodman[13] for the transformation, as shown in Figure 3, necessitates a structural collapse normal to the basal oxygen planes due to the removal of whole layers of oxygen (hydroxyl) ions. Because of experimental difficulties none of the investigators have been able to determine the extent of the dimensional change normal to the basal planes. However, if such a collapse occurs, it is possible that the presence of an external stress having a component parallel to the oxygen planes can cause deformation during the dehydroxylation.

Alternatively, if the decomposition proceeds by the inhomogeneous mechanism of Ball and Taylor[16], Figure 4, a stacking

sequence rearrangement is necessary at some time during the reaction. It can be shown that the necessary rearrangement can occur by the passage of a partial dislocation of the form $1/6\,[\bar{2}11]$ between every second oxygen layer. To provide the necessary stacking rearrangement without gross shape change of the crystallite the succession of shifts would be in the sequence $1/6\,\langle\bar{2}11\rangle$, $1/6\,\langle 1\bar{2}1\rangle$ ("b") and $1/6\,\langle 11\bar{2}\rangle$ ("c") on successive planes.

An arbitrarily chosen plane requiring shift from ABAB to ABCA could make the required change with a, b or c. In the presence of an applied stress the shift would be in the direction of that stress.

One property of the deformation could be related to this rearrangement. The observed dependence of strain rate on stress;

$$\dot{e} = \dot{e}_o + A\sigma$$

where $\dot{e}_o$ is the intercept with the rate axis, and A is a constant, could result from the fact that a small external stress could cause the sequence of partial dislocations to change from abc etc. to another sequence causing gross strain.

This hypothesis has not been developed in detail, as there is no direct indication in this study that deformation of the particles themselves is actually occurring.

## V. Summary and Conclusions

5. 1 Contact deformation and bond formation have been demonstrated in experiments in which tips of single crystal $Ca(OH)_2$ and cold-compacted $Mg(OH)_2$ powder were decomposed while loaded in contact.

5. 2 Compacts of $Mg(OH)_2$, of 0. 50 relative density have been decomposed under varying compressive loads. The shrinkage accompanying dehydroxylation in the absence of load was less than 0. 4%. A load-dependent deformation of up to 7% at 13. 6 kg/cm$^2$ (the maximum stress used) has been observed. The dependence of total strain on stress, at uniform heating rate takes the form:

$$e_T = e_{oT} + k\sigma^n$$

where $e_{oT}$ is less than 0. 4% and n is approximately 1/3.

These observations firmly establish for the first time that this material can be deformed plastically during a decomposition reaction.

5. 3 The creep behaviour of the compacts was explored, for different isothermal temperatures, stresses and relative densities. The compressive creep curve is of sigmoidal form, similar to the thermogravimetric curve for the same material. The creep curve has three stages;

Stage I - an initiation period, with rapid increase of creep rate.

Stage II - a period of nearly linear rapid creep.

Stage III - a decay region, with rapidly decreasing rate, apparently approaching zero asymptotically.

5.4 The maximum creep rate (slope of the creep curve) has been measured, and its dependence on temperature, stress and density determined.

The creep rate shows a temperature dependence of the Arrhenius form, with an activation energy of 17.5kcal/mol. This is approximately one-half the best published value for the activation energy of dehydroxylation, so the mechanisms of the two processes are thought to be different.

Comparison of the activation energy with those of grain growth and rehydration (17 and 16.1 kcal/mol, respectively) suggest that the creep process may be diffusion controlled.

The creep rate has a linear relationship with applied stress , in the stress range examined ( .54 to 13.6 $kg/cm^2$), and an apparent finite creep rate at zero stress:

$$\dot{e} = \dot{e}_o + A\sigma$$

A full explanation of this behaviour has not been developed, but it may relate to stacking sequence rearrangement during dehydroxylation.

The creep rate has been shown to be of the form

$$\dot{e} \propto 1/\rho$$

This has been explained in terms of an effective stress acting on interparticle contacts. The interparticle contact area is proportional to density, giving the above result.

The final form of the creep rate equation is:

$$\dot{e} = \dot{e}_o + \frac{A\sigma}{\rho} \exp\left(-\frac{17,500}{RT}\right) t^{-1}$$

5.5 The total creep strain developed under isothermal conditions has also been determined. The total strain has been found to be independent of temperature. Its variation versus stress is of the form

$$e_T = e_{oT} + e\sigma^n$$

where n is again approximately 1/3 and $e_{oT}$ less than 0.5%. The density dependence appears to be of the form

$$e_T \propto 1/\rho$$

5.6 The creep mechanism is postulated to be interparticle sliding, probably similar to grain boundary sliding in solid materials. However, it is possible that deformation of the particles occurs, probably by a mechanism associated with stacking sequence rearrangement, although this work does not permit the formulation of a rigorous hypothesis. It has, however, shown that load-dependent deformation can occur during dehydroxylation of $Mg(OH)_2$.

## VI Suggestions for Future Work

6.1 In order to establish more definitively the relationship between weight loss and creep, experiments should be devised to measure simultaneously, and accurately, the weight loss and dimensional change.

6.2 The effect of specimen size has not been studied, and experiments with varying diameters might permit extrapolation to zero diameter, and hence elimination of any back water vapour pressure effect due to the compact size.

6.3 As the $Mg(OH)_2$ particles in the compacts undoubtedly show a strong texture, due to their platy shape and the uniaxial pressing, it would be interesting to explore the effect of textural orientation on the deformation. This could be done by using specimens pressed sideways.

6.4 The effect of water vapour pressure on the deformation could also be studied. This might serve to clarify the mechanism.

6.5 The range of stresses used could be expanded, particularly to lower stresses, so that the true form of the stress dependence at very small stresses could be determined. This would probably require optical measurement of dimensional changes.

6.6 The activation energy for the creep process should be compared with one accurately determined for the dehydroxylation of the same material.

# APPENDICES

APPENDIX I

TEMPERATURE DISTRIBUTION WITHIN THE CYLINDRICAL SPECIMEN

In order to assess the possible time lag between the specimen's surface and its centre, an approximate calculation was performed using a method due to Carslaw and Jaeger [23].

Values for the thermal conductibity and specific heat were first estimated, as experimental values for $Mg(OH)_2$ were not available in the literature. The specific heat may be obtained in several ways. One estimate, based on comparison with values [20] for CaO, $Ca(OH)_2$, and MgO is 0.30 cal/gm°C. Values for the specific heat of MgO from Wicks [32] indicate a value between 0.30 to 0.40 for $Mg(OH)_2$, based on 0.265 cal/gm°C for MgO. A value of 0.35 cal/gm°C was selected for the calculations.

The thermal conductivity was estimated on the basis of the published values for MgO, which range from about 0.08 (cal/sec/$cm^2$/°C/cm)for pure, dense MgO, to $10^{-4}$ for powdered MgO. The relative bulk densities used in the experiments were somewhat greater than expected for loose powders, but it was felt that the reduced pressure ($10^{-2}$ Torr) would compensate, and a value of $K=10^{-4}$ was selected.

The method used permits the calculation of temperature as a function of time, the thermal diffusivity ($K/\rho$) and a reduced radius for an infinite cylinder subjected to a step increase in its surface temperature. The step increase is indicated by V on Figure 36 ,

and the local temperature at any time t by v. A typical steady state temperature of 400° is plotted on the left hand margin.

It can be seen that a temperature in excess of 390°F is reached at the specimen centre (v/R =O) in 8 to 10 minutes. This was felt to justify conducting the experiment and obtaining experimental verification of the specimen temperature during the tests.

It should be noted that the heat of reaction (endothermic) has not been taken into account in this calculation. Since it was found in the early tests that the maximum reaction rate did not develop until approximately 5 minutes after test temperature (405°C) had been reached (about 12 minutes from the start of the run), it was felt that the major endothermic reaction took place after the quasi-uniform temperature distribution has been achieved. Temperature measurements in the centre of the specimen during the test eventually confirmed the predicted temperature distribution.

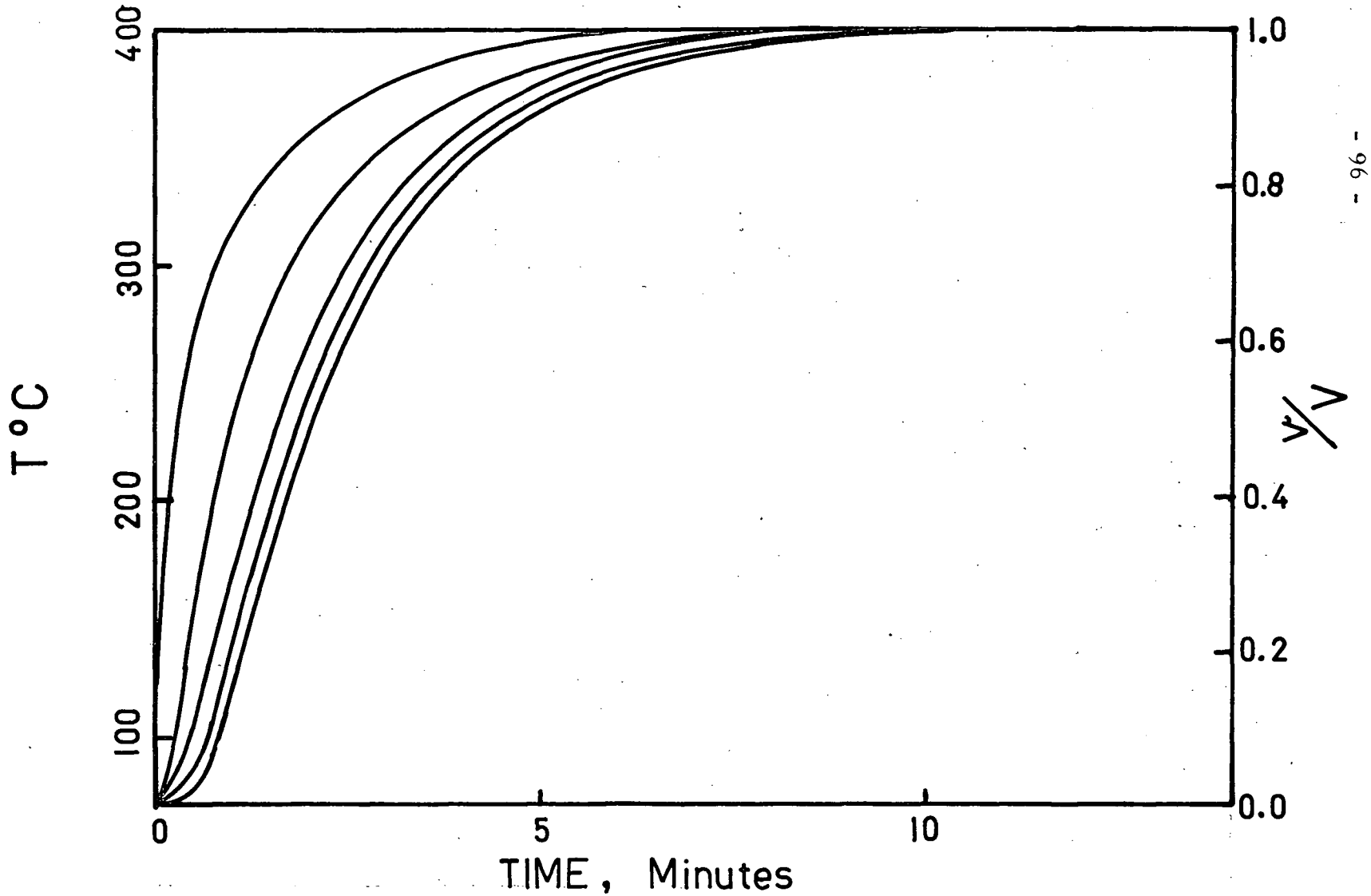


FIGURE 36 Theoretical temperature distribution in the specimens for the isothermal creep tests.

## APPENDIX II

## CREEP DATA - "ISOTHERMAL" CONDITIONS

The data is presented in tabular (columnar) form as time from the start of the run (minutes), specimen surface temperature ($T^{o}C$), and shrinkage from the initial length in inches $X10^{-5}$ (hundred thousandths). Duplicate runs are presented in the same table for comparison. The specimen particulars and run load are also presented. Initial length is given in inches and specimen density in $gm/cm^3$.

The specimen numbers are included on the Figures in Section 3, so that direct comparisons may be made. All the data presented have been corrected for thermal expansion by the method shown in Appendix III. The runs are grouped in the manner in which they were presented in Section 3. One set of four duplicate runs has been included (Nos. 85, 86, 96, 97). All runs were started with a system pressure of from 10 to 50 $\mu$ Hg, depending on the rate of reaction (temperature).

APPENDIX II (a)

| Specimen | 81 | 83 |
|---|---|---|
| $l_o$ | 0.3174 | 0.321 |
| $\rho_o$ | 1.206 | 1.206 |

Temperature 340°C Stress 13.6 kg/cm$^2$
Nominal relative density 0.50

| Time Min. | T°C | Specimen No. 81 | Specimen No. 83 | Time Min. | T°C | Specimen No. 81 | Specimen No. 83 |
|---|---|---|---|---|---|---|---|
| 0 | 40 | 0 | 0 | 31 | 340 | 1504 | |
| 1 | 40 | 2 | 0 | 32 | | 1564 | 1438 |
| 2 | 55 | 0 | -2 | 33 | | 1620 | 1506 |
| 3 | 125 | 29 | -74 | 34 | | 1674 | 1565 |
| 4 | 194 | 44 | -1 | 35 | 340 | 1727 | 1626 |
| 5 | 240 | 64 | 18 | 36 | | 1783 | 1691 |
| 6 | 280 | 70 | 32 | 37 | | 1835 | 1749 |
| 7 | 308 | 85 | 44 | 38 | | 1884 | 1809 |
| 8 | 336 | 106 | 70 | 39 | | 1932 | 1860 |
| 9 | 340 | 125 | 98 | 40 | 340 | 1976 | 1909 |
| 10 | 340 | 152 | 127 | 41 | | 2017 | 1951 |
| 11 | | 179 | 155 | 42 | | 2058 | 1996 |
| 12 | | 207 | 174 | 43 | | 2092 | 2036 |
| 13 | | 242 | 199 | 44 | | 2125 | 2072 |
| 14 | | 282 | 224 | 45 | 340 | 2160 | 2105 |
| 15 | 340 | 334 | 265 | 46 | | 2189 | 2136 |
| 16 | | 385 | 312 | 47 | | 2216 | 2165 |
| 17 | | 458 | 376 | 48 | | 2239 | 2188 |
| 18 | | 526 | 433 | 49 | | 2264 | 2211 |
| 19 | | 608 | 497 | 50 | 340 | 2296 | 2243 |
| 20 | 340 | 686 | 558 | 51 | | 2315 | 2248 |
| 21 | | 763 | 629 | 52 | | | 2259 |
| 22 | | 840 | 703 | 53 | | 2348 | 2279 |
| 23 | | 918 | 785 | 54 | | 2364 | 2283 |
| 24 | | 999 | 863 | 55 | 340 | 2386 | 2294 |
| 25 | 340 | 1070 | 934 | 56 | | 2393 | |
| 26 | | 1148 | 1003 | | | | |
| 27 | | 1220 | 1069 | | | | |
| 28 | | 1297 | 1144 | | | | |
| 29 | | 1371 | 1211 | | | | |
| 30 | 340 | 1438 | 1292 | | | | |

APPENDIX II (a)

| Specimen | 75 | 76 |
|---|---|---|
| $l_o$ | 0.318 | 0.3178 |
| $\rho_o$ | 1.208 | 1.203 |

Temperature 360°C Stress 13.6 kg/cm$^2$
Nominal relative density 0.50

| Time Min. | T°C | Specimen No. | | Time Min. | T°C | Specimen No. | |
|---|---|---|---|---|---|---|---|
| | | 75 | 76 | | | 75 | 76 |
| 0 | 40 | 0 | 0 | 31 | 360 | 2164 | 2095 |
| 1 | 40 | 0 | 0 | 32 | | 2204 | 2152 |
| 2 | 75 | -7 | 7 | 33 | | 2243 | 2210 |
| 3 | 145 | 13 | 0 | 34 | | 2264 | |
| 4 | 200 | 28 | -12 | 35 | 360 | 2284 | 2278 |
| 5 | 244 | 31 | -13 | 36 | | 2296 | 2291 |
| 6 | 283 | 27 | -12 | 37 | | 2310 | 2305 |
| 7 | 312 | 14 | -2 | 38 | | 2316 | 2321 |
| 8 | 344 | 16 | -2 | 39 | | 2346 | 2339 |
| 9 | 362 | 70 | | 40 | 360 | 2364 | 2355 |
| 10 | 360 | 113 | | 41 | | 2378 | 2369 |
| 11 | 360 | 190 | -130 | 42 | | 2385 | 2376 |
| 12 | 360 | 302 | 192 | 43 | | 2392 | |
| 13 | 360 | 416 | 275 | 44 | | 2399 | 2386 |
| 14 | 360 | 539 | 361 | 45 | 360 | | 2397 |
| 15 | 360 | | 459 | 46 | | 2423 | 2410 |
| 16 | | 816 | 580 | 47 | | 2435 | 2419 |
| 17 | | | 708 | 48 | | 2439 | 2423 |
| 18 | | 1050 | 850 | 49 | | | 2426 |
| 19 | | 1163 | 998 | 50 | 360 | | |
| 20 | 360 | 1270 | 1099 | | | | |
| 21 | | 1374 | 1246 | | | | |
| 22 | | 1493 | 1459 | | | | |
| 23 | | 1590 | | | | | |
| 24 | | 1669 | 1546 | | | | |
| 25 | 360 | 1755 | 1631 | | | | |
| 26 | | 1845 | 1726 | | | | |
| 27 | | 1913 | 1793 | | | | |
| 28 | | 1986 | 1880 | | | | |
| 29 | | 2067 | 1968 | | | | |
| 30 | 360 | 2116 | 2032 | | | | |

APPENDIX II (a)

| Specimen | 79 | 80 | 77 | 78 |
|---|---|---|---|---|
| $l_o$ | 0.3165 | 0.317 | 0.3166 | 0.3195 |
| $\rho_o$ | 1.202 | 1.206 | 1.204 | 1.199 |

Temperature 385°C, 405°C  Stress 13.6 kg/cm$^2$
Nominal relative density 0.50

| Time Min. | T°C | Specimen No. | | Time Min. | T°C | Specimen No. | |
|---|---|---|---|---|---|---|---|
| | | 79 | 80 | | | 77 | 78 |
| 0 | 40 | 0 | 0 | 0 | 40 | 0 | 0 |
| 1 | 40 | 4 | 0 | 1 | 45 | 0 | 0 |
| 2 | 60 | 3 | -1 | 2 | 102 | 0 | 0 |
| 3 | 125 | 7 | -3 | 3 | 191 | 23 | -5 |
| 4 | 205 | 5 | 20 | 4 | 255 | 45 | 17 |
| 5 | 255 | 2 | 32 | 5 | 300 | 58 | 22 |
| 6 | 292 | -3 | 25 | 6 | 334 | 60 | 32 |
| 7 | 320 | -16 | 33 | 7 | 360 | | 37 |
| 8 | 350 | -21 | 39 | 8 | 384 | 74 | 47 |
| 9 | 369 | 0 | 58 | 9 | 400 | 117 | 62 |
| 10 | 382 | 50 | 118 | 10 | 407 | 187 | 94 |
| 11 | 386 | 155 | 229 | 11 | 405 | 301 | 174 |
| 12 | 385 | 299 | 390 | 12 | 405 | 404 | 347 |
| 13 | 385 | 460 | 566 | 13 | 405 | 770 | 620 |
| 14 | 385 | 640 | 758 | 14 | 405 | 1045 | 928 |
| 15 | 385 | 831 | 956 | 15 | 405 | 1310 | 1223 |
| 16 | | 1011 | 1120 | 16 | | 1573 | |
| 17 | | 1199 | 1296 | 17 | | 1798 | 1723 |
| 18 | | 1265 | 1448 | 18 | | 1991 | 1911 |
| 19 | | 1517 | 1588 | 19 | | 2128 | 2077 |
| 20 | 385 | 1643 | 1717 | 20 | 405 | 2202 | 2204 |
| 21 | | 1767 | 1845 | 21 | | 2258 | 2277 |
| 22 | | 1858 | 1946 | 22 | | 2282 | 2306 |
| 23 | | 1950 | 2036 | 23 | | 2400 | 2333 |
| 24 | | 2073 | 2100 | 24 | | | 2360 |
| 25 | 385 | 2104 | 2152 | | | | |
| 26 | | 2156 | 2181 | | | | |
| 27 | | 2187 | 2200 | | | | |
| 28 | | 2214 | 2224 | | | | |
| 29 | | 2234 | 2244 | | | | |
| 30 | 385 | 2262 | 2272 | | | | |

APPENDIX II (b)

| Specimen | 85 | 86 | 96 | 97 |
|---|---|---|---|---|
| $l_o$ | 0.3182 | 0.3150 | 0.3135 | 0.3148 |
| $\rho_o$ | 1.204 | 1.211 | 1.217 | 1.216 |

Temperature 340°C Stress 6.0 kg/cm$^2$
Nominal relative density 0.50

| Time Min. | T°C | Specimen No. | | Time Min. | T°C | Specimen No. | |
|---|---|---|---|---|---|---|---|
| | | 85 | 86 | | | 96 | 97 |
| 0 | 40 | 0 | 0 | 0 | 40 | 0 | 0 |
| 1 | 40 | 3 | 0 | 1 | 40 | -2 | 1 |
| 2 | 84 | -3 | -2 | 2 | 84 | 1 | -2 |
| 3 | 165 | -3 | -16 | 3 | 165 | -1 | -19 |
| 4 | 228 | -5 | -14 | 4 | 228 | -11 | -42 |
| 5 | 285 | -4 | -17 | 5 | 285 | -18 | -52 |
| 6 | 320 | -4 | -32 | 6 | 320 | -15 | -62 |
| 7 | 340 | -1 | -42 | 7 | 340 | -4 | -68 |
| 8 | 340 | 18 | -41 | 8 | 340 | 31 | -61 |
| 9 | 340 | 32 | -25 | 9 | 340 | 58 | -35 |
| 10 | 340 | 61 | -7 | 10 | 340 | 78 | -14 |
| 11 | | 88 | 25 | 11 | | 96 | 11 |
| 12 | | 114 | 32 | 12 | | 111 | 29 |
| 13 | | 155 | 45 | 13 | | 120 | 66 |
| 14 | | 200 | 55 | 14 | | 132 | 78 |
| 15 | 340 | 149 | 81 | 15 | 340 | 157 | 104 |
| 16 | | 292 | 116 | 16 | | 179 | 136 |
| 17 | | 342 | 152 | 17 | | 216 | 196 |
| 18 | | 402 | 191 | 18 | | 256 | 237 |
| 19 | | 452 | 234 | 19 | | 300 | 296 |
| 20 | 340 | 509 | 283 | 20 | 340 | 349 | 352 |
| 21 | | 556 | 333 | 21 | | 387 | 413 |
| 22 | | 605 | 384 | 22 | | 437 | 483 |
| 23 | | 654 | 441 | 23 | | 494 | 547 |
| 24 | | 704 | 499 | 24 | | 550 | 611 |
| 25 | 340 | 756 | 549 | 25 | 340 | 608 | 678 |
| 26 | | 819 | 605 | 26 | | 659 | 741 |
| 27 | | 858 | 659 | 27 | | 715 | 799 |
| 28 | | 921 | 720 | 28 | | 774 | 857 |
| 29 | | 974 | 773 | 29 | | 840 | 907 |
| 30 | 340 | 1030 | 829 | 30 | 340 | 904 | 976 |

APPENDIX II (b) cont.

| Specimen | | 85 | 86 | | 96 | 97 | |
|---|---|---|---|---|---|---|---|
| Time Min. | T°C | Specimen No. | | Time Min. | T°C | Specimen No. | |
| | | 85 | 86 | | | 96 | 97 |
| 31 | 340 | 1080 | 883 | 31 | 340 | 970 | 1040 |
| 32 | | 1119 | 929 | 32 | | 1030 | 1091 |
| 33 | | 1168 | 974 | 33 | | 1087 | 1140 |
| 34 | | 1216 | 1024 | 34 | | 1144 | 1182 |
| 35 | 340 | 1266 | 1073 | 35 | 340 | 1192 | 1220 |
| 36 | | 1317 | 1117 | 36 | | 1243 | 1257 |
| 37 | | 1360 | 1160 | 37 | | 1304 | 1295 |
| 38 | | 1415 | 1200 | 38 | | 1334 | 1328 |
| 39 | | 1459 | 1235 | 39 | | 1379 | 1363 |
| 40 | 340 | 1497 | 1277 | 40 | 340 | 1422 | 1398 |
| 41 | | 1531 | 1317 | 41 | | 1456 | 1423 |
| 42 | | 1564 | 1361 | 42 | | 1493 | 1453 |
| 43 | | 1594 | 1395 | 43 | | 1528 | 1474 |
| 44 | | 1636 | 1431 | 44 | | 1558 | 1494 |
| 45 | 340 | 1680 | 1461 | 45 | 340 | 1589 | 1507 |
| 46 | | 1699 | 1492 | 46 | | 1610 | 1518 |
| 47 | | 1728 | 1525 | 47 | | 1636 | |
| 48 | | 1753 | 1542 | 48 | | 1659 | 1537 |
| 49 | | 1776 | 1565 | 49 | | 1680 | 1545 |
| 50 | 340 | 1821 | 1592 | 50 | 340 | 1703 | 1560 |

APPENDIX II (b)

| Specimen | | 84 | 98 | 99 | 100 |
|---|---|---|---|---|---|
| | $l$ | 0.3169 | 0.3140 | 0.3145 | 0.316 |
| | $\rho_o^o$ | 1.210 | 1.219 | 1.217 | 1.209 |

Temperature 385°C Stress 6.0 kg/cm$^2$
Nominal relative density 0.50

| Time Min. | T°C | Specimen No. | | Time Min. | T°C | Specimen No. | |
|---|---|---|---|---|---|---|---|
| | | 84 | 98 | | | 99 | 100 |
| 0 | 40 | 0 | 0 | 0 | 40 | 0 | 0 |
| 1 | 40 | 1 | 0 | 1 | 40 | 0 | 1 |
| 2 | 75 | 1 | 0 | 2 | 62 | -5 | 0 |
| 3 | 153 | 10 | -11 | 3 | 144 | -24 | -9 |
| 4 | 217 | 28 | -12 | 4 | 714 | -29 | -3 |
| 5 | 270 | 44 | -12 | 5 | 263 | -31 | -3 |
| 6 | 300 | 55 | -14 | 6 | 297 | -40 | -6 |
| 7 | 331 | 59 | -27 | 7 | 329 | -48 | -4 |
| 8 | 355 | 64 | -19 | 8 | 354 | -49 | 11 |
| 9 | 375 | 80 | -9 | 9 | 371 | -39 | 37 |
| 10 | 390 | 105 | 23 | 10 | 388 | -11 | 82 |
| 11 | 405 | 164 | 86 | 11 | 385 | 30 | 142 |
| 12 | 405 | 291 | 197 | 12 | 385 | 85 | 225 |
| 13 | 405 | 462 | 348 | 13 | 385 | 169 | 321 |
| 14 | 405 | 667 | 543 | 14 | 385 | 283 | 437 |
| 15 | 405 | 877 | 733 | 15 | 385 | 411 | 563 |
| 16 | | 1087 | 921 | 16 | | 521 | 687 |
| 17 | | 1305 | 1091 | 17 | | 664 | 814 |
| 18 | | 1430 | 1250 | 18 | | | 931 |
| 19 | | 1553 | 1389 | 19 | | 895 | 1045 |
| 20 | 405 | 1653 | 1499 | 20 | 385 | 1011 | 1152 |
| 21 | | 1717 | 1545 | 21 | | 1115 | 1259 |
| 22 | | 1747 | 1599 | 22 | | 1206 | 1348 |
| 23 | | 1773 | 1625 | 23 | | 1304 | 1423 |
| 24 | | 1803 | 1655 | 24 | | 1380 | 1490 |
| 25 | 405 | 1821 | 1675 | 25 | 385 | 1441 | 1546 |
| 26 | | 1825 | 1697 | 26 | | 1490 | 1599 |
| 27 | | 1837 | 1708 | 27 | | 1531 | 1624 |
| 28 | | 1852 | 1729 | 28 | | 1573 | 1651 |
| 29 | | 1867 | 1741 | 29 | | 1592 | 1671 |
| 30 | 405 | 1877 | 1747 | 30 | 385 | 1617 | 1702 |

APPENDIX II (c)

| Specimen | 103 | 104 | 105 |
|---|---|---|---|
| $l_o$ | 0.316 | 0.316 | 0.3167 |
| $\rho_o$ | 1.214 | 1.214 | 1.212 |

Temperature 360°C Stress 0.54 kg/cm$^2$
Nominal relative density 0.50

| Time Min. | T°C | Specimen No. | | Time Min. | T°C | Specimen No. |
|---|---|---|---|---|---|---|
| | | 103 | 104 | | | 105 |
| 0 | 40 | 0 | 0 | 0 | 40 | 0 |
| 1 | 40 | 0 | 0 | 1 | 40 | 0 |
| 2 | 78 | -5 | -5 | 2 | 78 | -5 |
| 3 | 148 | -9 | -11 | 3 | 148 | -17 |
| 4 | 214 | -5 | -18 | 4 | 214 | -14 |
| 5 | 267 | -23 | -19 | 5 | 267 | -30 |
| 6 | 302 | -37 | -43 | 6 | 302 | -48 |
| 7 | 322 | -52 | -63 | 7 | 322 | -65 |
| 8 | 354 | -57 | -63 | 8 | 354 | -65 |
| 9 | 360 | -50 | -58 | 9 | 360 | -61 |
| 10 | 360 | -47 | -50 | 10 | 360 | -60 |
| 11 | | -40 | -43 | 11 | | -60 |
| 12 | | -25 | -25 | 12 | | -59 |
| 13 | | -9 | 12 | 13 | | -47 |
| 14 | | 4 | 47 | 14 | | -34 |
| 15 | 360 | 26 | 96 | 15 | 360 | -17 |
| 16 | | 44 | 143 | 16 | | -4 |
| 17 | | 91 | 196 | 17 | | 32 |
| 18 | | 135 | 256 | 18 | | 74 |
| 19 | | 191 | 305 | 19 | | 119 |
| 20 | 360 | 245 | 365 | 20 | 360 | 164 |
| 21 | | 306 | 428 | 21 | | 211 |
| 22 | | 374 | 493 | 22 | | 272 |
| 23 | | 440 | 558 | 23 | | 341 |
| 24 | | 502 | 617 | 24 | | 384 |
| 25 | 360 | 570 | 676 | 25 | 360 | 443 |
| 26 | | 636 | 740 | 26 | | 500 |
| 27 | | 705 | 800 | 27 | | 562 |
| 28 | | 768 | 856 | 28 | | 608 |
| 29 | | 818 | 918 | 29 | | 659 |
| 30 | 360 | 862 | 964 | 30 | 360 | 698 |

APPENDIX II (c) cont.

| Specimen | | 103 | 104 | | 105 | |
|---|---|---|---|---|---|---|
| Time Min. | T°C | Specimen No. | | Time Min. | T°C | Specimen No. |
| | | 103 | 104 | | | 105 |
| 31 | 360 | 407 | 1006 | 31 | 360 | 732 |
| 32 | | 940 | 1042 | 32 | | 759 |
| 33 | | 966 | 1076 | 33 | | 786 |
| 34 | | 984 | 1099 | 34 | | 804 |
| 35 | 360 | 1004 | 1119 | 35 | 360 | 824 |

APPENDIX II (c)

| Specimen | 101 | 102 | 106 | 107 |
|---|---|---|---|---|
| $l_o$ | 0.3176 | 0.316 | 0.3194 | 0.3165 |
| $\rho_o$ | 1.208 | 1.214 | 1.205 | 1.212 |

Temperature 360°C Stress 6.0, 3.5 kg/cm$^2$
Nominal relative density 0.50

| Time Min. | T°C | Specimen No. | | Time Min. | T°C | Specimen No. | |
|---|---|---|---|---|---|---|---|
| | | 101 | 102 | | | 106 | 107 |
| 0 | 40 | 0 | 0 | 0 | 40 | 0 | 0 |
| 1 | 40 | 0 | 7 | 1 | 40 | 0 | 0 |
| 2 | 95 | -3 | 1 | 2 | 75 | -4 | -4 |
| 3 | 172 | -28 | -20 | 3 | 145 | -29 | -29 |
| 4 | 218 | -24 | -33 | 4 | 200 | -51 | -49 |
| 5 | 267 | -41 | -46 | 5 | 244 | -70 | -72 |
| 6 | 307 | -57 | -79 | 6 | 283 | -88 | -87 |
| 7 | 335 | -84 | -110 | 7 | 312 | -102 | -94 |
| 8 | 360 | -99 | -129 | 8 | 344 | -80 | -100 |
| 9 | 360 | -91 | -138 | 9 | 362 | -75 | -88 |
| 10 | 360 | -86 | -134 | 10 | 360 | -67 | -85 |
| 11 | | -70 | -129 | 11 | 360 | -50 | -66 |
| 12 | | -43 | -105 | 12 | 360 | -24 | -39 |
| 13 | | -4 | -74 | 13 | 360 | 6 | -5 |
| 14 | | 50 | -33 | 14 | 360 | 49 | 46 |
| 15 | 360 | 107 | 16 | 15 | 360 | 98 | 102 |
| 16 | | 195 | 94 | 16 | | 159 | 168 |
| 17 | | 263 | 152 | 17 | | 220 | 242 |
| 18 | | 345 | 231 | 18 | | 294 | 319 |
| 19 | | 33 | 316 | 19 | | 371 | 397 |
| 20 | 360 | 525 | 414 | 20 | 360 | 460 | 479 |
| 21 | | 617 | 508 | 21 | | 543 | 553 |
| 22 | | 703 | 602 | 22 | | 614 | 627 |
| 23 | | 783 | 696 | 23 | | 686 | 699 |
| 24 | | 869 | 795 | 24 | | 766 | 782 |
| 25 | 360 | 953 | 884 | 25 | 360 | 835 | 853 |
| 26 | | 1028 | 975 | 26 | | 898 | 916 |
| 27 | | 1098 | 1055 | 27 | | 954 | 978 |
| 28 | | 1176 | 1145 | 28 | | 1036 | 1047 |
| 29 | | 1247 | 1224 | 29 | | 1096 | 1104 |
| 30 | 360 | 1308 | 1294 | 30 | 360 | 1143 | 1152 |

APPENDIX II (c) cont.

| Specimen | | 101 | 102 | | 106 | 107 | |
|---|---|---|---|---|---|---|---|
| Time Min. | T°C | Specimen No. | | Time Min. | T°C | Specimen No. | |
| | | 101 | 102 | | | 106 | 107 |
| 31 | 360 | 1359 | 1359 | 31 | 360 | 1194 | 1199 |
| 32 | | 1410 | 1419 | 32 | | 1248 | 1248 |
| 33 | | 1458 | 1473 | 33 | | 1290 | 1283 |
| 34 | | 1500 | 1523 | 34 | | 1327 | 1329 |
| 35 | 360 | 1538 | 1564 | 35 | 360 | 1359 | 1349 |
| 36 | | 1568 | 1592 | 36 | | 1405 | 1391 |
| 37 | | 1598 | 1616 | 37 | | 1434 | 1411 |
| 38 | | 1644 | 1636 | 38 | | 1463 | 1430 |
| 39 | | 1771 | | 39 | | 1481 | 1447 |
| 40 | 360 | 1793 | | 40 | 360 | 1498 | 1464 |

APPENDIX II (d)

| Specimen | 136 | 137 |
|---|---|---|
| $l_o$ | 0.3045 | 0.3035 |
| $g_o$ | 1.702 | 1.700 |

Temperature 360°C Stress 9.2 kg/cm$^2$
Nominal relative density 0.70

| Time Min. | T°C | Specimen No. | | Time Min. | T°C | Specimen No. | |
|---|---|---|---|---|---|---|---|
| | | 136 | 137 | | | 136 | 137 |
| 0 | 40 | 0 | 0 | 31 | 360 | 417 | 523 |
| 1 | 40 | 2 | 1 | 32 | | 477 | 582 |
| 2 | 62 | -6 | -7 | 33 | | 533 | 638 |
| 3 | 132 | -22 | -29 | 34 | | 590 | 698 |
| 4 | 192 | -33 | -51 | 35 | 360 | 643 | 755 |
| 5 | 240 | -43 | -71 | 36 | | 717 | 820 |
| 6 | 277 | -56 | -94 | 37 | | 765 | 873 |
| 7 | 307 | -82 | -129 | 38 | | 821 | 928 |
| 8 | 336 | -111 | -162 | 39 | | 871 | 966 |
| 9 | 360 | -134 | -194 | 40 | 360 | 924 | 1014 |
| 10 | 360 | -152 | -122 | 41 | | 976 | 1055 |
| 11 | | -163 | -232 | 42 | | 1020 | 1090 |
| 12 | | -164 | -235 | 43 | | 1061 | 1124 |
| 13 | | -165 | -232 | 44 | | 1097 | 1157 |
| 14 | | -159 | -226 | 45 | 360 | 1133 | 1185 |
| 15 | 360 | -148 | -213 | 46 | | 1166 | 1211 |
| 16 | | -135 | -197 | 47 | | 1198 | 1237 |
| 17 | | -122 | -176 | 48 | | 1223 | 1256 |
| 18 | | -107 | -152 | 49 | | 1244 | 1274 |
| 19 | | -84 | -119 | 50 | 360 | 1263 | 1287 |
| 20 | 360 | -64 | -87 | | | | |
| 21 | | -39 | -50 | | | | |
| 22 | | -13 | -7 | | | | |
| 23 | | 19 | 45 | | | | |
| 24 | | 56 | 98 | | | | |
| 25 | 360 | 93 | 146 | | | | |
| 26 | | 139 | 207 | | | | |
| 27 | | 194 | 271 | | | | |
| 28 | | 248 | 331 | | | | |
| 29 | | 303 | 392 | | | | |
| 30 | 360 | 361 | 458 | | | | |

APPENDIX II (d)

| Specimen | 132 | 133 |
|---|---|---|
| $l_o$ | 0.309 | 0.3108 |
| $g_o$ | 1.537 | 1.535 |

Temperature 360°C Stress 9.2 kg/cm$^2$
Nominal relative density 0.65

| Time Min. | T°C | Specimen No. 132 | Specimen No. 133 | Time Min. | T°C | Specimen No. 132 | Specimen No. 133 |
|---|---|---|---|---|---|---|---|
| 0 | 40 | 0 | 0 | 31 | 360 | 736 | 727 |
| 1 | 42 | 0 | 3 | 32 | | 797 | 791 |
| 2 | 86 | -7 | -5 | 33 | | 854 | 850 |
| 3 | 156 | -25 | -17 | 34 | | 920 | 908 |
| 4 | 218 | -39 | -24 | 35 | 360 | 978 | 964 |
| 5 | 262 | -54 | -31 | 36 | | 1048 | 1031 |
| 6 | 298 | -74 | -57 | 37 | | 1103 | 1080 |
| 7 | 335 | -97 | -87 | 38 | | 1150 | 1127 |
| 8 | 360 | -120 | -110 | 39 | | 1200 | 1177 |
| 9 | 360 | -135 | -132 | 40 | 360 | 1248 | 1221 |
| 10 | 360 | -150 | -144 | 41 | | 1291 | 1264 |
| 11 | | -154 | -155 | 42 | | 1326 | 1301 |
| 12 | | -152 | -155 | 43 | | 1364 | 1336 |
| 13 | | -146 | -153 | 44 | | 1391 | 1363 |
| 14 | | -138 | -145 | 45 | 360 | 1418 | 1389 |
| 15 | 360 | -122 | -132 | 46 | | 1442 | 1418 |
| 16 | | -105 | -107 | 47 | | 1467 | 1446 |
| 17 | | -80 | -75 | 48 | | 1481 | 1475 |
| 18 | | -65 | -34 | 49 | | 1495 | 1484 |
| 19 | | 0 | 15 | 50 | 360 | 1506 | 1501 |
| 20 | 360 | 42 | 63 | | | | |
| 21 | | 93 | 117 | | | | |
| 22 | | 145 | 175 | | | | |
| 23 | | 209 | 235 | | | | |
| 24 | | 270 | 294 | | | | |
| 25 | 360 | 331 | 351 | | | | |
| 26 | | 398 | 411 | | | | |
| 27 | | 468 | 477 | | | | |
| 28 | | 536 | 539 | | | | |
| 29 | | 601 | 596 | | | | |
| 30 | 360 | 670 | 662 | | | | |

APPENDIX II (d)

| Specimen | 120 | 121 |
|---|---|---|
| $l_o$ | 0.3189 | 0.3148 |
| $g_o$ | 1.313 | 1.317 |

Temperature 360°C Stress 9.2 kg/cm$^2$
Nominal relative density 0.55

| Time Min. | T°C | Specimen No. 120 | Specimen No. 121 | Time Min. | T°C | Specimen No. 120 | Specimen No. 121 |
|---|---|---|---|---|---|---|---|
| 0 | 40 | 0 | 0 | 31 | 360 | 1536 | 1329 |
| 1 | 40 | 0 | 0 | 32 | | 1589 | 1390 |
| 2 | 80 | -8 | -6 | 33 | | 1632 | 1445 |
| 3 | 155 | -26 | -10 | 34 | | 1676 | 1499 |
| 4 | 210 | -37 | -17 | 35 | 360 | 1712 | 1550 |
| 5 | 246 | -59 | -26 | 36 | | 1758 | 1608 |
| 6 | 276 | -76 | -46 | 37 | | 1784 | 1648 |
| 7 | 300 | -95 | -72 | 38 | | 1802 | 1691 |
| 8 | 326 | -177 | -98 | 39 | | 1824 | 1713 |
| 9 | 354 | -125 | -109 | 40 | 360 | 1843 | 1740 |
| 10 | 363 | -114 | -114 | | | | |
| 11 | 360 | -99 | -108 | | | | |
| 12 | 360 | -67 | -91 | | | | |
| 13 | 360 | -22 | -63 | | | | |
| 14 | 360 | 40 | -19 | | | | |
| 15 | 360 | 111 | 36 | | | | |
| 16 | | 200 | 97 | | | | |
| 17 | | 290 | 166 | | | | |
| 18 | | 391 | 258 | | | | |
| 19 | | 495 | 336 | | | | |
| 20 | 360 | 597 | 434 | | | | |
| 21 | | 692 | 518 | | | | |
| 22 | | 793 | 618 | | | | |
| 23 | | 890 | 712 | | | | |
| 24 | | 995 | 801 | | | | |
| 25 | 360 | 1068 | 883 | | | | |
| 26 | | 1161 | 964 | | | | |
| 27 | | 1252 | 1047 | | | | |
| 28 | | 1322 | 1121 | | | | |
| 29 | | 1404 | 1191 | | | | |
| 30 | 360 | 1472 | 1258 | | | | |

APPENDIX II (d)

| Specimen | 129 | 130 | 108 | 109 |
|---|---|---|---|---|
| $l_o$ | 0.3142 | 0.3104 | 0.3165 | 0.3132 |
| $g_o$ | 0.963 | 0.972 | 1.212 | 1.220 |

Temperature 360°C Stress 9.2 kg/cm$^2$
Nominal relative density 0.40, 0.51

| Time Min. | T°C | Specimen No. | | Time Min. | T°C | Specimen No. | |
|---|---|---|---|---|---|---|---|
| | | 129 | 130 | | | 108 | 109 |
| 0 | 40 | 0 | 0 | 0 | 40 | 0 | 0 |
| 1 | 40 | 0 | 0 | 1 | 40 | 0 | 0 |
| 2 | 86 | -8 | -8 | 2 | 80 | -11 | -10 |
| 3 | 160 | 6 | -7 | 3 | 157 | -13 | -11 |
| 4 | 215 | 14 | -3 | 4 | 219 | -7 | -13 |
| 5 | 254 | 6 | -1 | 5 | 262 | 3 | -18 |
| 6 | 292 | -2 | -8 | 6 | 300 | -17 | -24 |
| 7 | 320 | -12 | -13 | 7 | 334 | -25 | -36 |
| 8 | 348 | 5 | 10 | 8 | 360 | -33 | -39 |
| 9 | 360 | 45 | 38 | 9 | 360 | -15 | -36 |
| 10 | 360 | 101 | 79 | 10 | 360 | -1 | -21 |
| 11 | 360 | 185 | 171 | 11 | | 33 | 4 |
| 12 | 360 | 290 | 246 | 12 | | 87 | 47 |
| 13 | 360 | 414 | 394 | 13 | | 160 | 102 |
| 14 | 360 | 545 | 541 | 14 | | 237 | 171 |
| 15 | 360 | 682 | 697 | 15 | 360 | 315 | 262 |
| 16 | | 822 | 865 | 16 | | 443 | 350 |
| 17 | | 967 | 1019 | 17 | | 498 | 451 |
| 18 | | 1110 | 1174 | 18 | | 603 | 555 |
| 19 | | 1251 | 1325 | 19 | | 704 | 659 |
| 20 | 360 | 1381 | 1464 | 20 | 360 | 802 | 751 |
| 21 | | 1510 | 1594 | 21 | | 908 | 848 |
| 22 | | 1639 | 1718 | 22 | | 1008 | 945 |
| 23 | | 1763 | 1832 | 23 | | 1110 | 1039 |
| 24 | | 1872 | 1967 | 24 | | 1199 | 1122 |
| 25 | 360 | 1976 | 2120 | 25 | 360 | 1280 | 1200 |
| 26 | | 2067 | | 26 | | 1362 | 1275 |
| | | | | 27 | | 1445 | 1352 |
| | | | | 28 | | 1524 | 1419 |
| | | | | 29 | | 1593 | 1479 |
| | | | | 30 | 360 | 1660 | 1535 |

APPENDIX II (d) cont.

Specimen 108 109

| Time Min. | T°C | Specimen No. 108 | 109 |
|---|---|---|---|
| 31 | 360 | 1725 | 1590 |
| 32 | | 1783 | 1643 |
| 33 | | 1833 | 1688 |
| 34 | | 1881 | 1732 |
| 35 | 360 | 1915 | 1766 |
| 36 | | 1948 | 1798 |
| 37 | | 1980 | 1826 |
| 38 | | 2005 | 1852 |
| 39 | | 2030 | 1874 |
| 40 | 360 | 2050 | 1889 |

APPENDIX II (d)

| Specimen | 124 | 125 |
|---|---|---|
| $l_o$ | 0.3275 | 0.3120 |
| $\rho_o$ | 1.072 | .073 |

Temperature 360°C Stress 9.2 kg/cm$^2$
Nominal relative density 0.45

| Time Min. | T°C | Specimen No. | | Time Min. | T°C | Specimen No. | |
|---|---|---|---|---|---|---|---|
| | | 124 | 125 | | | 124 | 125 |
| 0 | 40 | 0 | 0 | 31 | 360 | 2137 | 1989 |
| 1 | 40 | 0 | 1 | 32 | | 2186 | 2031 |
| 2 | 86 | -8 | -6 | 33 | | 2223 | 2068 |
| 3 | 160 | 0 | -1 | 34 | | 2260 | 2099 |
| 4 | 214 | 4 | 5 | 35 | 360 | 2292 | 2120 |
| 5 | 254 | -2 | 7 | 36 | | 2334 | |
| 6 | 293 | -9 | -2 | 37 | | 2357 | |
| 7 | 320 | -19 | -8 | 38 | | 2374 | |
| 8 | 347 | -8 | -7 | 39 | | 2395 | |
| 9 | 360 | 10 | 8 | | | | |
| 10 | 360 | 52 | 20 | | | | |
| 11 | | 117 | 52 | | | | |
| 12 | | 216 | 111 | | | | |
| 13 | | 320 | 180 | | | | |
| 14 | | 446 | 271 | | | | |
| 15 | 360 | 587 | 369 | | | | |
| 16 | | 718 | 600 | | | | |
| 17 | | 854 | 601 | | | | |
| 18 | | 986 | 728 | | | | |
| 19 | | 1103 | 861 | | | | |
| 20 | 360 | 1213 | 985 | | | | |
| 21 | | 1325 | 1105 | | | | |
| 22 | | 1439 | 1218 | | | | |
| 23 | | 1548 | 1332 | | | | |
| 24 | | 1642 | 1438 | | | | |
| 25 | 360 | 1734 | 1532 | | | | |
| 26 | | 1810 | 1631 | | | | |
| 27 | | 1892 | 1725 | | | | |
| 28 | | 1950 | 1799 | | | | |
| 29 | | 2021 | 1858 | | | | |
| 30 | 360 | 2088 | 1924 | | | | |

APPENDIX II (d)

| Specimen | 116 | 117 |
|---|---|---|
| $l_o$ | 0.3142 | 0.3130 |
| $\rho_o$ | 1.425 | 1.430 |

Temperature 360°C Stress 9.2 kg/cm$^2$
Nominal relative density 0.60

| Time Min. | T°C | Specimen No. | | Time Min. | T°C | Specimen No. | |
|---|---|---|---|---|---|---|---|
| | | 116 | 117 | | | 116 | 117 |
| 0 | 40 | 0 | 0 | 31 | 360 | 1074 | 1002 |
| 1 | 40 | 0 | 0 | 32 | | 1136 | 1062 |
| 2 | 78 | -8 | -8 | 33 | | 1195 | 1119 |
| 3 | 150 | -19 | -15 | 34 | | 1249 | 1178 |
| 4 | 208 | -33 | -14 | 35 | 360 | 1302 | 1235 |
| 5 | 256 | -32 | -16 | 36 | | 1380 | 1304 |
| 6 | 294 | -42 | -29 | 37 | | 1413 | 1360 |
| 7 | 326 | -75 | -51 | 38 | | 1456 | 1410 |
| 8 | 350 | -98 | -67 | 39 | | 1501 | 1464 |
| 9 | 362 | | -69 | 40 | 360 | 1540 | 1512 |
| 10 | 360 | 121 | -73 | 41 | | 1579 | 1557 |
| 11 | 360 | 122 | -66 | 42 | | 1600 | 1590 |
| 12 | 360 | 114 | -53 | 43 | | 1725 | 1623 |
| 13 | 360 | 101 | -40 | 44 | | 1641 | 1647 |
| 14 | 360 | -77 | -24 | 45 | 360 | 1657 | 1674 |
| 15 | 360 | -46 | -3 | | | | |
| 16 | | -2 | 28 | | | | |
| 17 | | 65 | 65 | | | | |
| 18 | | 106 | 111 | | | | |
| 19 | | 173 | 164 | | | | |
| 20 | 360 | 241 | 216 | | | | |
| 21 | | 313 | 279 | | | | |
| 22 | | 389 | 346 | | | | |
| 23 | | 472 | 416 | | | | |
| 24 | | 552 | 491 | | | | |
| 25 | 360 | 624 | 558 | | | | |
| 26 | | 705 | 637 | | | | |
| 27 | | 787 | 713 | | | | |
| 28 | | 863 | 786 | | | | |
| 29 | | 935 | 853 | | | | |
| 30 | 360 | 1005 | 926 | | | | |

## APPENDIX III

### Accuracy of the Thermal Expansion Correction

The data from the experimental runs were corrected for the thermal expansion of the loading frame by the subtraction of a correction obtained from runs made using a dummy quartz specimen to obtain the expansion curve for the frame alone. The corrections were averaged and subtracted from the indicated creep deformation values, i.e. :

$$L(t) = L'(t) - \bar{c}(t)$$

where $L(t)$ = the actual length at time t, $L'(t)$ = the indicated length and $\bar{c}(t)$ = the average change in length developed during the thermal expansion runs.

The correction has been verified by two methods:

1) Comparison of the total strain, (with a Micrometer) as determined by direct measurements of the specimens before and after dehydroxylation.
2) Direct measurement in the furnace using a travelling microscope. (Cathetometer).

The first method gave an apparent accuracy of about 0.001 inches for deformations of from 0.010 to 0.020 inches, indicating that the measurements are correct to one part in ten or twenty.

Figure 37 compares the deformation curve, as corrected by the normal procedure with lengths measured with the travelling microscope. The two are in agreement to within 10%, which is felt to be satisfactory.

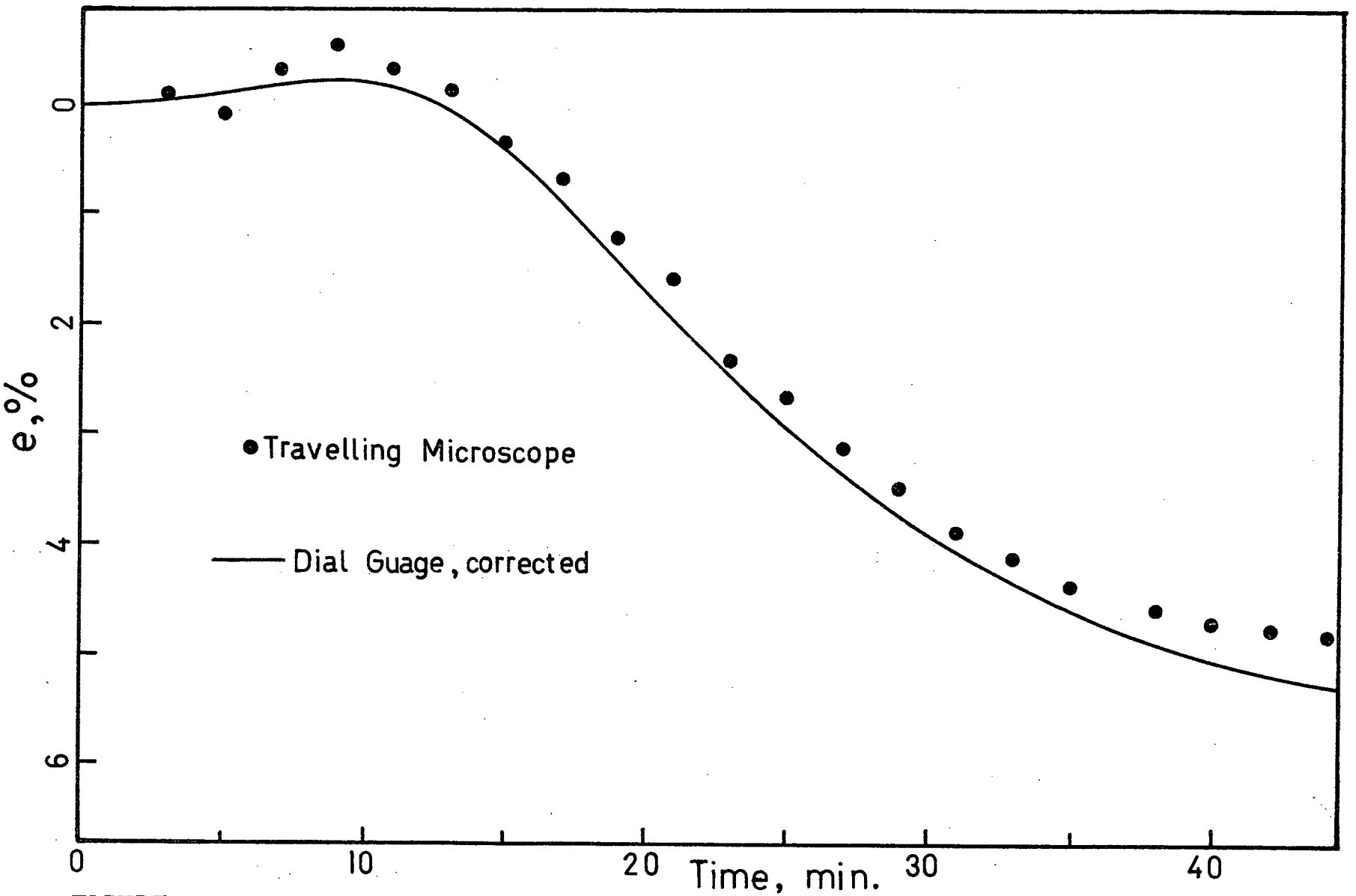


FIGURE 37 Comparative values of the deformation measured by the normal apparatus and a travelling microscope.

## BIBLIOGRAPHY


1. A. C. D. Chaklader, Nature, 206, 392 (1965)

2. P. E. D. Morgan and E. Scala, "High Density Oxides by Decomposition Pressure Sintering of Hydroxides", presented at the Sixty-Seventh Annual Meeting, The American Ceramic Society, Philadelphia, Pa., May 3rd, 1965.

3. T. G. Carruthers and T. A. Wheat, Proc. British Ceramic Society, 3, 259 (1965).

4. a) A. C. D. Chaklader and L. G. McKenzie, J. Am. Ceram. Soc., 49, 47 (1966).
   b) A. C. D. Chaklader and L. G. McKenzie, Am. Ceram. Soc. Bull., 43, 892 (1964).

5. A. C. D. Chaklader and V. T. Baker, Bull. Am. Ceram. Soc., 44, 258 (1965).

6. A. C. D. Chaklader and M. N. Shetty, Trans. Met. Soc. A. I. M. E., 233, 1441 (1965).

7. P. E. D. Morgan and N. C. Schaeffer, Tech. Rep. AFML-TR-66-356, Nov. 1966.

8. A. C. D. Chaklader and R. C. Cook, J. Am. Ceram. Soc. 47, 712 (1968).

9. J. A. Hedvall in Reaktionsfaehigheit fester Stoffe, V. J. A. Barth, (Leipzig), 1938. Reprinted by Edwards Brothers, Inc., Ann Arbor, Mich. (1943).

10. R. L. Coble and J. S. Ellis, J. Am. Ceram. Soc., 46, 438-41(1963).

11. I. B. Cutler in "Kinetics of High Temperature Processes", pp. 294-301, ed. W. D. Kingery, M. I. T. Press, and John Wiley & Sons, 1959.

12. N. G. Dave and S. K. Chopra, J. Am. Ceram. Soc., 49, 575 (1966).

13. J. F. Goodman, Proc. Royal Soc. (London), A 247, 346 - 52 (1958).

14. P. J. Anderson and R. F. Horlock, Trans. Faraday Soc., 58, 1993 - 2004 (1962).

15. a) R. S. Gordon and W. D. Kingery, J. Am. Ceram. Soc., 49, 654 - 660 (1966).
b) R. S. Gordon and W. D. Kingery, tbid., 50, 8 -14 (1967).

16. M. C. Ball and H. F. W. Taylor, Mineral Mag., 32, 754 - 66 (1961).

17. S. J. Gregg and R. I. Razouk, J. Chem. Soc., (London), 1949, pp. S36 - 44.

18. G. M. Zhabrova and V. A. Gordeeva, Kinetika i Katalis, Akad. Nauk. SSSR, Sb. Statei, 1960 pp. 31 - 42.

19. R. F. Horlock, P. L. Morgan and P. J. Anderson, Trans. Faraday Soc., 59, 721 - 28 (1963).

20. Handbook of Chemistry and Physics, 44th ed., pp. 2532, 2365. Edited by C. D. Hodgman, R. C. Weast and S. M. Selby. Chemical Rubber Publishing Co., Cleveland, (1962 - 1963).

21. X-Ray Powder Data File, Edited by Joseph V. Smith, ASTM, Philadelphia (1960).

22. A. Ferrari and C. Colla, International Critical Tables, IV, 63, McGraw Hill (1933).

23. H. S. Carslaw and J. C. Jaeger, Conduction of Heat in Solids, 2nd ed;, p. 200. Oxford University Press, London (1959).

24. R. L. Coble and W. D. Kingery, J. Am. Ceram. Soc., 39, 377 - 85 (1956).

25. A. K. Kakar and A. C. D. Chaklader, J. Appl. Phys., 38, 3223 - 30 (1967).

26. G. M. Fryer, Trans. Brit. Ceram. Soc., 39, 377 - 85 (1956).

27. K. Aihara, Graduate Student, Department of Metallurgy, U. B. C. Private Communication.

28. G. K. Layden and G. W. Brindley, J. Am. Ceram. Soc., 46, 518 - 22 (1963).

29. Y. Kotera, T. Saito and M. Terada, J. Jap. Ceram. Soc., 36, 195 - 199 (1963).

30. G. B. Smith, Metal & Ind. (London), 72, 427 (1948).

31. C. O. Hulse, S. M. Copley and J. A. Pask, J. Am. Ceram. Soc., 46, 317 - 323 (1963).

32. C. E. Wicks and F. E. Block, "Thermodynamic Properties of 65 Elements - Their Oxides, Halides, Carbides and Nitrides, Bull. 605, US Bureau of Mines, Washington (1963)."

33. A. C. D. Chaklader and G. Beynon, J. Am. Ceram. Soc., Oct. 1970, (To be published).